# Positively selected modifications in the pore of TbAQP2 allow pentamidine to enter *Trypanosoma brucei*

Ali H. Alghamdi[1], Jane C. Munday[1], Gustavo D. Campagnaro[1], Dominik Gurvič[2], Fredrik Svensson[3], Chinyere E. Okpara[4], Arvind Kumar ,[5] Maria Esther Martin Abril[1], Patrik Milić[1], Laura Watson[1], Daniel Paape,[1] Luca Settimo,[1] Anna Dimitriou[1], Joanna Wielinska[1], Graeme Smart[1], Laura F. Anderson[1], Christopher M. Woodley,[4] Siu Pui Ying Kelley[1], Hasan M.S. Ibrahim[1], Fabian Hulpia[6] , Mohammed I. Al-Salabi[1], Anthonius A. Eze[1], Ibrahim A. Teka[1], Simon Gudin[1], Christophe Dardonville[7], Richard R Tidwell[8], Mark Carrington[9], Paul M. O'Neill[4], David W Boykin[5], Ulrich Zachariae[2], Harry P. De Koning[1,*]

1. Institute of Infection, Immunity and Inflammation, University of Glasgow, Glasgow G12 8TA, UK
2. Computational Biology Centre for Translational and Interdisciplinary Research, University of Dundee, Dundee DD1 5EH, UK
3. IOTA Pharmaceuticals Ltd, St Johns Innovation Centre, Cowley Road, Cambridge CB4 0WS
4. Department of Chemistry, University of Liverpool, Liverpool, UK
5. Chemistry Department, Georgia State University, Atlanta, GA, US
6. Laboratory for Medicinal Chemistry, University of Ghent, Ghent, Belgium
7. Instituto de Química Médica - CSIC, Madrid, Spain
8. Department of Pathology and Lab Medicine, University of North Carolina at Chapel Hill, Chapel Hill, NC, USA
9. Department of Biochemistry, University of Cambridge, Cambridge, UK

*, to whom correspondence should be addressed:

email: Harry.de-Koning@glasgow.ac.uk

tel: +44-141-3303753

Running title : Mechanism of drug transport by TbAQP2

## Abstract

Mutations in the *Trypanosoma brucei* aquaporin AQP2 are associated with resistance to pentamidine and melarsoprol. We show that TbAQP2 but not TbAQP3 was positively selected for increased pore size from a common ancestor aquaporin. We demonstrate that TbAQP2's unique architecture permits pentamidine permeation through its central pore and show how specific mutations in highly conserved motifs affect drug permeation. Introduction of key TbAQP2 amino acids into TbAQP3 renders the latter permeable to pentamidine. Molecular dynamics demonstrates that permeation by dicationic pentamidine is energetically favourable in TbAQP2, driven by the membrane potential, although aquaporins are normally strictly impermeable for ionic species. We also identify the structural determinants that make pentamidine a permeant but exclude most other diamidine drugs. Our results have wide-ranging implications for optimising antitrypanosomal drugs and averting cross-resistance. Moreover, these new insights in aquaporin permeation may allow the pharmacological exploitation of other members of this ubiquitous gene family.



Keywords:

Drug transport / Aquaporin / evolution of membrane proteins / Trypanosoma brucei / pentamidine-melarsoprol cross-resistance

# Introduction

The *Trypanosoma brucei*-group species are protozoan parasites that cause severe and fatal infections in humans (sleeping sickness) and animals (nagana, surra, dourine) (Giordani *et al,* 2016; Büscher *et al,* 2017). The treatment is dependent on the sub-species of trypanosome, on the host, and on the stage of the disease (Giordani *et al,* 2016; De Koning, 2020). Many anti-protozoal drugs are inherently cytotoxic but derive their selectivity from preferential uptake by the pathogen rather than the host cell (Munday *et al,* 2015a; De Koning, 2020). Conversely, loss of the specific drug transporters is a main cause for drug resistance (Barrett *et al,* 2011; Baker *et al,* 2013; Munday *et al,* 2015a; De Koning, 2020). This is the case for almost all clinically used trypanocides, including diamidines such as pentamidine and diminazene (Carter *et al,* 1995; De Koning, 2001a; De Koning *et al,* 2004; Bridges *et al,* 2007), melaminophenyl arsenicals such as melarsoprol and cymelarsan for cerebral stage human and animal trypanosomiasis, respectively (Carter & Fairlamb, 1993; Bridges *et al,* 2007), and the fluorinated amino acid analogue eflornithine for human cerebral trypanosomiasis (Vincent *et al,* 2010). The study of transporters is thus important for anti-protozoal drug discovery programmes as well as for the study of drug resistance (Lüscher *et al,* 2007; Munday *et al,* 2015a).

In *Trypanosoma brucei*, the phenomenon of melarsoprol-pentamidine cross-resistance (MPXR) was first described shortly after their introduction (Rollo & Williamson, 1951), and was linked to reduced uptake rather than shared intracellular target(s) (Frommel & Balber, 1987). The first transporter to be implicated in MPXR was the aminopurine transporter TbAT1/P2 (Carter & Fairlamb, 1993; Mäser *et al,* 1999; Munday *et al,* 2015b) but two additional transport entities, named High Affinity Pentamidine Transporter (HAPT1) and Low Affinity Pentamidine Transporter (LAPT1), have been described (De Koning, 2001a; De Koning & Jarvis, 2001; Bridges *et al,* 2007). HAPT1 was identified as Aquaglyceroporin

2 (TbAQP2) via an RNAi library screen, and found to be the main determinant of MPXR (Baker *et al,* 2012, 2013; Munday *et al,* 2014). The apparent permissibility for high molecular weight substrates by TbAQP2 was attributed to the highly unusual selectivity filter of TbAQP2, which lacks the canonical aromatic/arginine (ar/R) and full NPA/NPA motifs, resulting in a much wider pore (Baker *et al,* 2012; Munday *et al,* 2014, 2015a). Importantly, the introduction of TbAQP2 into *Leishmania* promastigotes greatly sensitised these cells to pentamidine and melarsen oxide (Munday *et al,* 2014). Moreover, in several MPXR laboratory strains of *T. brucei* the *AQP2* gene was either deleted or chimeric after cross-over with the adjacent *TbAQP3* gene, which, unlike AQP2, contains the full, classical ar/R and NPA/NPA selectivity filter motifs and is unable to transport either pentamidine or melaminophenyl arsenicals (Munday *et al,* 2014). Similar chimeric genes and deletions were subsequently isolated from sleeping sickness patients unresponsive to melarsoprol treatment (Graf *et al,* 2013; Pyana Pati *et al,* 2014) and failed to confer pentamidine sensitivity when expressed in a *tbaqp2-tbaqp3* null *T. brucei* cell line whereas wild-type TbAQP2 did (Munday *et al,* 2014; Graf *et al,* 2015).

The model of drug uptake through a uniquely permissive aquaglyceroporin (Munday *et al,* 2015a) was challenged by a study arguing that instead of traversing the TbAQP2 pore, pentamidine merely binds to an aspartate residue (Asp265) near the extracellular end of the pore, above the selectivity filter, followed by endocytosis (Song *et al,* 2016). This alternative, 'porin-receptor' hypothesis deserves careful consideration given that (i) it is an exceptional assertion that drug-like molecules with molecular weights grossly exceeding those of the natural substrates, can be taken up by an aquaglyceroporin and (ii) the fact that bloodstream form trypanosomes do have, in fact, a remarkably high rate of endocytosis (Field & Carrington, 2009; Zoltner *et al,* 2016). The question is also important because aquaporins are found in almost all cell types and the mechanism by which they convey therapeutic agents

and/or toxins into cells is of high pharmacological and toxicological interest. While TbAQP2 is the first aquaporin described with the potential to transport drug-like molecules, this ability might not be unique, and the mechanism by which the transport occurs should be carefully investigated.

We therefore conducted a mutational analysis was undertaken, swapping TbAQP2 and TbAQP3 selectivity filter residues and altering pore width at its cytoplasmic end. This was complemented with a thorough structure-activity relationship study of the interactions between pentamidine and TbAQP2, using numerous chemical analogues for which inhibition constants were determined and interaction energy calculated. The pentamidine-TbAQP2 interactions were further modelled by running a molecular dynamics simulation on a protein-ligand complex, and In addition, we investigated a potential correlation between the *T. brucei* endocytosis rate and the rate of pentamidine uptake. Our results unequivocally show that pentamidine permeates directly through the central pore of TbAQP2 and that uptake is dependent on the microbial membrane potential. Having identified the essential characteristics that allow the transport of large, flexible molecules through TbAQP2, this should now allow the evaluation of aquaporins in other species for similar adaptations.

# Results

*12. Investigation of the structural determinants of AQP2 for pentamidine transport*

*1.1. Positive selection for pore size*

In *T. brucei*, the AQP2 and AQP3 genes are arranged as a tandem pair on chromosome 10 and have 74% amino acid identity. Whereas TbAQP2 clearly mediates pentamidine uptake, TbAQP3 does not (Baker *et al,* 2012; Munday *et al,* 2014), nor do various chimeric AQP2/3 rearrangements that give rise to pentamidine resistance (Munday *et al,* 2014; Graf *et al,* 2015). To investigate the origin of the AQP2 gene, a phylogenetic analysis of AQPs in African trypanosomes was performed. The number of aquaporin genes varies: there is a single aquaporin in *T. vivax* and *T. congolense,* two in *T. suis* and three in *T. brucei* and its derivatives (Supplemental Fig. 1A). The most probable tree (Supplemental Fig. 1B) is consistent with the evolutionary history of the four species (Hutchinson & Gibson, 2015) and indicates AQP1 as the ancestral AQP present in all trypanosome species. A duplication occurred in the common ancestor of *T. suis* and *T. brucei* after divergence from *T. congolense* and a further duplication, to form AQP2 and AQP3, in the ancestor of *T. brucei* after divergence from *T. suis*. Multiple alignment (Supplemental Fig. 1A) shows that the classical NPA/NPA and ar/R AQP selectivity filter elements are present in all AQPs except *T. brucei* AQP2. The divergence of *T. brucei* AQP2 and 3 was investigated by calculating the non-synonymous/synonymous codon ratio (dN/dS) for different AQPs (Supplemental Fig. 1C). For *T. brucei* aligned with *T. suis* AQP1, dN/dS is 0.21 and for AQP3, dN/dS is 0.30 indicating purifying selection. However, comparing *T. brucei* AQP2 with *T. brucei* AQP3, dN/dS is 2.0 indicating strong selection pressure for divergence on AQP2 towards an aquaporin with increased pore size. In order to verify any role of amino

139 acids along the TbAQP2 pore in facilitating pentamidine sensitivity and/or uptake, we
140 performed a mutational analysis.
141
142 *1.2 Introduction of AQP3 residues into the AQP2 selectivity filter*
143 One highly conserved motif of aquaporins, believed to be essential for permeant selectivity,
144 is NPA/NPA which is present in TbAQP3 but not in TbAQP2, where, uniquely, it is
145 N**S**$^{131}$A/NP**S**$^{263}$ instead. We therefore constructed a TbAQP2 variant with the classical
146 NPA/NPA motif (TbAQP2$^{S131P/S263A}$) and expressed it in the *aqp2/aqp3* null cell line (Baker
147 *et al,* 2012; Munday *et al,* 2014). In this cell line, uptake of 30 nM [$^3$H]-pentamidine was
148 reduced to 4.40 ± 0.71% (*n*=4) of the rate in the control line expressing TbAQP2WT (P<0.05,
149 Student's unpaired t-test), as well as significantly different from the rate measured in parallel
150 in the *tbaqp2/tbaqp3* null cells (P<0.01) (Fig. 1A). The remaining pentamidine uptake was
151 sufficient to strongly sensitise the TbAQP2$^{S131P/S263A}$ cells to pentamidine in a standard
152 protocol of 48 h incubation with the drug followed by a further 24 h in the presence of the
153 resazurin indicator dye (P<0.0001 vs *tbaqp2/tbaqp3* null) but the $EC_{50}$ was still significantly
154 higher than the TbAQP2WT control (P<0.05) (Fig. 1B). A similar effect was observed for the
155 melaminophenyl arsenical drug cymelarsan, but there was no change in sensitivity to
156 diminazene or the control drug phenylarsine oxide (PAO), which is believed to diffuse
157 directly across the membrane (Fairlamb *et al,* 1992) (Fig. 1B).
158 The mutant L258Y, which has the AQP3 Tyr-250 half of the highly conserved
159 aromatic/arginine (ar/R) motif, responsible for pore restriction and proton exclusion (Wu *et*
160 *al,* 2009), introduced into the TbAQP2 pore, yielded a drug transport phenotype similar to
161 TbAQP2$^{S131P/S263A}$. The [$^3$H]-pentamidine transport rate was reduced to 6.6 ± 1.4% of
162 TbAQP2WT (P<0.05) but remained above the rate in the *tbaqp2/tbaqp3* null cells (P<0.01)

(Fig. 1A). Pentamidine and cymelarsan $EC_{50}$ values were also significantly different from both the TbAQP2WT and the *tbaqp2/tbaqp3* null controls (Fig. 1C).

The ar/R motif is part of the larger selectivity filter, usually WGYR, present in both TbAQP1 and TbAQP3 but uniquely consisting of $I^{110}VL^{258}L^{264}$ in TbAQP2 (Baker *et al,* 2013), all non-polar, open chained residues. Cell lines expressing mutations $AQP2^{I110W}$ and $AQP2^{L264R}$, either alone or in combination, displayed pentamidine transport rates, and pentamidine and cymelarsan $EC_{50}$ values that were not significantly different from the *tbaqp2/tbaqp3* null controls but highly significantly different from the TbAQP2WT drug-sensitive controls, showing that their capacity for pentamidine and cymelarsan uptake had been reduced to zero (Fig. 1A, D-F).

We conclude that the unique TbAQP2 replacement of the NPA/NPA motif and all of the WGYR selectivity filter mutations are necessary for the observed pentamidine and melaminophenyl arsenical sensitivity observed in cells expressing wild-type TbAQP2.

*1.3 Introduction of TbAQP2 selectivity filter residues into the AQP3 pore enables pentamidine transport*

An interesting question was whether the introduction of (some of) the critical TbAQP2 residues in TbAQP3 might give the latter the capacity to take up pentamidine. We therefore constructed $TbAQP3^{W102I/R256L}$ and $TbAQP3^{W102I/R256L/Y250L}$ and tested whether *tbaqp2/tbaqp3* null cells transfected with these mutant aquaporins were able to take up 25 nM [$^3$H]-pentamidine in the presence of 1 mM adenosine (which blocks uptake via TbAT1/P2). Pentamidine uptake in the tested cell lines was very low compared to the same cells expressing TbAQP2WT (Fig. 1G). However, by measuring [$^3$H]-pentamidine uptake over 30 min it was possible to reliably and reproducibly measure radiolabel accumulation in each cell line. This showed that while uptake in $TbAQP3^{W102I/R256L}$ only trended slightly upwards

188 (P>0.05), the mutant AQP3 with all three AQP2 WGYR residues (W102I, R256L and
189 Y250L) accumulated significantly more [$^3$H]-pentamidine than the *tbaqp2/tbaqp3* null cells
190 (P<0.01) or the null cells expressing TbAQP3WT (P=0.011). This is further corroborated by
191 comparing the pentamidine sensitivity profile of these cell lines: only TbAQP3$^{W102I/R256L/Y250L}$
192 conveyed significant sensitisation to *tbaqp2/tbaqp3* null cells (P<0.0001; Fig. 1H). Thus,
193 TbAQP3 is converted into a pentamidine transporter by the insertion of the AQP2 WGYR
194 residues, although this does not convey as high a rate of pentamidine uptake as TbAQP2.
195
196 *1.4 Mutations of amino acids modelled to potentially bind pentamidine or melarsoprol*
197 *dramatically reduce pentamidine transport*
198 Our previous attempts at modelling the binding of pentamidine and melarsoprol into
199 the pore of TbAQP2 tentatively identified several residues that could be involved in this
200 process (Munday *et al,* 2015a), from which we selected two residues, Ile190 and Trp192, at
201 the extracellular end of the channel (position shown in Fig. 6), to swap with the
202 corresponding residues of TbAQP3, creating TbAQP2$^{I190T}$ and TbAQP2$^{W192G}$. Both residues
203 were predicted to interact with the substrate(s) via main-chain carbonyl oxygen atoms, but the
204 side chains could nonetheless affect the interactions.
205 TbAQP2$^{I190T}$ displayed dramatically reduced [$^3$H]-pentamidine uptake, at 2.7 ± 0.7%
206 (P<0.01, *n*=4) of the TbAQP2WT control, although significantly higher than the rate of the
207 *tbaqp2/tbaqp3* null negative control (P<0.05) (Fig. 2A). The reduced rate was the result of a
208 reduced $V_{max}$ of the high affinity [$^3$H]-pentamidine uptake, rather than a change in Km; the
209 LAPT1 $V_{max}$ and $K_m$ were unchanged in cells expressing TbAQP2$^{I190T}$ or TbAQP2WT
210 (Supplemental Fig. S2). TbAQP2$^{I190T}$ still conferred some increased pentamidine sensitivity
211 in the standard resazurin test (P<0.0001), although highly significantly less sensitizing than
212 TbAQP2WT (P<0.001); an intermediate sensitivity was also observed for cymelarsan (Fig.

2B). Substitution W192G also produced intermediate sensitivity to both drugs (Fig. 2C) but the double substitution TbAQP2$^{I190T/W192G}$ displayed no significant pentamidine uptake above *tbaqp2/tbaqp3* null (Fig. 3A) and did not sensitise to pentamidine or cymelarsan (Fig. 2D).

*1.5. The effect of large amino acids at the cytoplasmic end of the pore.*

To test whether restrictions at the cytoplasmic end of TbAQP2 would impact on pentamidine transport, we selected three leucine residues and exchanged each with tryptophan, creating L84W, L118W and L218W (positions indicated in Fig. 6). Expressing each of the L-to-W mutants in *tbaqp2/tbaqp3* null cells revealed significantly reduced pentamidine sensitivity compared to the same cells expressing TbAQP2WT (Fig. 3A), while also exhibiting dramatically reduced rates of [$^3$H]-pentamidine transport (Fig. 3B). This effect was additive, with TbAQP2$^{L84W/L118W}$ not significantly sensitising for pentamidine and displaying no detectable increase in [$^3$H]-pentamidine transport relative to *tbaqp2/tbaqp3* null cells (Fig. 3A,B). None of these L-to-W mutants sensitised the cells to cymelarsan, diminazene or PAO (Supplemental Fig. S3). When the same leucine residues were replaced with methionine instead of tryptophan, variants L84M and L218M were not or barely different from TbAQP2WT with respect to pentamidine sensitisation (Fig. 3A) or transport (but highly significantly different from their respective tryptophan variants). For position 118 the Met replacement had similar effects as the Trp variant had, albeit with a significantly higher rate of pentamidine transport (1.88 ± 0.20 ($n$=6) *versus* 9.38 ± 0.63% ($n$=3) of TbAQP2WT, P<0.001; Fig. 3A,B). The L84M and L218M mutants also sensitised to cymelarsan (P<0.01) and, surprisingly, the L218 W and M mutants also sensitised slightly to diminazene (~2-fold, P<0.05) (Supplemental Fig. S3).

These results strongly argue that the introduction of large amino acids at the cytosolic end significantly blocks the transport of pentamidine, whereas the change to Leu→Met

mutants were more permissive for pentamidine, but not cymelarsan. In order to check whether these variants were still functional aquaglyceroporins, we used the observation of Jeacock *et al,* (2017) that *T. brucei* cells lacking all three AQPs are sensitised to the Trypanosome Alternative Oxidase inhibitor SHAM, as a result of cellular glycerol accumulation. By this measure, all of the position 84, 118 and 218 Trp and Met mutants were able to transport glycerol, as each displayed SHAM $EC_{50}$ values significantly different from the *tbaqp1-2-3* null cells (Fig. 3C,D); several variants displayed an intermediate SHAM $EC_{50}$, being also significantly different from TbAQP2WT, indicating some attenuation of glycerol efflux capacity for those mutants. Indeed, uptake of [$^3$H]-glycerol closely mirrored the SHAM observations (Fig. 3E).

*1.6. Overall correlation between [$^3$H]-pentamidine transport rate and pentamidine $EC_{50}$*

The results presented in Figures 2-4 consistently show that even TbAQP2 mutants that display a large reduction in [$^3$H]-pentamidine uptake rate results can show intermediate pentamidine sensitivity phenotypes ($EC_{50}$s), due to the nature of the standard drug sensitivity test employed, which involves a 48-h incubation with the drug prior to a further 24-h incubation with resazurin: even a much-reduced transport rate will be sufficient to accumulate significant amounts of intracellular pentamidine over 3 days. A plot of [$^3$H]-pentamidine transport rates versus pentamidine $EC_{50}$, using the data for all 19 TbAQP2 and TbAQP3 mutants for which the transport rates were determined, shows that relatively small changes in $EC_{50}$ occur, even with up to approximately 95% reduction in transport rates; at >95% reduction large $EC_{50}$ increases become apparent (Supplemental Fig. S4).

*2. Partially blocking endocytosis does not alter the rate of pentamidine transport*

The knockdown of the CRK12 kinase in *T. brucei* causes a highly reproducible defect in endocytosis that affects an estimated one third of cells 12 h after RNAi induction and is ultimately lethal (Monnerat *et al,* 2013). We utilized this system to investigate whether a link between endocytosis and pentamidine transport exists. At 12 h of CRK12 RNAi induction with tetracycline, CRK12 mRNA levels were reduced by 42% ($P<0.001$) relative to uninduced controls as determined by qRT-PCR (Fig. 4A). Samples from the culture taken at this time point showed an increased abundance of cells with swelling characteristic of endocytosis defects, although this was hard to quantify as a minority of cells were affected, and to various degrees, as the 12 h time point was deliberately taken as an early point that would not yet affect cell viability (Supplemental Fig. S5) or cause excessive cellular pathology. We thus performed parallel uptake experiments with [$^3$H]-pentamidine and [$^3$H]-suramin, with suramin acting as positive control as it is known to enter *T. brucei* bloodstream forms through endocytosis after binding to surface protein ISG75 (Zoltner *et al,* 2016). After 12 h of CRK12 RNAi induction, pentamidine uptake was not significantly less than in the *T. brucei* 2T1 parental cells, whereas uptake of [$^3$H]-suramin was ($P=0.019$, $n=5$; Fig. 4B,C).

*3. The protonmotive force drives AQP2-mediated pentamidine uptake in bloodstream forms of T. brucei*

It has been reported that knock-down of the HA1–3 plasma membrane proton pumps of *T. brucei* (which are essential for maintaining the plasma membrane potential), confers pentamidine resistance (Alsford *et al,* 2012; Baker *et al,* 2013). Interestingly, this locus only conferred resistance to (dicationic) pentamidine, not to the (neutral) melaminophenyl arsenicals, unlike knockdown of the TbAQP2/TbAQP3 locus (Alsford *et al,* 2012). We have previously reported that the HAPT-mediated pentamidine uptake in *T. brucei* procyclics correlates strongly with the proton-motive force (PMF) (De Koning, 2001a). However, it is

not clear whether this dependency indicates that pentamidine uptake is mediated by a proton symporter, as known for many *T. brucei* nutrient transporters (De Koning & Jarvis, 1997a,b, 1998; De Koning *et al,* 1998), or reflects the energetics of uptake of cationic pentamidine being driven by the strong inside-negative membrane potential $V_m$. The absence of an effect of HA1–3 knockdown on sensitivity to the neutral melaminophenyl arsenicals strongly argues against a mechanism of proton symport for HAPT1/AQP2 but a (partial) dependency of HAPT1/AQP2-mediated uptake of dicationic pentamidine on PMF or $V_m$ would be expected if the substrate traverses the channel, as opposed to binding a single Asp residue on the extracellular side of the protein, as suggested in the endocytosis model (Song *et al,* 2016). Here we show that the same ionophores that inhibit HAPT1-mediated pentamidine transport in procyclic cells, and inhibit hypoxanthine uptake in both bloodstream form (BSF) (De Koning & Jarvis, 1997b) and procyclic (De Koning & Jarvis, 1997a) *T. brucei*, also dose-dependently inhibit [$^3$H]-pentamidine uptake in BSF (Fig. 5A). This confirms that pentamidine needs the membrane potential for rapid uptake, as predicted by the dependence on the HA1–3 proton pumps. Using [$^3$H]-suramin as an endocytosed substrate (Zoltner *et al,* 2016), we found that 20 μM CCCP also inhibits endocytosis in *T. brucei*, by 32.6% (P=0.029; pre-incubation 3 min, plus suramin accumulation over 10 minutes) (Fig. 5B). While that means that the ionophore experiments do not perfectly discriminate between endocytosis and trans-channel transport for di-cationic pentamidine, they do for neutral melaminophenyl arsenicals: the non-dependence of these neutral TbAQP2 substrates on the proton gradient (Alsford *et al,* 2012) indicates that, unlike suramin, they are not endocytosed.

Although there is a good correlation between the proton-motive force and TbAQP2-mediated pentamidine transport (Fig. 5C), the effect of CCCP was stronger than expected, and stronger than previously observed for [$^3$H]-hypoxanthine uptake in *T. brucei* bloodstream forms (De Koning & Jarvis 1997b) and we thus investigated whether CCCP might have a

direct effect on TbAQP2. Indeed, CCCP inhibited uptake of (neutral) [$^3$H]-glycerol in *tbaqp1-2-3* null cells expressing TbAQP2-WT, with an $IC_{50}$ of 20.7 ± 2.6 µM (n=3) and inhibited [$^3$H]-pentamidine uptake in the same cells with a similar $IC_{50}$ (Fig. 5D,E), showing CCCP to inhibit TbAQP2 directly, irrespective of effects on the membrane potential.

*4. Molecular dynamics modelling of pentamidine interactions with TbAQP2*

To further investigate pentamidine binding and permeation in TbAQP2, we used the coordinates of the TbAQP2-pentamidine complex that was modelled in our previous study (Munday *et al,* 2015a). The stability of the protein model was first confirmed by unbiased atomistic molecular dynamics simulations (Supplemental Fig. S6). We then conducted force-probe simulations, in which a moving spring potential was used to enforce unbinding of pentamidine from its docked binding position and subsequently reconstructed the free-energy profile of pentamidine association-dissociation along the pore axis by employing Jarzynski's equality (Park *et al,* 2003).

Figure 6 shows that the docked position of pentamidine correctly identified its minimum free-energy binding site inside the TbAQP2 pore. Pentamidine adopts an extended state inside the TbAQP2 pore, adapting its molecular shape to the narrow permeation channel; pentamidine binding poses display inter-amidine lengths in the range 16.5 – 17 Å. Importantly, our steered simulations reveal that pentamidine can exit the channel in either direction, and that unbinding on the route towards the cytoplasm occurs on a free-energy surface roughly symmetric to that towards the extracellular side. Apart from overcoming the strongly attractive binding interaction in the centre, there are no major further free-energy barriers in either direction. The computed free-energy profile of pentamidine binding to the TbAQP2 structural model slightly overestimates its experimentally recorded binding affinity. However, the pentamidine conformation binding the narrow pore may not be the lowest-

energy internal conformation of the small molecule, a factor that may be underrepresented in the profile as simulations were started from the protein-bound state. A further source of uncertainty stems from the protein model, which is expected to be somewhat less accurate than a crystal structure.

Due to the dicationic character of pentamidine, the free-energy profile of the molecule within TbAQP2 strongly depends on the membrane voltage. The voltage drop of -125 mV across the cytoplasmic membrane of *T. b. brucei* (De Koning & Jarvis, 1997b), with a negative potential inside the cell, results in an overall inward attraction of ~22 kJ/mol (Fig. 6, arrow), i.e. exit from TbAQP2 into the cytoplasm is substantially more favourable for pentamidine than towards the extracellular side. Taken together, the free-energy profile under membrane voltage explains the strong coupling between pentamidine uptake and $V_m$ observed in the experiments. The high affinity of the binding interaction leads to slow off-rates and a relatively low $V_{max}$ ($0.0044 \pm 0.0004$ pmol$(10^7$ cells$)^{-1}s^{-1}$) (De Koning, 2001a).

*5. SAR of the pentamidine-AQP2 interaction*

In order to study substrate binding and selectivity by the *T. b. brucei* High Affinity Pentamidine Transporter (HAPT1/TbAQP2), competition assays were performed with a series of pentamidine analogues and other potential inhibitors, in the presence of 1 mM unlabelled adenosine to block diamidine uptake by the TbAT1 aminopurine transporter (De Koning, 2001a; Bridges *et al,* 2007). High specific activity [$^3$H]-pentamidine was used at 30 nM, below the $K_m$ value (De Koning, 2001a). Uptake was linear for at least 3 min (De Koning, 2001a) and we utilized 60 s incubations for the determination of inhibition constants ($K_i$). At 30 nM [$^3$H]-pentamidine there is virtually no uptake through LAPT1 (Bridges *et al,* 2007) ($K_m$ value ~1000-fold higher than HAPT1) (De Koning, 2001a). The full dataset of 71 compounds is presented in Supplemental Table S1, featuring $K_i$s spanning 5 log units.

362

363 *5.1. The linker length and composition is a strong determinant for high affinity binding of*
364 *pentamidine*

365 We determined the $K_i$ values for analogues with a 2–8 methylene unit linker (Fig. 7A, Table
366 1). Pentamidine analogues featuring 5-7 units displayed submicromolar binding affinities (5
367 > 6 > 7), while fewer (3-4) or more (8) only conveyed low micromolar binding affinity,
368 equivalent to a decrease in Gibbs free energy of binding ($\Delta G^0$) from 10.2 to 13.0 kJ/mol
369 (Table 1). Energy minimalization using Gaussian16 yielded an elongated conformation for
370 pentamidine, with an inter-amidine length of 17.8 Å (Fig. 7B). Replacement of the ether
371 oxygens with S or NH, analogues RT-48 and RT-50, respectively (Table 1) resulted in
372 $\delta(\Delta G^0)$ of 10.0 and 12.9 kJ/mol, respectively, indicating that the ether oxygens potentially act
373 as H-bond acceptors: the NH group serves only as an H-bond donor, as its lone pair is
374 conjugated with the aromatic system, and the sulphur mimics an aromatic NH (Beno *et al,*
375 2015). The sulfone analogue (RT-49), which introduces a dihedral angle of 180° between the
376 benzamidine and the linker (Brameld *et al,* 2008), displayed no binding affinity. We propose
377 that a near-planar conformation of the Phe-O-$CH_2$ segment is required for efficient
378 engagement of the binding site. This is supported by examining the binding affinities found
379 for the analogous benzofuramidine series (e.g. RT-14, Fig. 7B), which has a conformationally
380 predefined ether-methylene bond orientation. Replacement of the middle methylene unit of
381 pentamidine with an isosteric oxygen (ethylene glycol derivative DB1699, Table 1) results in
382 a less flexible linker and a remarkable drop in binding affinity ($\delta(\Delta G^0)$ = 15.3 kJ/mol).

383

384 *5.2. Two amidine groups are required for high affinity binding*

385 Matched-molecular pair analysis of non-symmetric analogues identified that both amidines
386 contribute to high affinity binding (compare pairs pentamidine/RT-36 and

pentamidine/CHI/1/72/1; Table 1). Removal of an H-bond donor (as in CHI/1/72/1) leads to a loss in $\Delta G^0$ >10 kJ/mol. The aniline derivative RT-36 can still act as an H-bond donor, albeit with significantly reduced basicity (and thus H-bond acceptor propensity), and accordingly displayed intermediate affinity ($\delta(\Delta G^0)$ = 6.2 kJ/mol). Interestingly, the removal of one amidine (compare butamidine and CHI/1/69/1) did not produce a significant effect on the binding affinity ($K_i$ = 3.87 μM and $K_i$ = 2.33 μM, respectively), indicating that the low affinity of butamidine (compare 36 nM for pentamidine) is due to an inability to attain a productive interaction with the second amidine. Capping of the amidine group, resulting in imidazoline analogue RT-32, or methylation (analogue RT-30) reduced binding to HAPT1, probably due to increased steric crowding at the interaction site, impairing H-bonding. Reducing pentamidine to just 4-hydroxybenzamidine removed essentially all affinity ($K_i$ = 2.9 mM; $\delta(\Delta G^0)$ = 28.1 kJ/mol), and the replacement of one amidine with a carboxylic group (compare propamidine, RT-38) was highly deleterious for engagement with the binding site. Finally, the orientation of the amidine group is crucial as shown by a *meta* to *para* change on the phenyl ring (*meta*-pentamidine, Table 1). We conclude that for high affinity both amidine groups must be able to interact unimpeded with the transporter, and in the linear (*para*) conformation.

*5.3. Fully conjugated linking units*

Stilbamidine and the short-linker analogues FR39 and CRMI8 (Ríos Martínez *et al,* 2015) displayed low binding affinity (Table 1). Diminazene also displayed similar low affinity ($K_i$ = 63 μM), and [$^3$H]-diminazene uptake can only just be detected in procyclic *T. b. brucei*, *i.e.* in the absence of the TbAT1/P2 transporter (Teka *et al,* 2011), potentially indicating a minimal uptake via HAPT1. Stilbamidine and diminazene feature a similar inter-amidine distance, much shorter than pentamidine (12.35 and 12.25 Å, respectively). DB75

(furamidine) likewise displayed low affinity (Table 2) and is only internalised by TbAT1/P2 (Ward *et al,* 2011). The 2,5-furan linker imposes a fixed, inflexible angle of 136º on the benzamidine moieties and the phenyl rings will adopt a planar orientation with respect to the furan plane. This appears to allow only one benzamidine end to interact with the transporter, as (unlike the flexible linker of aliphatic diamidines, *vide supra*) the replacement of one amidine group actually increases the binding affinity, presumably by allowing an improved bonding orientation of the remaining amidine. Thus, DB607 (methoxy for amidine) and DB960 (*N*-methyl benzimidazole for benzamidine) display a somewhat higher affinity than DB75, although the fixed angle was unchanged. Introduction of a pyridine-N in the *ortho*-position with respect to the amidine functionality (DB994), dramatically reduces the $pK_a$ of the amidine moiety (Wang *et al,* 2010), resulting in a complete loss of binding affinity ($K_i$ = 167 ± 20 μM), while this was not observed for the corresponding *meta*-pyridine derivative (DB829). The unfavourable furan bond angle is further demonstrated by the distally elongated analogues DB1061 and DB1062 that approximate the inter-amidine distance of pentamidine but showed no improvement in binding affinity (Table 2). Replacement of furan with thiazole (ER1004) or methylpyrrole (DB320), which feature a similar bond angle, also revealed comparable binding affinities. In contrast, a 2,5-substituted thiophene (DB686 and DB1063) or 2,5-substituted selenophene (DB1213) as a bio-isosteric replacement for the furan linker resulted in significantly higher binding affinities when compared to their matched pair analogue (DB1063/DB1061 and DB1213/DB75), which we attribute to a larger benzamidine-benzamidine angle. This is corroborated by the much weaker binding of the 2,4-thiophene derivative DB1077. A terminal amidine cap (imidazoline) reduced affinity as it did for pentamidine (compare DB1061/DB1062 and DB1063/DB1064 (Table 2)). A difuran spacer (DB914) resulted in a high affinity binder ($K_i$ = 0.073 μM) because the two furans orient themselves in a *trans* conformation, resulting in a near-linear molecule.

437

438 *5.4. Modifications to the phenyl rings of pentamidine*

439 Substituents in the *ortho*-position (relative to the alkyloxy substituent) of pentamidine were
440 poorly tolerated, including chloride or iodide (RT-43, iodopentamidine; Table 1); the amide
441 analogue displayed no affinity at all (RT-46). Such substituents will cause an out-of-plane
442 conformation of the alkoxy-group to avoid clashing with the *ortho*-substituent; high-affinity
443 pentamidine binding appears to require a coplanar arrangement of the first methylene bound
444 to the oxygen. Similarly, the introduction of an *ortho*-pyridine N (RT-52) led to a $\delta(\Delta G^0)$ of
445 13.7 kJ/mol. This derivative exhibits a conformational bias towards an *anti*-orientation of the
446 ether oxygen and pyridine nitrogen (Fig. 7C) (Chein & Corey, 2010). The regio-isomeric
447 *meta*-pyridine (RT-53) was completely inactive, reflecting the need for a positively charged
448 amidine, as this analogue has a significantly reduced pKa (Wang *et al,* 2010) (see furan-
449 spaced analogue DB994, *supra*).

450

451 *5.5. Non-diamidine trypanocides*

452 The important veterinary trypanocide isometamidium, a hybrid of the phenanthridine
453 ethidium and the diamidine diminazene, inhibited HAPT1-mediated [$^3$H]-pentamidine uptake
454 with a $K_i$ of only 3.5 μM (Supplemental Table S1), most probably through an interaction with
455 its benzamidine moiety, as ethidium displayed virtually no affinity ($K_i$ = 97 μM). However,
456 we found no evidence that HAPT1/AQP2 is able to transport the bulky isometamidium
457 molecule. For instance, the 2T1, *tbaqp2* null, TbAQP2 expressed in *tbaqp2* null, and the
458 *tbaqp2/tbaqp3* null strains displayed statistically identical $EC_{50}$ values for isometamidium
459 (112 ± 12 nM, 103 ± 14 nM, 98 ± 24 nM and 95 ± 12 nM, respectively; P>0.05, Student's
460 unpaired t-test), and the $EC_{50}$ values for ethidium were also identical for each of these strains
461 (1.32 ± 0.07 μM, 1.39 ± 0.08 μM, 1.35 ± 0.11 μM and 1.38 ± 0.14 μM, respectively). It is

462 thus likely that isometamidium acts as an extracellular inhibitor rather than a substrate for
463 HAPT/AQP2, as it does for the TbAT1/P2 transporter (De Koning, 2001b). The nitro-
464 heterocyclic trypanocide megazol (Carvalho *et al,* 2014), curcumin and its trypanocidal
465 analogue AS-HK14 (Alkhaldi *et al,* 2015) failed to inhibit HAPT1. Two trypanocidal bis-
466 phosphonium compounds, CD38 (Taladriz *et al,* 2012) and AHI43 (Alkhaldi *et al,* 2016) did
467 inhibit pentamidine uptake ($K_i$ 5-10 µM), whereas two related compounds, CDIV31 and
468 AHI15 (Taladriz *et al,* 2012), did not. Phloretin, which inhibits human AQP9 and AQP3
469 (Geng *et al,* 2017),[47] displayed a $K_i$ of 1.76 µM for HAPT1/TbAQP2.
470
471 *5.6. Are all the HAPT1/AQP2 inhibitors transported?*
472 In an uptake-by-endocytosis model it would be expected that TbAQP2 binding energy
473 correlates well with TbAQP2-mediated uptake rates for each analogue. We were unable to
474 ascertain the existence of such a correlation directly, for lack of radiolabelled substrates other
475 than pentamidine and diminazene and thus used the Resistance Factor (RF; $EC_{50}$(aqp2/3
476 null)/$EC_{50}$(TbAQP2-WT)) as a proxy: clearly, a compound with a significant RF is
477 internalized by TbAQP2. We observed a poor correlation between HAPT1 binding affinity
478 and the level of resistance in the *tbaqp2/tbaqp3* null strain ($r^2$=0.039, Supplemental Fig. S7;
479 n=30), with many inhibitors, even those with high affinity, not displaying any significant
480 resistance in the null line. This indicates that many of these inhibitors inhibit
481 HAPT1/TbAQP2 but are not transported by it. This is not compatible with a model in which
482 pentamidine binds and is then internalized by endocytosis: the inhibitors do not show
483 resistance in the *tbaqp2/tbaqp3* null line, whereas substrates do. The caveat inherent to using
484 the RF instead of rate of transport is that it cannot be excluded that some of the test
485 compounds are AQP2 substrates yet predominantly taken up by transporters other than
486 TbAQP2, and hence show a low RF.

487

488 *5.7. SAR summary*

489 Figure 7D summarises the structure-activity relationship of pentamidine interactions with
490 HAPT1/TbAQP2. No modification in any part of the molecule improved affinity for
491 TbAQP2, but virtually every modification resulted in a significant loss of binding activity.
492 The results clearly demonstrate that at least both amidine groups and one or both ether
493 oxygens are involved in interactions with AQP2, the sum of which adds up to the unusually
494 high binding energy for this substrate-transporter pair ($\Delta G^0$ = -42.6 kJ/mol). These results,
495 unambiguously demonstrating pentamidine binding in an elongated orientation, are in
496 complete agreement with the modelling and molecular dynamics, and the mutational analysis
497 presented above, strengthening those conclusions using a completely different approach.

498

## Discussion and conclusion

There is overwhelming consensus that expression of TbAQP2 is associated with the extraordinary sensitivity of *T. brucei* to pentamidine and melaminophenyl arsenicals, and that mutations and deletions in this locus cause resistance (Baker *et al,* 2012, 2013; Graf *et al,* 2013, 2015, 2016; Pyana Pati *et al,* 2014; Munday *et al,* 2014, 2015a; Unciti-Broceta *et al,* 2015). What has remained however unclear is the mechanism underpinning these phenomena – there are currently no documented other examples of aquaporins transporting such large molecules.. Yet, considering how ubiquitous aquaporins are to almost all cell types, this question is of wide pharmacological importance: if large cationic and neutral drugs (pentamidine and melarsoprol, respectively) can be taken up via an aquaglyceroporin of *T. brucei*, what other pharmacological or toxicological roles may these channels be capable of in other cell types? This manuscript shows clearly that changes in the TbAQP2 WGYR and NPA/NPA motifs, which collectively enlarge the pore and remove the cation filter, allow the passage of these drugs into the cell, and thereby underpin the very high sensitivity of the parasite to these drugs.

TbAQP2 has evolved, apparently by positive selection given the high dN/dS ratio, to remove all main constriction points, including the aromatic amino acids and the cationic arginine of the selectivity filter, and the NPA/NPA motif, resulting in an unprecedentedly enlarged pore size. Whereas the advantage of this to *T. b. brucei* is yet unknown, the adaptation is stable within the *brucei* group of trypanosomes, and found in *T. b. rhodesiense* (Munday *et al,* 2014; Graf *et al,* 2016), *T. b. gambiense* (Graf *et al,* 2013, 2015; Munday *et al,* 2014; Pyana Pati *et al,* 2014), *T. equiperdum* and *T. evansi* (Philippe Büscher and Nick Van Reet, unpublished). As such, it is not inappropriate to speculate that the wider pore of TbAQP2 (i) allows the passage of something not transported by TbAQP1 and TbAQP3; (ii)

that this confers an a yet unknown advantage to the cell; and (iii) that uptake of pentamidine is a by-product of this adaptation.

It is difficult to reconcile the literature on pentamidine transport/resistance with uptake via endocytosis. For instance, the rate of endocytosis in bloodstream trypanosomes is much higher than in the procyclic lifecycle forms (Langreth & Balber, 1975; Zoltner *et al,* 2016), yet the rate of HAPT-mediated [$^3$H]-pentamidine uptake in procyclics is ~10-fold higher than in bloodstream forms (De Koning, 2001a; Teka *et al,* 2011), despite the level of TbAQP2 expression being similar in both cases (Siegel *et al,* 2010; Jensen *et al,* 2014). Moreover, in procyclic cells TbAQP2 is spread out over the cell surface (Baker *et al,* 2012) but endocytosis happens exclusively in the flagellar pocket (Field & Carrington, 2009) (which is 3-fold smaller in procyclic than in bloodstream forms (Demmel *et al,* 2014)), as the pellicular microtubule networks below the plasma membrane prevent endocytosis (Zoltner *et al,* 2016). Similarly, the expression of TbAQP2 in *Leishmania mexicana* promastigotes produced a rate of [$^3$H]-pentamidine uptake more than 10-fold higher than observed in *T. brucei* BSF (Munday *et al,* 2014), despite these cells also having a low endocytosis rate (Langreth & Balber, 1975). The $K_m$ and inhibitor profile of the TbAQP2-mediated pentamidine transport in these promastigotes was indistinguishable from HAPT in procyclic or bloodstream form *T. brucei* (De Koning, 2001a). Moreover, the experimental $V_{max}$ for HAPT-mediated pentamidine uptake in *T. brucei* BSF and procyclics (Baker *et al,* 2013) can be expressed as $9.5\times10^5$ and $8.5\times10^6$ molecules/cell/h, respectively; given a 1:1 stoichiometry for AQP2:pentamidine the endocytosis model would require the internalisation and recycling of as many units of TbAQP2 and this seems unlikely, especially in procyclic cells. These observations are all inconsistent with the contention that pentamidine uptake by trypanosomes is dependent on endocytosis.

548 Furthermore, the Gibbs free energy of -42 kJ/mol for the pentamidine/AQP2
549 interaction (De Koning, 2001a; Zoltner *et al,* 2016) is highly unlikely to be the result of the
550 one interaction between one terminal amidine and Asp265 as required in the endocytosis
551 model (Song *et al,* 2016). For the TbAT1 transporter, a double H-bond interaction of Asp140
552 with the N1(H)/C(6)$NH_2$ motif of adenosine or with one amidine of pentamidine (Munday *et*
553 *al,* 2015b) is estimated to contribute only ~16 kJ/mol to the total $\Delta G^0$ of -34.5 kJ/mol for
554 adenosine (-36.7 kJ/mol, pentamidine) (De Koning & Jarvis, 1999). The endocytosis model
555 also does not address the internalisation of melaminophenyl arsenicals, which presumably
556 would equally need access to Asp265.

557 Here we systematically mapped the interactions between the aquaporin and
558 pentamidine ($\Delta G^0$ for 71 compounds), yielding a completely consistent SAR with multiple
559 substrate-transporter interactions, summarised in Fig. 7D. The evidence overwhelmingly
560 supports the notion that pentamidine engages TbAQP2 with both benzamidine groups and
561 most probably with at least one of the linker oxygens, and that its flexibility and small width
562 are both required to optimally interact with the protein. This is completely corroborated by
563 molecular dynamics modelling, which shows minimal energy to be associated with a near-
564 elongated pentamidine centrally in the TbAQP2 pore, without major energy barriers to
565 exiting in either direction, but driven to the cytoplasmic side by the membrane potential. This
566 contrasts with the contention (Song *et al,* 2016) that pentamidine could not be a permeant for
567 TbAQP2 because it did not transport some small cations and that this proves that the larger
568 pentamidine cannot be a substrate either. There is scant rationale for that assertion: out of
569 many possible examples: there are 5 orders of magnitude difference in affinity for
570 pentamidine and *para*-hydroxybenzamidine (35 nM *vs* 2.9 mM; Supplemental Table S1);
571 adenine is not a substrate for the *T. brucei* P1 adenosine transporter (De Koning & Jarvis,
572 1999), the SLC1A4 and SLC1A5 neutral amino acid transporters transport Ala, Ser, Cys and

573 Thr but not Gly (Kania *et al,* 2013), and $Na^+$ is not a permeant of $K^+$ channels (Zhorov &
574 Tikhonov, 2013).

575 The endocytosis model identifies only two key residues for pentamidine access
576 (Leu264) and binding (Asp265) in TbAQP2 (Song *et al,* 2016). Yet, multiple clinical isolates
577 and laboratory strains contain chimeric AQP2/3 genes associated with resistance and/or non-
578 cure that have retained those residues and should thus allow binding and internalisation of
579 pentamidine (Graf *et al,* 2013; Pyana Pati, 2014; Unciti Broceta *et al,* 2015; Munday *et al,*
580 2014). Although we find that introduction of the AQP3 Arg residue in position 264
581 ($TbAQP2^{L264R}$) disables pentamidine transport, this is because the positively charged
582 arginine, in the middle of the pore, is blocking the traversing of all cations through the pore,
583 as is its common function in aquaporins (Beitz *et al,* 2006; Wu *et al,* 2009). Indeed, the
584 W(G)YR filter residues appear to be key determinants for pentamidine transport by AQPs
585 and the introduction of all three TbAQP2 residues into TbAQP3 ($AQP3^{W102I/R256L/Y250L}$) was
586 required to create an AQP3 that at least mildly sensitised to pentamidine, and facilitated a
587 detectable level of pentamidine uptake. Conversely, any one of the mutations I110W, L258Y
588 or L264R was sufficient to all but abolish pentamidine transport by TbAQP2. Similarly, the
589 conserved NPA/NPA motif, and particularly the Asp residues, present in TbAQP3 but
590 NSA/NPS in TbAQP2, is also associated with blocking the passage of cations (Wree *et al,*
591 2011). The unique serine residues in this TbAQP2 motif, halfway down the pore, might be
592 able to make hydrogen bonds with pentamidine. Reinstating the NPA/NPA motif resulted in a
593 TbAQP2 variant with a 93.5% reduced rate of [$^3$H]-pentamidine transport.

594 Tryptophan residues were introduced towards the cytoplasmic end of the TbAQP2
595 pore (L84W, L118W, L218W) to test the hypothesis that introducing bulky amino acids in
596 that position would block the passage of pentamidine. Each of these mutants was associated
597 with reduced sensitivity to pentamidine and cymelarsan and a >90% reduction in [$^3$H]-

598 pentamidine uptake. This effect was size-dependent as the pentamidine transport rate of
599 L84M and L218M was statistically identical to that of control TbAQP2 cells, and L118M
600 also displayed a higher transport rate than L118W ($P<0.0001$). These mutant AQPs were still
601 functional aquaglyceroporins as their expression in *tbaqp1-2-3* null cells made those cells less
602 sensitive to the TAO inhibitor SHAM, and increased glycerol uptake.

603 Independence from endocytosis was demonstrated by employing the tetracycline-
604 inducible CRK12 RNAi cell line previously described to give a highly reproducible and
605 progressive endocytosis defect in *T. brucei* (Monnerat *et al,* 2013), and unambiguously
606 distinguishes between uptake via endocytosis and transporters. Twelve hours after CRK12
607 RNAi induction pentamidine transport was not significantly reduced although uptake of [$^3$H]-
608 suramin, which is accumulated by endocytosis through the *T. brucei* flagellar pocket (Zoltner
609 *et al,* 2016), was reduced by 33% ($P=0.0027$), indicating successful timing of the experiment
610 to the early stage of endocytosis slow-down. Although several ionophores, including CCCP,
611 nigericin and gramicidin strongly inhibited pentamidine uptake, similar to what has been
612 previously reported for transport processes in *T. brucei* that are linked to the protonmotive
613 force (De Koning & Jarvis, 1997a,b, 1998; De Koning *et al,* 1998), this is probably due to the
614 inside-negative membrane potential of -125 mV (De Koning & Jarvis, 1997b) attracting the
615 dicationic pentamidine. This is consistent with the prediction of the molecular dynamics
616 modelling, and the reported role of the HA1–3 proton pumps in pentamidine but not
617 melarsoprol resistance (Alsford *et al,* 2012; Baker *et al,* 2013).

618 Altogether, we conclude that the primary entry of the sleeping sickness drugs
619 pentamidine and melarsoprol into *T. brucei* spp. is through the unusually large pore of
620 TbAQP2, rendering the parasite extraordinarily sensitive to the drugs (compare *Leishmania*
621 *mexicana* (Munday *et al,* 2014)). This is the first report providing detailed mechanistic
622 evidence of the uptake of organic drugs (of MW 340 and 398, respectively) by an aquaporin.

623 We show that this porin has evolved through positive selection and identify the adaptations in
624 the constriction motifs that enabled it. We consider that other pore-opening adaptations may
625 have evolved in other organisms, including pathogens, which could initiate the
626 pharmacological exploitation of aquaporins and lead to the design of new drug delivery
627 strategies.
628
629

# Materials and Methods

*Trypanosome strains and cultures.*

The drug-sensitive clonal *T. b. brucei* strain 427 (MiTat 1.2/BS221) (De Koning *et al,* 2000) was used for all the work on the SAR of pentamidine transport. The *tbaqp2/tbaqp3* null cells (Baker *et al,* 2012) and *tbaqp1-2-3* null cells (Jeacock *et al,* 2017) (both obtained from David Horn, University of Dundee, UK) are derived from the 2T1 strain of *T. b. brucei* (Alsford & Horn, 2008). The *CRK12* RNAi cell line[28] was obtained from Dr Tansy Hammarton (University of Glasgow, UK) and is also based on the 2T1 cell line; RNAi expression was induced with 1 µg/ml tetracycline in the medium. All experiments were performed with bloodstream form trypanosomes grown *in vitro* in HMI-11 medium as described (Wallace *et al,* 2002) at 37 °C in a 5% $CO_2$ atmosphere. Cultures were routinely maintained in 10 ml of this medium, being seeded at $5\times10^4$ cells/ml and passed to fresh medium at reaching approximately $3\times10^6$ cells/ml after 48 h. For transport experiments 150 or 200 ml of culture was seeded at the same density in large flasks and incubated until the culture reached late-log phase.

*Materials*

A complete list of diamidine analogues and other chemicals used for the SAR study is given as a table in the supplemental materials with their sources (Supplemental Table S1). Ionophores and uncouplers nigericin, gramicidin, carbonyl cyanide m-chlorophenyl hydrazone (CCCP) and valinomycin, as well as the *T. brucei* proton pump inhibitor *N*-ethylmaleimide (NEM) were all purchased from Sigma-Aldrich. New compounds synthesised for this study are listed and described in the Supplemental Materials.

*Transport of [$^3$H]-pentamidine* - Transport of [$^3$H]-pentamidine was performed exactly as previously described for various permeants (Wallace *et al,* 2002; Bridges *et al,* 2007; Teka *et al,* 2011) in a defined assay buffer (AB; 33 mM HEPES, 98 mM NaCl, 4.6 mM KCl, 0.55 mM $CaCl_2$, 0.07 mM $MgSO_4$, 5.8 mM $NaH_2PO_4$, 0.3 mM $MgCl_2$, 23 mM $NaHCO_3$, 14 mM glucose, pH 7.3). [$^3$H]-pentamidine was custom-made by GE Healthcare Life Sciences (Cardiff, UK) with a specific activity of 88 Ci/mmol. Incubations of bloodstream form trypanosomes with 30 nM of this label (unless otherwise indicated) were performed in AB at room temperature for 60 s (unless otherwise indicated) and terminated by addition of 1 ml ice-cold 'stop' solution (1 mM unlabelled pentamidine (Sigma) in AB) and immediate centrifugation through oil (7:1 dibutylphthalate:mineral oil v/v (both from Sigma)). Transport was assessed in the presence of 1 mM adenosine to block uptake through the P2 aminopurine transporter; adenosine does not affect HAPT1-mediated transport (De Koning, 2001a; Bridges *et al,* 2007). Inhibition assays were performed routinely with 6 - 10 different concentrations of inhibitor over the relevant range, diluting stepwise by one third each time, in order to obtain a well-defined and accurate sigmoid plot and $IC_{50}$ value (inhibitor concentration giving 50% inhibition of pentamidine transport; calculated by non-linear regression using Prism 6.0 (GraphPad), using the equation for a sigmoid curve with variable slope). Highest concentration was usually 1 mM unless this was shown to be insufficient for good inhibition, or when limited by solubility. $K_i$ values were obtained from $IC_{50}$ values using

$$K_i = IC_{50}/[1 + (L + K_m)] \quad \text{(Eq. 1)}$$

in which L is the [$^3$H]-pentamidine concentration and $K_m$ the Michaelis-Menten constant for pentamidine uptake by HAPT1 (Wallace *et al,* 2002). The Gibbs Free energy of interaction $\Delta G^0$ was calculated from

$$\Delta G^0 = -RT\ln K_i \quad \text{(Eq. 2)}$$

680 in which R is the gas constant and T is the absolute temperature (Wallace *et al,* 2002).

681

682 *Construction of AQP mutants and transfection*

683 All mutations in the TbAQP2 and TbAQP3 genes were introduced to the relevant backbone
684 WT vector, either pRPa$^{GFP\text{-}AQP2}$ or pRPa$^{GFP\text{-}AQP3}$ (Baker *et al,* 2012), by site-directed
685 mutagenesis. For mutations S131P, S263A, I110W, L264R, L258Y, I190T and W192G in
686 AQP2, and W102I, R256L and Y250L in AQP3 mutations were inserted using the
687 QuikChange II kit (Agilent, Santa Clara, CA, USA), following the manufacturer's
688 instructions. For mutations L84W, L118W, L218W, L84M, L118M and L218M were
689 introduced using the Q5 Site-Directed Mutagenesis Kit (E0554S), (New England BioLabs)
690 according to manufacturer's instructions.

691 The following primer pairs (itemised in Supplemental Table S2) were used to insert
692 the named TbAQP2 mutations: for S131P, primers HDK1062 and HDK1063; in combination
693 with mutation S263A, using primers HDK1064 and HDK1065 to produce plasmid
694 pHDK166. For I110W, primers HDK607 and HDK608, to produce pHDK84; for L264R,
695 primers HDK609 and HDK610 to produce pHDK167; the combination I110W/L264R was
696 produced using primers HDK609 and HDK610 on plasmid pHDK84 to give plasmid
697 pHDK78; for L258Y, primers HDK1109 and HDK1110 to produce pHDK168; for I190T,
698 primers HDK1056 and HDK1057 to produce pHDK163; for W192G, primers HDK1058 and
699 HDK1059 to produce pHDK164; the combination I190T/W192G was produced using
700 primers HDK1060 and HDK1061 on plasmid pHDK163 to give plasmid pHDK165; for
701 L84W, primers HDK1276 and HDK1277, producing pHDK210; for L118W, primers
702 HDK1274 and HDK1275, producing pHDK208; for L218W, primers HDK1272 and
703 HDK1273, producing pHDK209; for the combination L84W/L118W, primers HDK1276 and
704 HDK1277 on template pHDK208, producing pHDK227; for L84M, primers HDK1364 and

HDK1367, producing pHDK234; for L118M, primers HDK1365 and HDK1367, producing pHDK235; and for L218M, primers HDK1366 and HDK1367, producing pHDK236. To insert the named mutations into TbAQP3, the following primers were used (Supplemental Table S3): for W102I, primers HDK511 and HDK512, in combination with mutation R256L, with primers HDK513 and HDK514, to produce plasmid pHDK71; and to add mutation Y250L to this combination, primers HDK795 and HDK796, to produce pHDK121. All plasmids were checked by Sanger Sequencing (Source BioScience, Nottingham, UK) for the presence of the correct mutation(s) and the cassette for integration digested out with *Asc*I (NEB, Hitchin, UK) prior to transfection.

For transfection, 10 µg of digested plasmid and 1-2×$10^7$ parasites of the desired cell line (either *aqp2/aqp3* null or *aqp1/aqp2/aqp3* null) were resuspended in transfection buffer and transfected using an Amaxa Nucleofector, with program X-001. After a recovery period (8-16 h) in HMI-11 at 37 °C and 5% $CO_2$, the parasites were cloned out by limiting dilution with the selection antibiotic (2.5 µg/ml hygromycin). In all cases the correct integration of the expression cassettes was analysed by PCR.

*Drug sensitivity assays*

Drug sensitivity assays for *T. b. brucei* bloodstream forms used the cell viability dye resazurin (Sigma) and were performed exactly as described (Wallace *et al,* 2002; Bridges *et al,* 2007) in 96-well plates with doubling dilutions of test compound, starting at 100 µM, over 2 rows of the plate (23 dilutions plus no-drug control). Incubation time with test compound was 48 h (37 ºC/5% $CO_2$), followed by an additional 24 h in the presence of the dye.

*Molecular dynamics*

Molecular dynamics simulations were performed using the GROMACS software package, version 5.1.1 (Abraham *et al,* 2015). We used the coordinates from the homology model of TbAQP2 published in Figure 2A in Munday et al (2015a), which was inserted into POPC/POPE (4:1) membranes, approximately reflecting the membrane composition of *T. b. brucei* (Smith & Bütikofer, 2010). The membrane models were constructed using the CHARMM-GUI webserver (Jo *et al,* 2008). Subsequently, extended stability tests of the modelled structure and the bound pentamidine were carried out using unbiased simulations of 100 ns length. The root-mean-square deviation (RMSD) of the protein remained relatively low with a backbone RMSD converging to ~3 Å after 100 ns simulated time (Supplemental Fig. S6) bound to the binding site defined previously using molecular docking (Fig. 6) (Munday *et al,* 2015a). For these and all following simulations, we used the CHARMM36 force field (Klauda *et al,* 2010); pentamidine was parameterised using the CHARMM generalized force field approach (CHGenFF (Vanommeslaeghe *et al,* 2010)). All simulations employed a time step of 2 fs under an NPT ensemble at p = 1 bar and T = 310 K. To obtain non-equilibrium work values for removing pentamidine from the internal AQP2 binding site, we then conducted steered MD simulations with a probe speed of 0.005 nm/ns and a harmonic force constant of 300 kJ/mol $nm^2$, pulling pentamidine in both directions along the pore axis. The free energy profile of pentamidine binding to the AQP2 pore was reconstructed by using the Jarzynski equality (Jarzynski, 1997).

*Statistical analysis*

All transport experiments were performed in triplicate and all values such as rate of uptake, percent inhibition, $K_i$, $K_m$, $V_{max}$ etc were performed at least three times completely independently. For drug sensitivity tests, all $EC_{50}$ values were based on serial dilutions over two rows of a 96-well plate (23 doubling dilutions plus no-drug control), which were

obtained independently at least three times. $EC_{50}$ and $IC_{50}$ values were determined by non-linear regression using the equation for a sigmoid curve with variable slope and are presented as average ± SEM. Statistical significance between any two data points was determined using Student's t-test (unpaired, two-tailed).

**Acknowledgements**

This work was supported by the UK Medical Research Council (MRC) [grant 84733 to HPdK] and by the US National Institutes of Health (NIH) [Grant No. GM111749 to DWB]. DC was supported by an MRC iCASE award [MR/R015791/1]. UZ acknowledges funding from the Scottish Universities Physics Alliance. AHA is funded through a PhD studentship from Albaha University, Saudi Arabia. GDC was funded by a PhD Studentship from Science Without Borders [206385/2014-5, CNPq, Brazil]. The authors thank Dr Tansy Hammarton for the use of the CRK2 RNAi cell line and Prof David Horn for the use of the aqp1-3 null cell line.

**Author contributions**

Performed experiments: AHA, JCM, GDC, MEMA, PM, LW, DP, AD, JW, GS, LFA, SPYK, HMSI, MIAS, AAE, IAT, SG, HPDK

Chemical synthesis and SAR: CEO, AK, FH, CD

Computational analysis and modelling: DG, FS, LS, CMW, MC

Supervision: RRT, DWB, PMON, UZ, HPDK

Writing manuscript: FH, UZ, HPDK

**Conflict of Interest**

The authors declare that they have no conflict of interest**.**

# References

Abraham MJ, Murtola T, Schulz R, Pálla S, Smith JC, Hessa B, Lindahl E (2015) GROMACS: high performance molecular simulations through multi-level parallelism from laptops to supercomputers. *SoftwareX* 1–2: 19–25. doi.org/10.1016/j.softx.2015.06.001

Alkhaldi AA, Creek DJ, Ibrahim H, Kim DH, Quashie NB, Burgess KE, Changtam C, Barrett MP, Suksamrarn A, De Koning HP (2015) Potent trypanocidal curcumin analogs bearing a monoenone linker motif act on *Trypanosoma brucei* by forming an adduct with trypanothione. *Mol Pharmacol* 87: 451–464. doi.org/10.1124/mol.114.096016

Alkhaldi AAM, Martinek J, Panicucci B, Dardonville C, Ziková A, De Koning HP (2016) Trypanocidal action of bisphosphonium salts through a mitochondrial target in bloodstream form *Trypanosoma brucei*. *Int J Parasitol Drugs Drug Resist* 6: 23–34. doi.org/10.1016/j.ijpddr.2015.12.002

Alsford S, Eckert S, Baker N, Glover L, Sanchez-Flores A, Leung KF, Turner DJ, Field MC, Berriman M, Horn D (2012) High-throughput decoding of antitrypanosomal drug efficacy and resistance. *Nature* 482: 232–236. doi.org/ 10.1038/nature10771

Alsford S, Horn D (2008) Single-locus targeting constructs for reliable regulated RNAi and transgene expression in *Trypanosoma brucei*. *Mol Biochem Parasitol* 161: 76–79. doi.org/10.1016/j.molbiopara.2008.05.006

Baker N, De Koning HP, Mäser P, Horn D (2013) Drug resistance in African trypanosomiasis: the melarsoprol and pentamidine story. *Trends Parasitol* 29, 110–118. doi.org/10.1016/j.pt.2012.12.005

Baker N, Glover L, Munday JC, Aguinaga Andrés D, Barrett MP, De Koning HP, Horn D (2012) Aquaglyceroporin 2 controls susceptibility to melarsoprol and pentamidine in

803 African trypanosomes. *Proc Natl Acad Sci USA* 109: 10996–11001.
804 doi.org/10.1073/pnas.1202885109

805 Barrett MP, Vincent IM, Burchmore RJ, Kazibwe AJ, Matovu E (2011) Drug resistance in
806 human African trypanosomiasis. *Future Microbiol* 6: 1037-1047.
807 doi.org/10.2217/fmb.11.88

808 Beitz E, Wu B, Holm LM, Schultz JE, Zeuthen T. (2006) Point mutations in the
809 aromatic/arginine region in aquaporin 1 allow passage of urea, glycerol, ammonia and
810 protons. *Proc Natl Acad Sci USA* 103: 269–274. doi.org/ 10.1073/pnas.0507225103

811 Beno BR, Yeung KS, Bartberger MD, Pennington LD, Meanwell NA (2015) A survey of the
812 role of noncovalent sulfur interactions in drug design. *J Med Chem* 58: 4383–4438.
813 doi.org/10.1021/jm501853m

814 Brameld KA, Kuhn B, Reuter DC, Stahl M (2008) Small molecule conformational
815 preferences derived from crystal structure data. A medicinal chemistry focused analysis.
816 *J Chem Inf Model* 48: 1–24. doi.org/10.1021/ci7002494

817 Bridges D, Gould MK, Nerima B, Mäser P, Burchmore RJS, De Koning HP (2007) Loss of
818 the High Affinity Pentamidine Transporter is responsible for high levels of cross-
819 resistance between arsenical and diamidine drugs in African trypanosomes. *Mol*
820 *Pharmacol* 71: 1098–1108. doi.org/10.1124/mol.106.031351

821 Büscher P, Cecchi,G, Jamonneau V, Priotto G (2017) Human African trypanosomiasis.
822 *Lancet* 390**:** 2397–2409. doi.org/10.1016/S0140-6736(17)31510-6

823 Carter NS, Berger BJ, Fairlamb AH (1995) Uptake of diamidine drugs by the P2 nucleoside
824 transporter in melarsen-sensitive and -resistant *Trypanosoma brucei brucei*. *J Biol*
825 *Chem* 270: 28153-28157. doi.org/10.1074/jbc.270.47.28153

826 Carter NS, Fairlamb AH (1993) Arsenical-resistant trypanosomes lack an unusual adenosine
827 transporter. *Nature* 361: 173–176. doi.org/10.1038/361173a0

828 Carvalho, A. S, Salomão, K, Castro, S. L, Conde, T. R, Zamith, H. P. Caffarena, E. R, Hall,
829 B. S, Wilkinson, S. R, Boechat, N (2014) Megazol and its bioisostere 4H-1,2,4-triazole:
830 comparing the trypanocidal, cytotoxic and genotoxic activities and their in vitro and in
831 silico interactions with the *Trypanosoma brucei* nitroreductase enzyme. *Mem Inst*
832 *Oswaldo Cruz* 109: 315–323. doi.org/10.1590/0074-0276140497
833 Chein RJ, Corey EJ (2010) Strong conformational preferences of heteroaromatic ethers and
834 electron pair repulsion. *Org Lett* 12: 132–135. doi.org/10.1021/ol9025364
835 De Koning H.P (2020) The drugs of sleeping sickness: their mechanisms of action and
836 resistance, and a brief history. *Trop Med Infect Dis* 5: 14.
837 doi.org/10.3390/tropicalmed5010014
838 De Koning HP (2001a) Uptake of pentamidine in *Trypanosoma brucei brucei* is mediated by
839 three distinct transporters. Implications for crossresistance with arsenicals. *Mol*
840 *Pharmacol* 59: 586–592. doi.org/10.1016/S0001-706X(01)00177-2
841 De Koning HP (2001b) Transporters in African trypanosomes: role in drug action and
842 resistance. *Int J Parasitol* 31: 512–522. doi.org/10.1016/S0020-7519(01)00167-9
843 De Koning HP, Jarvis SM (1997a) Hypoxanthine uptake through a purine-selective
844 nucleobase transporter in *Trypanosoma brucei brucei* procyclics is driven by
845 protonmotive force. *Eur J Biochem* 247: 1102–1110. doi.org/10.1111/j.1432-
846 1033.1997.01102.x
847 De Koning HP, Jarvis SM (1997b) Purine nucleobase transport in bloodstream forms of
848 *Trypanosoma brucei brucei* is mediated by two novel transporters. *Mol Biochem*
849 *Parasitol* 89: 245–258. doi.org/10.1016/S0166-6851(97)00129-1
850 De Koning HP, Jarvis SM (1998) A highly selective, high affinity transporter for uracil in
851 *Trypanosoma brucei brucei*; evidence for proton-dependent transport. *Biochem Cell Biol*
852 76: 853–858. doi.org/10.1139/o98-086

De Koning HP, Jarvis SM (1999) Adenosine transporters in bloodstream forms of T. b. brucei: Substrate recognition motifs and affinity for trypanocidal drugs. *Mol Pharmacol* 56: 1162–1170. doi.org/10.1124/mol.56.6.1162

De Koning HP, Jarvis SM (2001) Uptake of pentamidine in *Trypanosoma brucei brucei* is mediated by the P2 adenosine transporter and at least one novel, unrelated transporter. Acta Trop 80: 245-250. doi.org/10.1016/S0001-706X(01)00177-2

De Koning HP, MacLeod A, Barrett MP, Cover B, Jarvis SM (2000) Further evidence for a link between melarsoprol resistance and P2 transporter function in African trypanosomes. *Mol Biochem Parasitol* 106: 181–185. doi.org/10.1016/s0166-6851(99)00206-6

De Koning HP, Stewart M, Anderson L, Burchmore R, Wallace LJM, Barrett MP (2004) The trypanocide diminazene aceturate is accumulated predominantly through the TbAT1 purine transporter; additional insights in diamidine resistance in African trypanosomes. *Antimicrob Agents Chemother* 48: 1515–1519. doi.org/10.1128/AAC.48.5.1515-1519.2004

De Koning HP, Watson CJ, Jarvis SM (1998) Characterisation of a nucleoside/proton symporter in procyclic *Trypanosoma brucei brucei*. *J Biol Chem* 273: 9486–9494. doi.org/10.1074/jbc.273.16.9486

Demmel L, Schmidt K, Lucast L, Havlicek K. Zankel A, Koestler T, Reithofer V, de Camilli P, Warren G (2014) The endocytic activity of the flagellar pocket in *Trypanosoma brucei* is regulated by an adjacent phosphatidylinositol phosphate kinase. *J Cell Sci* 127: 2351–2364. doi.org/10.1242/jcs.146894

Fairlamb AH, Carter NS, Cunningham M, Smith K (1992) Characterisation of melarsen-resistant *Trypanosoma brucei brucei* with respect to cross-resistance to other drugs and

877 trypanothione metabolism. *Mol Biochem Parasitol* 53: 213–222. doi.org/10.1016/0166-
878 6851(92)90023-D

879 Field MC, Carrington M (2009) The trypanosome flagellar pocket. *Nat Rev Microbiol* 7:
880 775–786. doi.org/10.1038/nrmicro2221

881 Frommel TO, Balber AE (1987) Flow cytofluorimetric analysis of drug accumulation by
882 multidrug-resistant *Trypanosoma brucei brucei* and *T. b. rhodesiense*. *Mol Biochem*
883 *Parasitol* 26: 183–191. doi.org/10.1016/0166-6851(87)90142-3

884 Geng X, McDermott J, Lundgren J, Liu L, Tsai KJ, Shen J, Liu Z (2017) Role of AQP9 in
885 transport of monomethylselenic acid and selenite. *Biometals* 30: 747–755.
886 doi.org/10.1007/s10534-017-0042-x

887 Giordani F, Morrison LJ, Rowan TG, De Koning HP, Barrett MP (2016) The animal
888 trypanosomiases and their chemotherapy: a review. *Parasitology* 143: 1862–1889.
889 doi.org/10.1017/S0031182016001268

890 Graf FE, Baker N, Munday JC, De Koning HP, Horn D, Mäser P (2015) Chimerization at the
891 *AQP2-AQP3* locus is the genetic basis of melarsoprol-pentamidine cross-resistance in
892 clinical *Trypanosoma brucei gambiense* isolates. *Int J Parasitol Drugs Drug Resist* 5:
893 65–68. doi.org/10.1016/j.ijpddr.2015.04.002

894 Graf FE, Ludin P, Arquint C, Schmidt RS, Schaub N, Kunz-Renggli C, Munday JC,
895 Krezdorn J, Baker N, Horn D, Balmer O, Caccone A, De Koning HP, Mäser P. (2016)
896 Comparative genomics of drug resistance of the sleeping sickness parasite *Trypanosoma*
897 *brucei rhodesiense*. *Cell Mol Life Sci* 73: 3387–3400. doi.org/10.1007/s00018-016-2173-
898 6

899 Graf FE, Ludin P, Wenzler T, Kaiser M, Pyana P, Büscher P, De Koning HP, Horn D, Mäser
900 P (2013) Aquaporin 2 mutations in *Trypanosoma b. gambiense* field isolates correlate

with decreased susceptibility to pentamidine and melarsoprol. *PLoS Negl Trop Dis* 7: e2475. doi.org/10.1371/journal.pntd.0002475

Hutchinson R, Gibson W (2015) Rediscovery of *Trypanosoma* (Pycnomonas) *suis*, a tsetse-transmitted trypanosome closely related to *T. brucei*. *Infect Genet Evol* 36: 381–388. doi.org/10.1016/j.meegid.2015.10.018

Jarzynski C (1997) Nonequilibrium equality for free energy differences. *Phys Rev Lett* 78: 2690–2693. doi.org/10.1103/PhysRevE.56.5018

Jeacock L, Baker N, Wiedemar N, Mäser P, Horn D (2017) Aquaglyceroporin-null trypanosomes display glycerol transport defects and respiratory-inhibitor sensitivity. *PLoS Pathog* 13: e1006307. doi.org/10.1371/journal.ppat.1006307

Jensen BC, Ramasamy G, Vasconcelos EJ, Ingolia NT, Myler PJ, Parsons M (2014) Extensive stage-regulation of translation revealed by ribosome profiling of *Trypanosoma brucei*. *BMC Genomics* 15: 911. doi.org/10.1186/1471-2164-15-911

Jo S, Kim T, Iyer VG, Im W (2008) CHARMM-GUI: A Web-based Graphical User Interface for CHARMM. *J Comput Chem* 29: 1859-1865. doi.org/10.1002/jcc.20945

Kanai Y, Clémençon B, Simonin A, Leuenberger M, Lochner M, Weisstanner M, Hediger MA (2013) The SLC1 high-affinity glutamate and neutral amino acid transporter family. *Mol Aspects Med* 34: 108–120. doi.org/10.1016/j.mam.2013.01.001

Klauda JB, Venable RM, Freites JA, O'Connor JW, Tobias DJ, Mondragon-Ramirez C, Vorobyov I, MacKerell AD Jr, Pastor RW (2010) Update of the CHARMM all-atom additive force field for lipids: validation on six lipid types. *J. Phys. Chem. B* 114, 7830–7843. doi.org/10.1021/jp101759q

Langreth SG, Balber AE (1975) Protein uptake and digestion in bloodstream and culture forms of *Trypanosoma brucei*. *J Protozool* 22: 40–55. doi.org/10.1111/j.1550-7408.1975.tb00943.x

926 Lüscher A, De Koning HP, Mäser P (2007) Chemotherapeutic strategies against
927 *Trypanosoma brucei*: Drug targets vs. drug targeting. *Curr Pharm Des* 13: 555–567.
928 doi.org/10.2174/138161207780162809
929 Mäser P, Sütterlin C, Kralli A, Kaminsky RA (1999) nucleoside transporter from
930 *Trypanosoma brucei* involved in drug resistance. *Science* 285: 242–244. doi.org/
931 10.1126/science.285.5425.242
932 Monnerat S, Almeida Costa CI, Forkert AC, Benz C, Hamilton A, Tetley L, Burchmore R,
933 Novo C, Mottram JC, Hammarton TC (2013) Identification and functional
934 characterisation of CRK12:CYC9, a novel cyclin-dependent kinase (CDK)-cyclin
935 complex in *Trypanosoma brucei*. *PLoS One* 8: e67327.
936 doi.org/10.1371/journal.pone.0067327
937 Munday JC, Eze AA, Baker N, Glover L, Clucas C, Aguinaga Andrés D, Natto MJ, Teka IA,
938 McDonald J, Lee RS, Graf FE, Ludin P, Burchmore RJS, Turner CMR, Tait A, MacLeod
939 A, Mäser P, Barrett MP, Horn D, De Koning HP (2014) *Trypanosoma brucei*
940 Aquaglyceroporin 2 is a high affinity transporter for pentamidine and melaminophenyl
941 arsenic drugs and is the main genetic determinant of resistance to these drugs. *J*
942 *Antimicrob Chemother* 69: 651–663. doi.org/doi.org/10.1093/jac/dkt442
943 Munday JC, Settimo L, De Koning HP (2015a) Transport proteins determine drug sensitivity
944 and resistance in a protozoan parasite, *Trypanosoma brucei*. *Frontiers Pharmacol* 6: 32.
945 doi.org/10.3389/fphar.2015.00032
946 Munday JC, Tagoe DNA, Eze AA, Krezdorn JA, Rojas López KE, Alkhaldi AAM,
947 McDonald F, Still J, Alzahrani KJ, Settimo L, De Koning HP (2015b) Functional
948 analysis of drug resistance-1 associated mutations in the *Trypanosoma brucei* Adenosine
949 Transporter 1 (TbAT1) and the proposal of a structural model for the protein. *Mol*
950 *Microbiol* 96: 887–900. doi.org/10.1111/mmi.12979

951 Park S, Khalili-Araghi F, Tajkhorshid E, Schulten K (2003) Free energy calculation from
952 steered molecular dynamics simulations using Jarzynski's equality. *J Chem Phys* 119:
953 3559. doi.org/10.1063/1.1590311
954 Pyana Pati P, Van Reet N, Mumba Ngoyi D, Ngay Lukusa I, Karhemere Bin Shamamba S,
955 Büscher P (2014) Melarsoprol sensitivity profile of *Trypanosoma brucei gambiense*
956 isolates from cured and relapsed sleeping sickness patients from the Democratic
957 Republic of the Congo. *PLoS Negl Trop Dis* 8: e3212.
958 doi.org/10.1371/journal.pntd.0003212
959 Ríos Martínez CH, Miller F, Ganeshamoorthy K, Glacial F, Kaiser M, De Koning HP, Eze
960 AA, Lagartera L, Herraiz T, Dardonville C (2015) A new nonpolar *N*-hydroxy
961 imidazoline lead compound with improved activity in a murine model of late-stage
962 *Trypanosoma brucei brucei* infection is not cross-resistant with diamidines. *Antimicrob*
963 *Agents Chemother* 59: 890–904. doi.org/10.1128/AAC.03958-14
964 Rollo IM, Williamson J (1951) Acquired resistance to 'Melarsen', tryparsamide and amidines
965 in pathogenic trypanosomes after treatment with 'Melarsen' alone. *Nature* 167: 147–148
966 doi.org/10.1038/167147a0
967 Siegel TN, Hekstra DR, Wang X, Dewell S, Cross GA (2010) Genome-wide analysis of
968 mRNA abundance in two life-cycle stages of *Trypanosoma brucei* and identification of
969 splicing and polyadenylation sites. *Nucleic Acids Res* 38: 4946–4957.
970 doi.org/10.1093/nar/gkq237
971 Smith TK, Bütikofer P (2010) Lipid metabolism in *Trypanosoma brucei*. *Mol Biochem*
972 *Parasitol* 172: 66–79. doi.org/10.1016/j.molbiopara.2010.04.001
973 Song J, Baker N, Rothert M, Henke B, Jeacock L, Horn D, Beitz E (2016) Pentamidine is not
974 a permeant but a nanomolar inhibitor of the *Trypanosoma brucei* Aquaglyceroporin-2.
975 *PLoS Pathog* 12: e1005436. doi.org/10.1371/journal.ppat.1005436

976 Taladriz A, Healy A, Flores Pérez EJ, Herrero García V, Ríos Martínez C, Alkhaldi AAM,
977 Eze AA, Kaiser M, Brun R, de Koning HP, Chana A, Dardonville C (2012) Synthesis
978 and structure-activity analysis of new phosphonium salts with potent activity against
979 African trypanosomes. *J Med Chem* 55: 2606–2622. doi.org/10.1021/jm2014259
980 Teka IA, Kazibwe A, El-Sabbagh N, Al-Salabi MI, Ward CP, Eze AA, Munday JC, Mäser P,
981 Matovu E, Barrett MP, De Koning HP (2011) The diamidine diminazene aceturate is a
982 substrate for the High Affinity Pentamidine Transporter: implications for the
983 development of high resistance levels. *Mol Pharmacol* 80: 110–116.
984 doi.org/10.1124/mol.111.071555
985 Unciti-Broceta JD, Arias JL, Maceira J, Soriano M, Ortiz-González M, Hernández-Quero J,
986 Muñóz-Torres M, De Koning HP, Magez S, Garcia-Salcedo JA (2015) Specific cell
987 targeting therapy bypasses drug resistance mechanisms in African trypanosomiasis. *PloS*
988 *Pathog* 11: e1004942. doi.org/10.1371/journal.ppat.1004942
989 Vanommeslaeghe K, Hatcher E, Acharya C, Kundu S, Zhong S, Shim J, Darian E, Guvench
990 O, Lopes P, Vorobyov I, Mackerell AD, Jr (2010) CHARMM general force field: A
991 force field for drug-like molecules compatible with the CHARMM all-atom additive
992 biological force fields. *J. Comput. Chem*. 31, 671–690. doi.org/10.1002/jcc.21367
993 Vincent IM, Creek D, Watson DG, Kamleh MA, Woods DJ, Wong PE, Burchmore RJ,
994 Barrett MP (2010) A molecular mechanism for eflornithine resistance in African
995 trypanosomes. *PLoS Pathog* 6: e1001204. doi.org/ 10.1371/journal.ppat.1001204
996 Wallace LJM, Candlish D, De Koning HP (2002) Different substrate recognition motifs of
997 human and trypanosome nucleobase transporters: selective uptake of purine
998 antimetabolites. *J Biol Chem* 277: 26149–26156. doi.org/10.1074/jbc.M202835200
999 Wang MZ, Zhu X, Srivastava A, Liu Q, Sweat JM, Pandharkar T, Stephens CE, Riccio E,
1000 Parman T, Munde M, Mandal S, Madhubala R, Tidwell RR, Wilson WD, Boykin DW,

Hall JE, Kyle DE, Werbovetz KA (2010) Novel arylimidamides for treatment of visceral leishmaniasis. *Antimicrob Agents Chemother* 54: 2507–2516. doi.org/10.1128/AAC.00250-10

Ward CP, Wong PE, Burchmore RJ, De Koning HP, Barrett MP (2011) Trypanocidal furamidine analogues: influence of pyridine nitrogens on trypanocidal activity, transport kinetics and resistance patterns. *Antimicrob Agents Chemother* 55: 2352–2361. doi.org/10.1128/AAC.01551-10

Wree D, Wu B, Zeuthen T, Beitz E (2011) Requirement for asparagine in the aquaporin NPA signature motifs for cation exclusion. *FEBS J* 278: 740–748. doi.org/10.1111/j.1742-4658.2010.07993.x

Wu B, Steinbronn C, Alsterfjord M, Zeuthen T, Beitz E (2009) Concerted action of two cation filters in the aquaporin water channel. *EMBO J* 28: 2188–2194. doi.org/10.1038/emboj.2009.182

Zhorov BS, Tikhonov DB (2013) Ligand action on sodium, potassium, and calcium channels: role of permeant ions. *Trends Pharmacol Sci* 34: 154–161. doi.org/10.1016/j.tips.2013.01.002

Zoltner M, Horn D, De Koning HP, Field MC (2016) Exploiting the Achilles' heel of membrane trafficking in trypanosomes. *Curr Opin Microbiol* 34: 97–103. doi.org/10.1016/j.mib.2016.08.005

## Figures and Legends

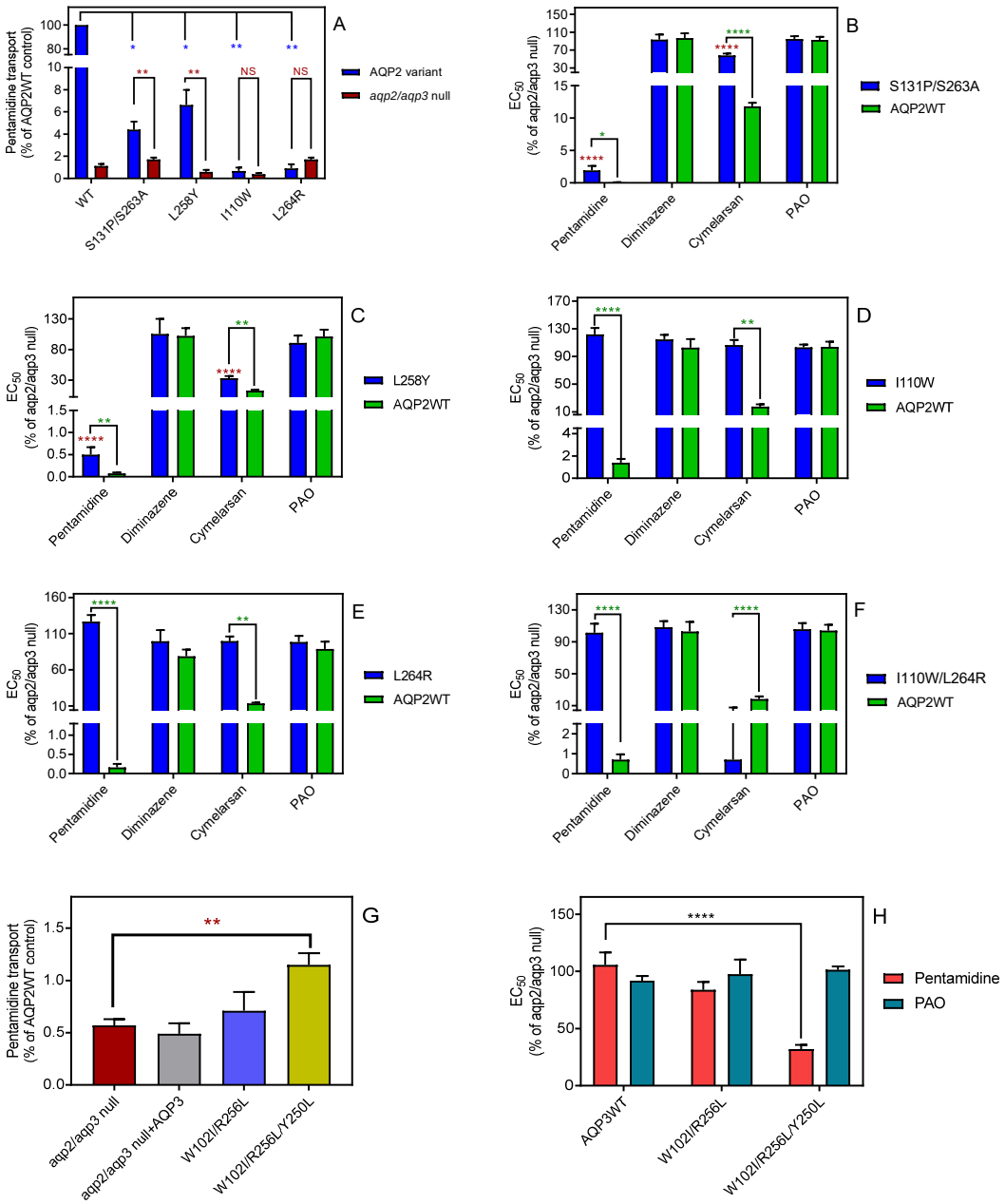


**Fig. 1. The selectivity filter differences between TbAQP2 and TbAQP3 are largely responsible for their differences in pentamidine sensitivity and transport rates**.

(A) Transport of 30 nM [$^3$H]-pentamidine by *tbaqp2/aqp3* null cells expressing TbAQP2-WT or one of the TbAQP2 mutants as indicated (blue bars). The corresponding brown bars are

pentamidine transport in the control *tbaqp2/aqp3* null cells assessed in parallel in each experiment. Transport was determined in the presence of 1 mM adenosine to block the TbAT1/P2 transporter. Bars represent the average and SEM of at least three independent experiments, each performed in triplicate. Blue stars: statistical significance comparison, by two-tailed unpaired Student's tests, between the cells expressing TbAQP2WT and mutants; red stars: statistical comparison between the AQP2-expressing cells and control cells; NS, not significant. (B-F) $EC_{50}$ values indicated test drugs, expressed as a percentage of the resistant control (*tbaqp2/tbaqp3* null), against cell lines either expressing the indicated TbAQP2 mutant or TbAQP2WT (sensitive control). Red stars and green stars: comparison with *tbaqp2/aqp3* null or TbAQP2WT-expressing cells, respectively, which were always assessed in parallel in each experiment. (G) Transport of 30 nM [$^3$H]-pentamidine by *tbaqp2/aqp3* null cells expressing TbAQP3 or an AQP3 mutant as indicated. (H) $EC_{50}$ values of the indicated drugs against *tbaqp2/aqp3* null cells expressing either TbAQP3 or a mutant thereof, expressed as percentage of *tbaqp2/aqp3* null.

All experiments are the average and SEM of at least 3 independent experiments. *, $P<0.05$; **, $P<0.01$; ***, $P<0.001$, ****, $P<0.0001$ by unpaired Student's t-test, two-tailed.

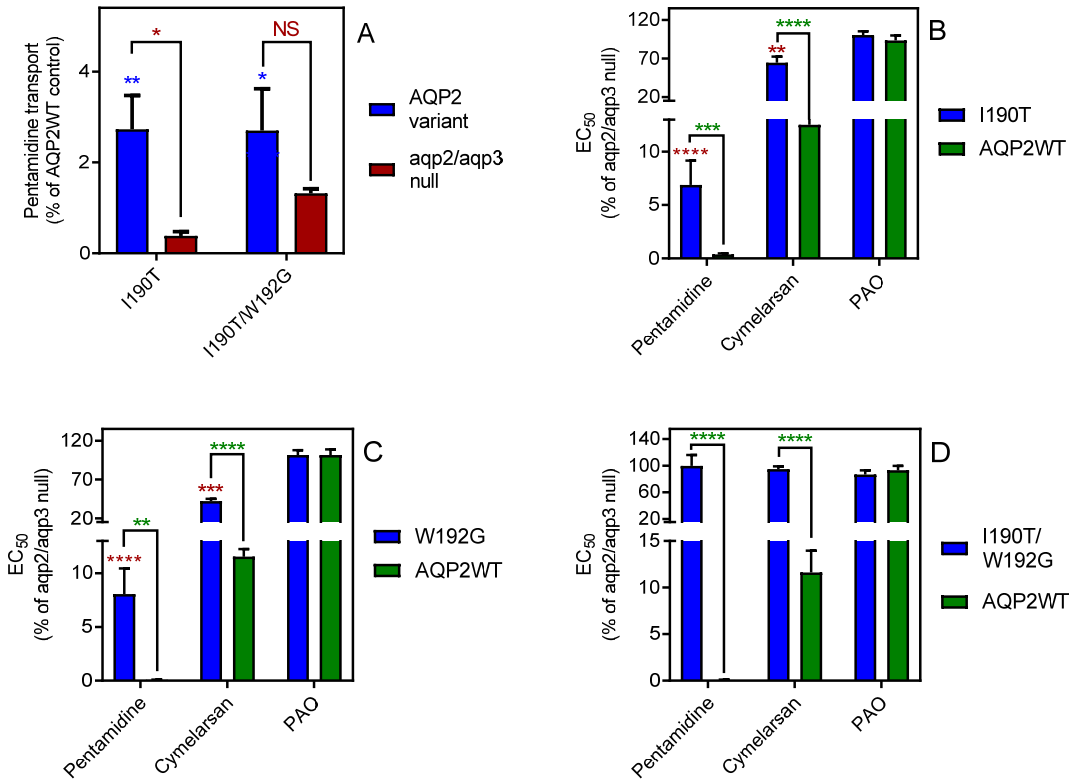


**Fig. 2. Mutational analysis of TbAQP2 residues I190 and W192.** (A) Transport of 30 nM [$^3$H]-pentamidine by *tbaqp2/tbaqp3* null cells or TbAQP2 variants expressed therein. Transport was expressed as a percentage of the rate of the AQP2WT control, performed in parallel. Blue stars are comparison with TbAQP2WT, red stars, comparison with the *tbaqp2/tbaqp3* null control. NS, not significant. (B) $EC_{50}$ values for the indicated drugs against *tbaqp2/tbaqp3* null cells, and against TbAQP2WT and TbAQP2$^{I190T}$ expressed therein; values were expressed as % of the *tbaqp2/tbaqp3* null (resistant) control. Red stars, comparison with the resistant control; green stars, comparison with the internal sensitive control (TbAQP2WT). The assays for all three strains and all three drugs were done simultaneously on at least 3 different occasions. (C) As B but for TbAQP2$^{W192G}$. (D) As B but for TbAQP2$^{I190T/W192G}$.

*, P<0.05; **, P<0.01; ***, P<0.001, ****, P<0.0001 by unpaired Student's t-test.

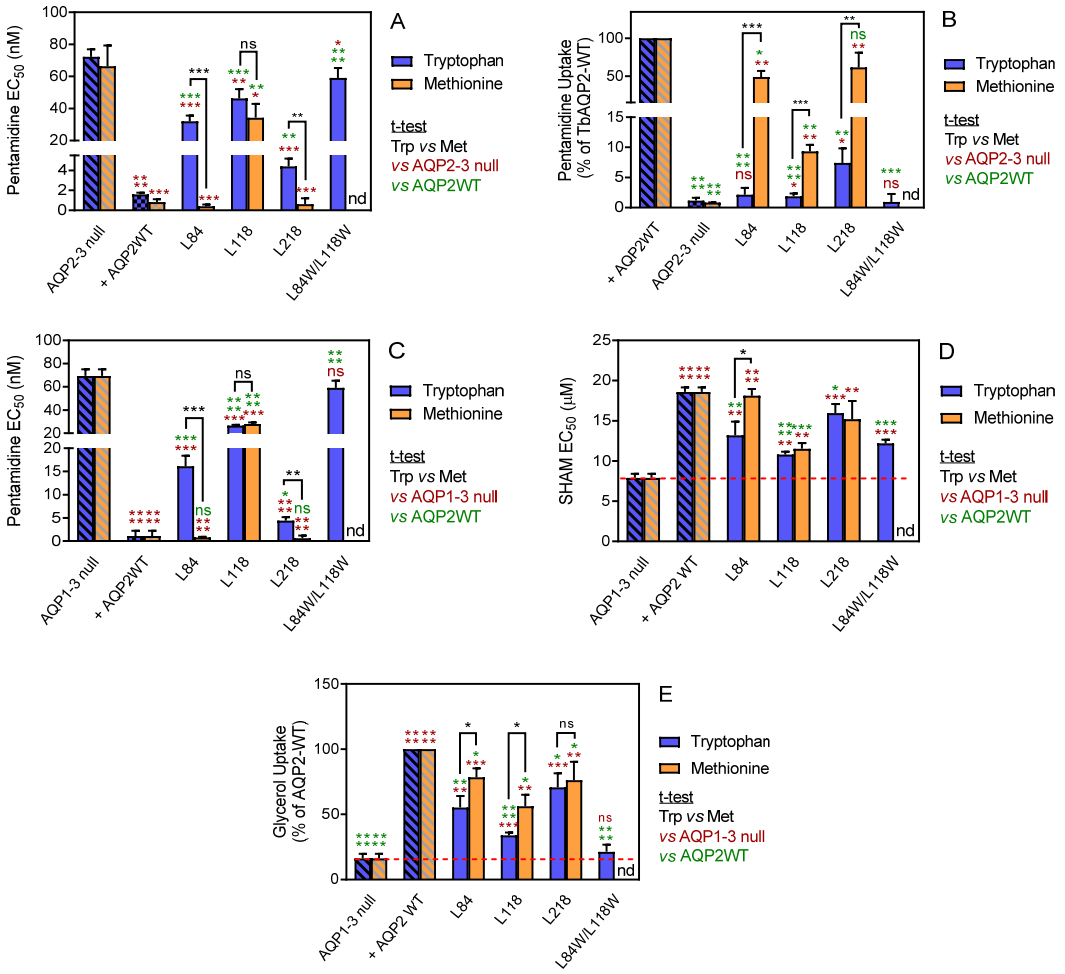


**Fig. 3. Analysis of TbAQP2 variants with a leucine-to-tryptophan or leucine-to-methionine substitution near the cytoplasmic end of the pore**. (A) Pentamidine $EC_{50}$ values (nM) for mutant and WT TbAQP2 expressed in *tbaqp2/tbaqp3* cells (aqp2-3 null). The mutants are either a Trp (dark blue bars) or Met (orange bars) substitution at the indicated positions. The resistant control (aqp2-3 null) and sensitive control (AQP2WT) for the separate datasets (Trp or Met) are indicated as hatched bars in the same colours. (B) As (A) but showing transport of 30 nM [$^3$H]-pentamidine by the same cell lines, expressed as percentage of the transport rate in the TbAQP2 control cells. (C) Pentamidine $EC_{50}$ values for the same mutants as in (A) but expressed in the *tbaqp1-2-3* null cells, performed in parallel with the determination of $EC_{50}$ values for SHAM, shown in (D). As all cell lines were done

simultaneously, the resistant and sensitive strain control values are identical for the Trp and Met mutants in this series.

All bars represent the average and SEM of at least three independent replicates. *, P<0.05; **, P<0.01; ***, P<0.001, ****, P<0.0001 by unpaired Student's t-test; ns, not significant; nd, not determined.

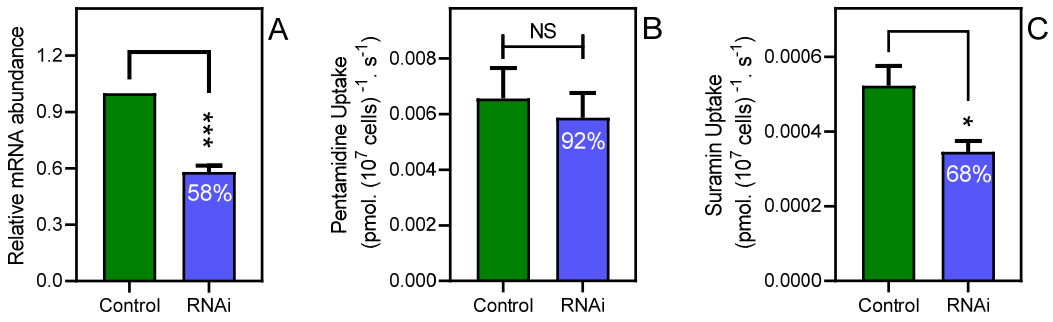


**Fig. 4. Disabling endocytosis does not reduce uptake of pentamidine.** (A) qRT-PCR of CRK12, normalised to housekeeping gene GPI-8 (n=3). (B) Transport of 0.025 µM [$^3$H]-Pentamidine measured in control (non-induced) and CRK12 cell after exactly 12 h of tetracycline induction; incubation time with label was 30 s. Bar is average and SEM of 5 independent determinations, each performed in triplicate. NS, not significant by unpaired Student's t-test. (C) As frame B but uptake of 0.25 µM [$^3$H]-suramin over 15 min; average and SEM of 5 independent determinations, each in quadruplicate. **, P=0.0027 by Student's unpaired, two-tailed t-test.

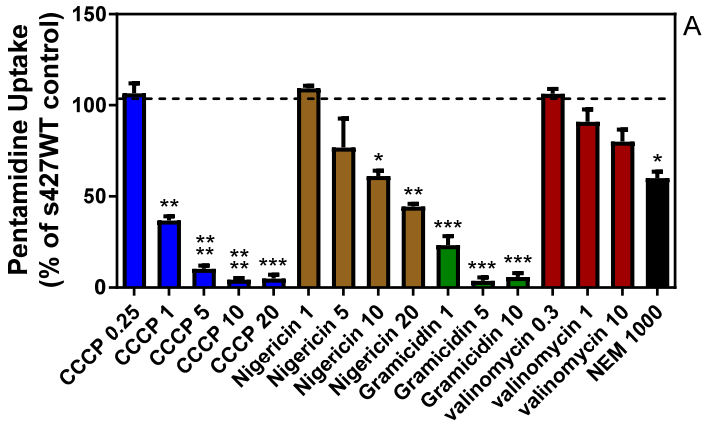


1084

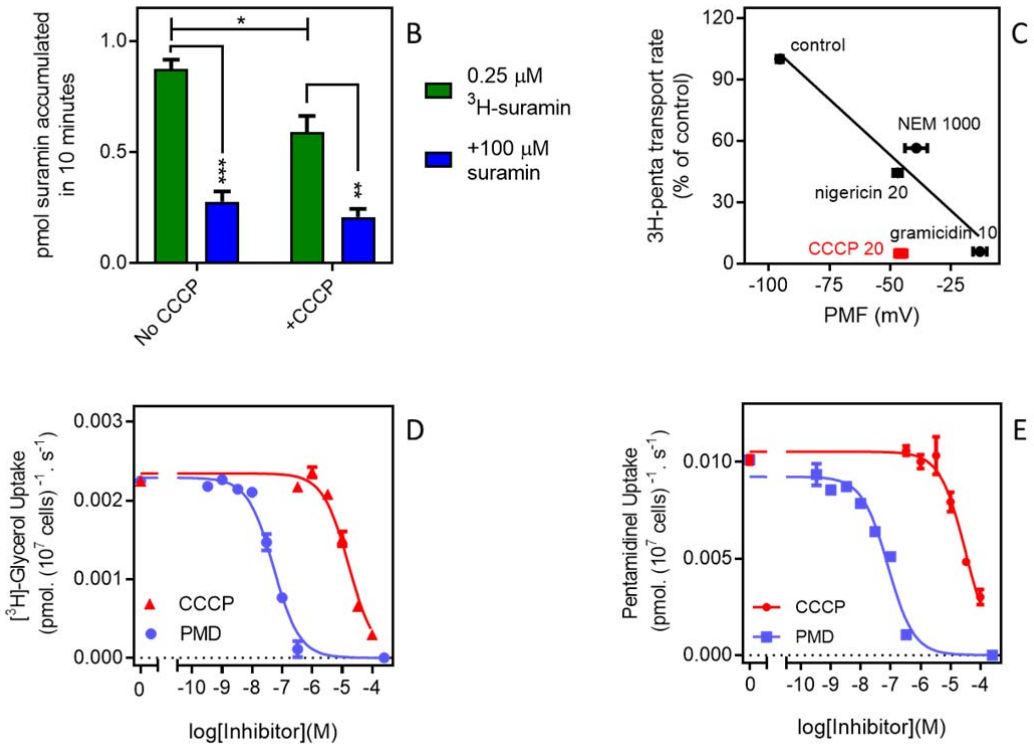


1085

1086 **Fig. 5. High affinity pentamidine uptake in *T. b. brucei* is sensitive to ionophores.** (A)
1087 Uptake of 25 nM [$^3$H]-pentamidine in s427WT bloodstream forms was measured in the
1088 presence of 1 mM adenosine to block the P2 transporter, and in the further presence of
1089 various ionophores at the indicated concentrations in µM. Incubation with radiolabel was 5
1090 min after a 3 min pre-incubation with ionophore. Accumulation of radiolabel was expressed
1091 as a percentage of the control, being a parallel incubation in the absence of any ionophore.

Bars represent the average of 3 – 5 independent determinations (each performed in quadruplicate) and SEM. (B) Uptake of 0.25 µM [$^3$H]-suramin by *T. b. brucei* s427WT cells over 10 minutes. Cells were incubated in parallel, with or without the presence of 20 µM CCCP (plus 3-minute pre-incubation). Saturation of the suramin-receptor interaction was demonstrated by including 100 µM unlabelled suramin (blue bars). Bars represent average and SEM or three independent experiments, each performed in quadruplicate. (C) Correlation plot of pentamidine transport rate versus protonmotive force (PMF), $r^2 = 0.93$, $P<0.05$ by F-test. Concentrations in µM are indicated in the frame. CCCP is shown in red and not included in the regression analysis. Each data point is the average of 4 or more independent repeats performed in quadruplicate. The values for PMF were taken from (De Koning and Jarvis, 1997b). (D) Uptake of 0.25µM [$^3$H]-glycerol by *aqp1/aqp2/aqp3* null cells expressing TbAQP2-WT. Dose response with CCCP and pentamidine (PMD), using an incubation time of 1 min. The graph shown was performed in triplicate and representative of three independent repeats. (E) As C but using 0.025 µM [$^3$H]-pentamidine and 30 s incubations. Representative graph in triplicate from 3 independent repeats.

*, $P<0.05$; **, $P<0.01$; ***, $P<0.001$ by Student's unpaired t-test.

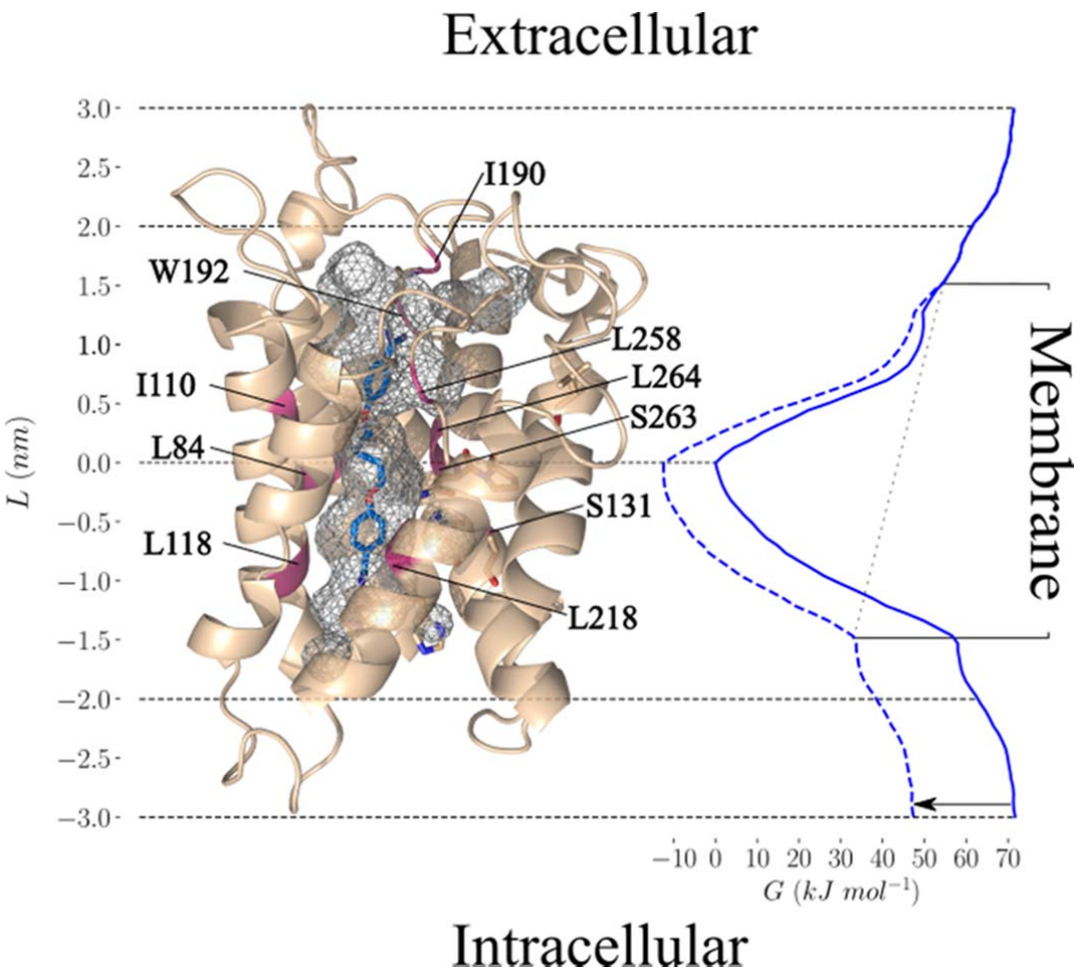


**Fig. 6. Pentamidine binding in TbAQP2 and free-energy profile of permeation (Left).** Docked conformation of pentamidine (blue) bound to the TbAQP2 (wheat). The protein and the ligand were modelled as described.[4] The protein pore is shown in grey mesh, and the mutated positions described in the text are in magenta. (Right) Free-energy profile G(L) (solid blue line) along the pore axis of TbAQP2 (L). The membrane voltage of *T. b. brucei* gives rise to a voltage drop across the membrane (gray dotted line), which alters the free-energy profile (dashed blue line includes $V_m$ effect) and reduces the free-energy of pentamidine exit into the intracellular bulk by ~22 kJ/mol as compared to the extracellular side (black arrow).

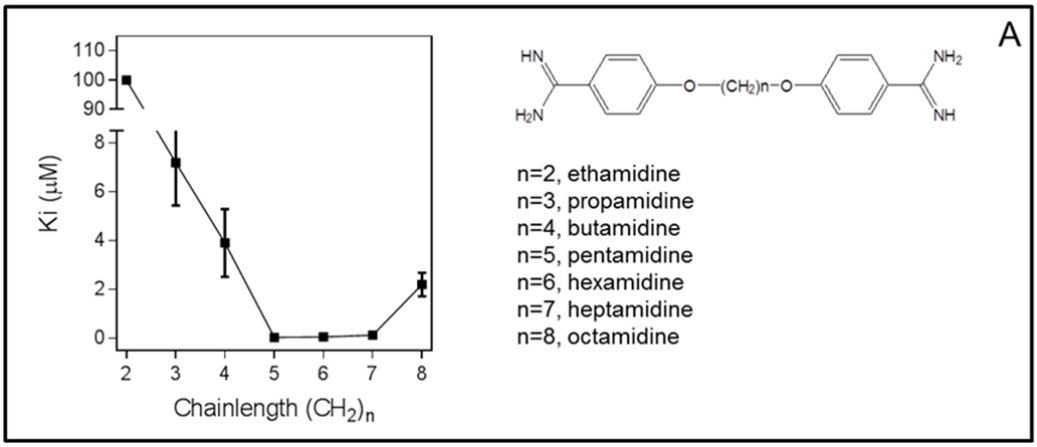


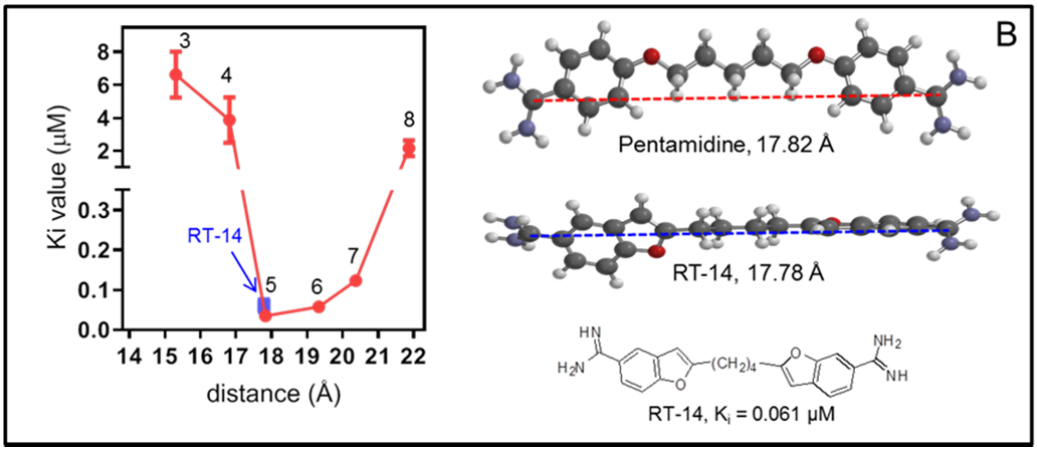


1121

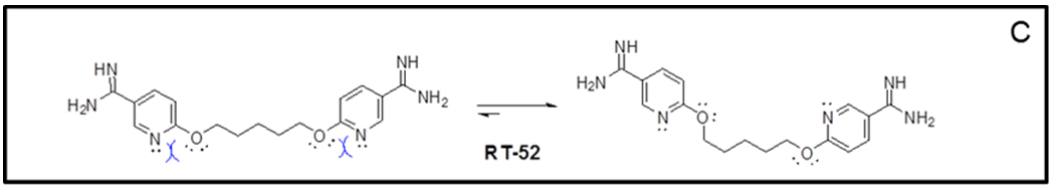


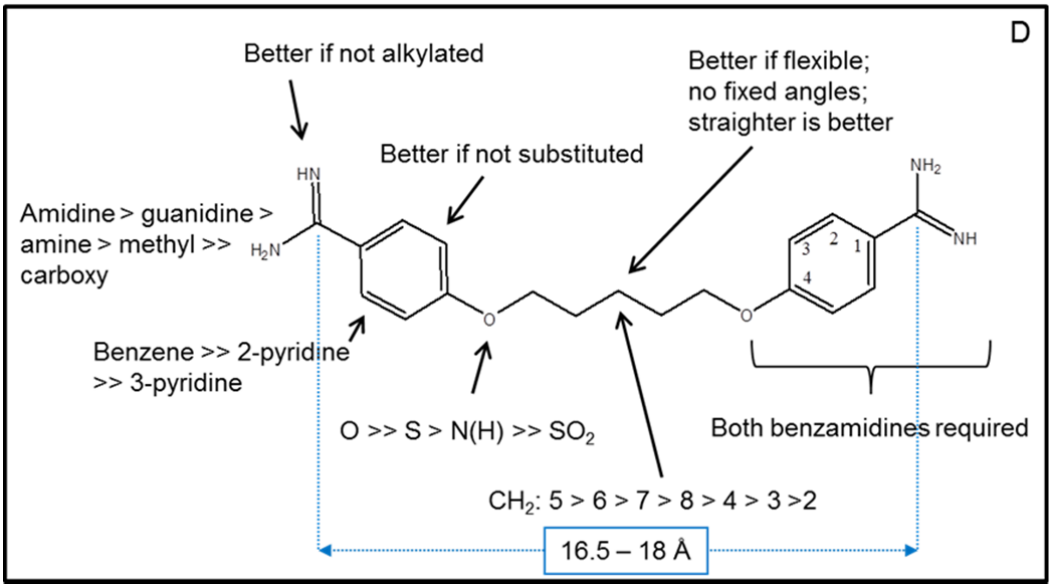


1122

**Fig. 7. Correlation between linker chain length and affinity to HAPT1.**

(A) A series of pentamidine analogues with different methylene linker length was tested for inhibition of TbAQP2/HAPT1-mediated 25 nM [$^3$H]-pentamidine transport (i.e. in the presence of adenosine to block the TbAT1/P2 transporter). The $K_i$ values are listed in Table 1. All $K_i$ values are shown as average and SEM of 3 or more independent experiments, each performed in triplicate. (B) The distance between the amidine carbon atoms in the lowest-energy conformation was calculated using density functional theory as implemented in Spartan '16 v2.0.7. Geometry optimisations were performed with the wB97XD functional and the 6-31G* basis set at the ground state in gas phase. Structures and distances shown represent the dication state that is overwhelmingly prevalent in aqueous solution at neutral pH. The numbered red data points correspond to the propamidine - octamidine series in frame A. (C) Repulsion between free electron pairs (double dots), indicated by curved blue lines for RT-52 in the *cis*-conformation, causing it to exist overwhelmingly in the *anti*-conformation. (D) Overview of SAR observations on the binding preferences of TbAQP2 for pentamidine and its analogues.

1139 **Table 1**. Pentamidine analogues with an aliphatic linker

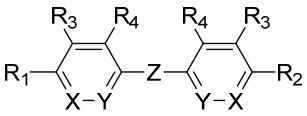


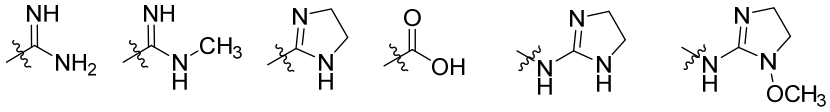


Am MeAm Im CA $G_1$ $G_2$

1140

| Compound | $R_1$ | $R_2$ | $R_3$ | $R_4$ | X | Y | Z | $K_i$ (μM) | $\delta(\Delta G^0)$ PMD (kJ/mol) |
|---|---|---|---|---|---|---|---|---|---|
| Ethamidine | Am | Am | H | H | CH | CH | -O-$(CH_2)_2$-O- | >100 | >19.7 |
| Propamidine | Am | Am | H | H | CH | CH | -O-$(CH_2)_3$-O- | 6.63 ± 1.40 | 13.0 |
| Butamidine | Am | Am | H | H | CH | CH | -O-$(CH_2)_4$-O- | 3.87 ± 1.38 | 11.7 |
| **Pentamidine** (PMD) | Am | Am | H | H | CH | CH | -O-$(CH_2)_5$-O- | **0.036 ± 0.0006** | -- |
| Hexamidine | Am | Am | H | H | CH | CH | -O-$(CH_2)_6$-O- | 0.058 ± 0.011 | 1.3 |
| Heptamidine | Am | Am | H | H | CH | CH | -O-$(CH_2)_7$-O- | 0.123 ± 0.010 | 3.1 |
| Octamidine | Am | Am | H | H | CH | CH | -O-$(CH_2)_8$-O- | 2.16 ± 0.48 | 10.2 |
| RT-48 | Am | Am | H | H | CH | CH | -S-$(CH_2)_5$-S- | 2.01 ± 0.86 | 10.0 |
| RT-50 | Am | Am | H | H | CH | CH | -NH-$(CH_2)_5$-NH- | 6.27 ± 1.30 | 12.9 |
| RT-49 | Am | Am | H | H | CH | CH | -$SO_2$-$(CH_2)_5$-$SO_2$- | >150 | >20.7 |

| | | | | | | | | | |
|---|---|---|---|---|---|---|---|---|---|
| DB1699 | Am | Am | H | H | CH | CH | -O-$(CH_2)_2$-O-$(CH_2)_2$-O- | 16.6 ± 2.1 | 15.3 |
| RT-36 | Am | $NH_2$ | H | H | CH | CH | -O-$(CH_2)_5$-O- | 0.43 ± 0.07 | 6.2 |
| CHI/1/72/1 | Am | $CH_3$ | H | H | CH | CH | -O-$(CH_2)_5$-O- | 3.1 ± 0.7 | 10.7 |
| CHI/1/69/1 | Am | H | H | H | CH | CH | -O-$(CH_2)_4$-O- | 2.3 ± 0.5 | 10.4 |
| RT-38 | Am | CA | H | H | CH | CH | -O-$(CH_2)_3$-O- | NI, 100 | >19.7 |
| *meta*-PMD | H | H | Am | H | CH | CH | -O-$(CH_2)_5$-O- | 2890 ± 1050 | 28.1 |
| RT-32 | Im | Im | H | H | CH | CH | -O-$(CH_2)_5$-O- | 0.40 ± 0.08 | 6.0 |
| RT-30 | MeAm | MeAm | H | H | CH | CH | -O-$(CH_2)_5$-O- | 0.30 ± 0.07 | 5.3 |
| Stilbamidine | Am | Am | H | H | CH | CH | -CH=CH- | 54.8 ± 3.2 | 18.3 |
| FR39 | G1 | G1 | H | H | CH | CH | -$(CH_2)_2$- | 41.7 ±15.2 | 17.6 |
| CRMI8 | G2 | G2 | H | H | CH | CH | -$(CH_2)_2$- | 52.8 ±12.7 | 18.1 |
| RT-43 | Am | Am | H | Cl | CH | CH | -O-$(CH_2)_5$-O- | 0.51 ± 0.15 | 6.6 |
| Iodo-PMD | Am | Am | H | I | CH | CH | -O-$(CH_2)_5$-O- | 2.15 ± 0.04 | 8.4 |
| RT-46 | Am | Am | H | -C(O)$NH_2$ | CH | CH | -O-$(CH_2)_5$-O- | >100 | >19.7 |
| RT-52 | Am | Am | H | H | CH | N | -O-$(CH_2)_5$-O- | 8.84 ± 0.88 | 13.7 |
| RT-53 | Am | Am | H | H | N | CH | -O-$(CH_2)_5$-O- | NI, 250 | >22 |

Am, amidine; MeAm, Methyl-amidine; Im, imidazole; CA, carboxylic acid; G1, 2-aminoimidazoline; G2, 1-methoxy-2-aminoimidazoline. PMD, pentamidine, NI, no inhibition at the indicated concentration in μM. $K_i$ is the inhibition constant for [$^3$H]-pentamidine transport by TbAQP2/HAPT1. $\delta(\Delta G^0)$ PMD is the difference in Gibbs Free Energy of interaction of the substrate with TbAQP2 with the same value for pentamidine (PMD). All $K_i$ values are the average and SEM of at least 3-4 independent experiments.

1148 Table 2. Selection of diamidine analogues with aromatic linkers

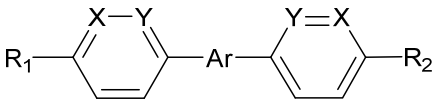


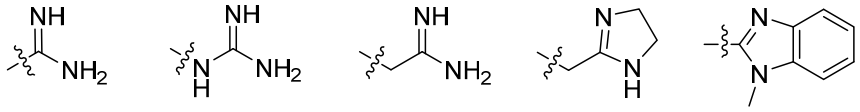


1149

| Compound | $R_1$ | $R_2$ | Ar | X | Y | $K_i$ (μM) | $\delta(\Delta G^0)$ PMD (kJ/mol) |
|---|---|---|---|---|---|---|---|
| DB75 | Am | Am | 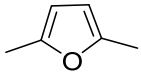 | CH | CH | 38.2 ± 10.2 | 17.3 |
| DB607 | Am | $OCH_3$ | 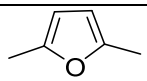 | CH | CH | 18.1 ± 1.9 | 15.5 |
| DB960 | Am | NMB[a] | 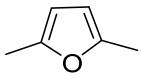 | CH | CH | 16.6 ± 3.5 | 15.3 |
| DB994 | Am | Am | 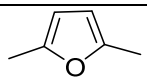 | N | CH | 167 ± 20 | 21.0 |
| DB829 | Am | Am | 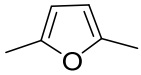 | CH | N | 39.9 ± 8.0 | 17.4 |
| DB1061 | EtAm | EtAm | 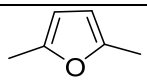 | CH | CH | 32.3 ± 6.0 | 16.9 |
| DB1062 | 2MeIm | 2MeIm | 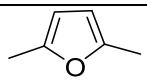 | CH | CH | 59.6 ± 11.2 | 18.4 |
| ER1004 | Am | Am | 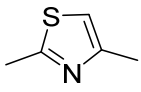 | CH | CH | 68.7 ± 16.0 | 18.8 |
| DB320 | Am | Am | 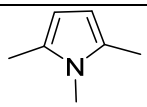 | CH | CH | 71.3 ± 12.1 | 18.9 |

| | | | | | | | |
|---|---|---|---|---|---|---|---|
| DB686 | Gua | Gua | 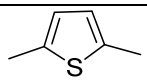 | CH | CH | 0.29 ± 0.11 | 5.2 |
| DB1063 | EtAm | EtAm | 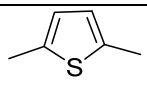 | CH | CH | 0.40 ± 0.10 | 6.0 |
| DB1064 | 2MeIm | 2MeIm | 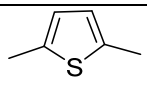 | CH | CH | 3.0 ± 0.82 | 11.0 |
| DB1213 | Am | Am | 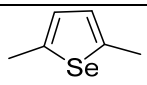 | CH | CH | 0.72 ± 0.17 | 7.5 |
| DB1077 | Am | Am | 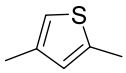 | CH | CH | 13.8 ± 3.1 | 14.8 |
| DB914 | Am | Am | 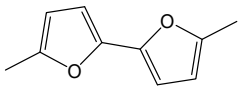 | CH | CH | 0.073 ± 0.013 | 1.8 |

Am, amidine; Im, imidazole; EtAm, ethylamidine; 2MeIm, 2-methylimidazoline; NMB, *N*-methyl benzimidazole. [a]This compound lacks the second benzene ring and features the terminal NMB moiety instead. $K_i$ is the inhibition constant for [$^3$H]-pentamidine transport by TbAQP2/HAPT1. $\delta(\Delta G^0)$ PMD is the difference in Gibbs Free Energy of interaction of the substrate with TbAQP2 with the same value for pentamidine (PMD). All $K_i$ values are the average and SEM of at least 3-4 independent experiments.

# Supplemental Materials with:

## Pentamidine enters *Trypanosoma brucei* by passing through the pore of the aquaglyceroporin TbAQP2

Ali H. Alghamdi[1], Jane C. Munday[1], Gustavo D. Campagnaro[1], Dominik Gurvič[2], Fredrik Svensson[3], Chinyere E. Okpara[4], Arvind Kumar ,[5] Maria Esther Martin Abril[1], Patrik Milić[1], Laura Watson[1], Daniel Paape,[1] Luca Settimo,[1] Anna Dimitriou[1], Joanna Wielinska[1], Graeme Smart[1], Laura F. Anderson[1], Christopher M. Woodley,[4] Siu Pui Ying Kelley[1], Hasan M.S. Ibrahim[1], Fabian Hulpia[6] , Mohammed I. Al-Salabi[1], Anthonius A. Eze[1], Ibrahim A. Teka[1], Simon Gudin[1], Christophe Dardonville[7], Richard R Tidwell[8], Mark Carrington[9], Paul M. O'Neill[4], David W Boykin[5], Ulrich Zachariae[2], Harry P. De Koning[1,*]

Content:


| *Supplemental figures* | page |
|---|---|
| Supplemental Figure S1 | 2 |
| Supplemental Figure S2 | 5 |
| Supplemental Figure S3 | 7 |
| Supplemental Figure S4 | 8 |
| Supplemental Figure S5 | 10 |
| Supplemental Figure S6 | 11 |
| Supplemental Figure S7 | 12 |
| | |
| *Supplemental tables* | |
| Supplemental Table S1 | separate file |
| Supplemental Table S2 | 14 |
| Supplemental Table S3 | 15 |
| | |
| *Chemical synthesis and analysis of new compounds* | |
| Paul O'Neill laboratory | 16 |
| Dave Boykin laboratory | 24 |

A.

```
Tco       MTSPTVPNPMSTVPMTEM----TE-ANGTTNPPIPDAGERTAV---NFDTEQCK-TKEIL  51
Tbr1      MSD--EKINVHQYPSETDVRGLKARNGGACEVPFEENN-EPIPNRSANPQEKNE--NELV  55
Tsu1      MSS--EPVNVHRYTAEGDRSGLKDRHGKTCEVCVGDESAAAVPSAVYNPQEQSGDGPEVK  58
Tsu2      MQN--QPDAMTH-STAVQMV-NKNPEDGTGGADTERSDEMTAP--------TTRTGDAQK  48
Tbr2      MQS--QPDNVAY-PMELQAV-NKDGT---VEVRVQGNVDNSSN--------ERWDADVQK  45
Tbr3      MQS--QPDNVAY-PMELQAV-NKDGT---VEVRVQGNDDSS----------------NRK  37
          * .      :             .

Tco       -AGEGEAPHGPMDINYWPLRNLRMDFREYVGEFLGTFVLLFMGNGVVATTLLDNNLGFLS  110
Tbr1      GDNADNEAHDAVDVNYWAPRQLRLDYRNYMGEFLGTFVLLFMGNGVVATTILDKDLGFLS  115
Tsu1      AGGGEAEVQNAADVNNWAPRRLRLDYRDYMGEFLGTFVLLFMGNGVVATTMLDDGLGFLS  118
Tsu2      CETTNTPKEGAGGINYWAPRELRLKYRDYMGELLGTFVLLLMGNGVVATVVVDGKLGFLS  108
Tbr2      HEVAEAQEKPVGGINFWAPRELRLNYRDYVAEFLGNFVLIYIAKGAVITSLLVPDFGLLG  105
Tbr3      HEVAEAQEEVPGGINFWAPRELRLNYRDYMGELLGTFVLLFMGNGVVATVIIDGKLGFLS  97
                    .   .:* *  *.**:.:*:*:.*:**.***: :.:*.* * ::   :*:*.

Tco       ITFGWGIAVTMGLYVSLGTSSGHLNPAVTVANAFFGGFPWKKVPGYIAMQMLGAFVGAAC  170
Tbr1      ITLGWGIAVTMGLYISLGISCGHLNPAVTLANAVFGCFPWRRVPGYIAAQMLGAFVGAAC  175
Tsu1      ITLGWGIAVTMGLYISLGTSCGHLNPAVTVANAVFGCFPWKKVAGYIAMQMLGAFVGAAC  178
Tsu2      ITLGWGIAVTMALYISLGISSGHLNPAVTVGNAVFGDFPWRKVPGYIAAQMFGAFLGAAC  168
Tbr2      LTIGIGVAVTMALYVSLGISGGHLNSAVTVGNAVFGDFPWRKVPGYIAAQMLGTFLGAAC  165
Tbr3      ITLGWGIAVTMALYVSLGISSGHLNPAVTVGNAVFGDFPWRKVPGYIAAQMLGAFLGAAC  157
          :*:* *:****.**:*** * **** ***:.**.** ***::* **** **:*:*:****

Tco       AYGVYADLLNKKVSDG----EIEDYAGMFSTYPRDGNSLFSCIFGEFICTAMLTFCVCGI  226
Tbr1      AYGVYADLLKQHSGG-LVGFGDKGFAGMFSTYPREGNRLFYCIFSEFICTAILLFCVGGI  234
Tsu1      AYGVFADLLKQHSGG-LIPFGDKGFAGMFSTYPRDGNRLFYCIFGEFICTAMLLFCVSGI  237
Tsu2      AYGVFADLLKEYCGGKLLAFGAKGIAGVFSTYPKEANSVFACVFGEFICTAILLFCVCGI  228
Tbr2      AYGVFADLLKAHGGGELIAFGEKGIAWVFAMYPAEGNGIFYPIFAELISTAVLLLCVCGI  225
Tbr3      AYGVFADLLKAHGGGELIAFGEKGTAGVFSTYPRDSNGLFSCIFGEFICTAMLLFCVCGI  217
          ****:****:   ..       :. * :*: ** :.* :*  :*.*:*.**:* :** **

Tco       FDTHNAPATGHEPLAVGALVFAIGNNVGYATGYAINPARDFGPRVFSAILYGSTVFTRGD  286
Tbr1      FDPNNSPAKGHEPLAVGALVFAIGNNIGYASGYAINPARDFGPRVFSAILFGSEVFTTGN  294
Tsu1      FDANNSPAKGHEPLAVGALVFAIGNNIGYATGYAINPARDFGPRLFSAILFGSEVFTAGN  297
Tsu2      FDPNNSPAKKHEPLAVGSLIFAIGNNIGYSTGYAMNPARDFAPRVFSALLLGGEVFSHGN  288
Tbr2      FDPNNSPAKGYETVAIGALVFVMVNNFGLASPLAMNPSLDFGPRVFGAILLGGEVFSHAN  285
Tbr3      FDPNNSPAKGHEPLAVGALVFAIGNNIGYSTGYAINPARDFGPRVFSSFLYGGKVFSHAN  277
          ** :*:**. :* :*:*:*:*.: **.* ::  *:**: **.**:*.::* *. **: .:

Tco       YYFWVPLFIPLLGGIFGIILYKYFVPH     313
Tbr1      YYFWVPLFIPFLGGIFGLFLYKYFVPY     321
Tsu1      YYFWVPLFIPFLGGIFGLLLYKYFVPH     324
Tsu2      YYFWVPLFIPFLGAIFGLFLYKYFVPH     315
Tbr2      YYFWVPLVVPFFGAILGLFLYKYFLPH     312
Tbr3      YYFWVPLVIPLFGGIFGLFLYKYFVPH     304
          *******.:*::*.*:*::*****:*:
```

```
>Tco AQP1
MTSPTVPNPMSTVPMTEMTEANGTTNPPIPDAGERTAVNFDTEQCKTKEILAGEGEAPHGPMDINYWPLRNLRMD
FREYVGEFLGTFVLLFMGNGVVATTLLDNNLGFLSITFGWGIAVTMGLYVSLGTSSGHLNPAVTVANAFFGGFPW
KKVPGYIAMQMLGAFVGAACAYGVYADLLNKKVSDGEIEDYAGMFSTYPRDGNSLFSCIFGEFICTAMLTFCVCG
IFDTHNAPATGHEPLAVGALVFAIGNNVGYATGYAINPARDFGPRVFSAILYGSTVFTRGDYYFWVPLFIPLLGG
IFGIILYKYFVPH

>Tbr AQP1
MSDEKINVHQYPSETDVRGLKARNGGACEVPFEENNEPIPNRSANPQEKNENELVGDNADNEAHDAVDVNYWAPR
QLRLDYRNYMGEFLGTFVLLFMGNGVVATTILDKDLGFLSITLGWGIAVTMGLYISLGISCGHLNPAVTLANAVF
GCFPWRRVPGYIAAQMLGAFVGAACAYGVYADLLKQHSGGLVGFGDKGFAGMFSTYPREGNRLFYCIFSEFICTA
ILLFCVGGIFDPNNSPAKGHEPLAVGALVFAIGNNIGYASGYAINPARDFGPRVFSAILFGSEVFTTGNYYFWVP
LFIPFLGGIFGLFLYKYFVPY

>Tbr AQP2
```

```
MQSQPDNVAYPMELQAVNKDGTVEVRVQGNVDNSSNERWDADVQKHEVAEAQEKPVGGINFWAPRELRLNYRDYV
AEFLGNFVLIYIAKGAVITSLLVPDFGLLGLTIGIGVAVTMALYVSLGISGGHLNSAVTVGNAVFGDFPWRKVPG
YIAAQMLGTFLGAACAYGVFADLLKAHGGGELIAFGEKGIAWVFAMYPAEGNGIFYPIFAELISTAVLLLCVCGI
FDPNNSPAKGYETVAIGALVFVMVNNFGLASPLAMNPSLDFGPRVFGAILLGGEVFSHANYYFWVPLVVPFFGAI
LGLFLYKYFLPH

>Tbr AQP3
MQSQPDNVAYPMELQAVNKDGTVEVRVQGNDDSSNRKHEVAEAQEEVPGGINFWAPRELRLNYRDYMGELLGTFV
LLFMGNGVVATVIIDGKLGFLSITLGWGIAVTMALYVSLGISSGHLNPAVTVGNAVFGDFPWRKVPGYIAAQMLG
AFLGAACAYGVFADLLKAHGGGELIAFGEKGTAGVFSTYPRDSNGLFSCIFGEFICTAMLLFCVCGIFDPNNSPA
KGHEPLAVGALVFAIGNNIGYSTGYAINPARDFGPRVFSSFLYGGKVFSHANYYFWVPLVIPLFGGIFGLFLYKY
FVPH

>Tsu AQP1
MSSEPVNVHRYTAEGDRSGLKDRHGKTCEVCVGDESAAAVPSAVYNPQEQSGDGPEVKAGGGEAEVQNAADVNNW
APRRLRLDYRDYMGEFLGTFVLLFMGNGVVATTMLDDGLGFLSITLGWGIAVTMGLYISLGTSCGHLNPAVTVAN
AVFGCFPWKKVAGYIAMQMLGAFVGAACAYGVFADLLKQHSGGLIPFGDKGFAGMFSTYPRDGNRLFYCIFGEFI
CTAMLLFCVSGIFDANNSPAKGHEPLAVGALVFAIGNNIGYATGYAINPARDFGPRLFSAILFGSEVFTAGNYYF
WVPLFIPFLGGIFGLLLYKYFVPH

>Tsu AQP2
MQNQPDAMTHSTAVQMVNKNPEDGTGGADTERSDEMTAPTTRTGDAQKCETTNTPKEGAGGINYWAPRELRLKYR
DYMGELLGTFVLLLMGNGVVATVVVDGKLGFLSITLGWGIAVTMALYISLGISSGHLNPAVTVGNAVFGDFPWRK
VPGYIAAQMFGAFLGAACAYGVFADLLKEYCGGKLLAFGAKGIAGVFSTYPKEANSVFACVFGEFICTAILLFCV
CGIFDPNNSPAKKHEPLAVGSLIFAIGNNIGYSTGYAMNPARDFAPRVFSALLLGGEVFSHGNYYFWVPLFIPFL
GAIFGLFLYKYFVPH
```

B.

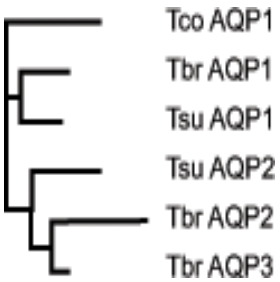


C.

| | dN/dS |
|---|---|
| T. brucei AQP1 v T. suis AQP1 | 0.21 |
| T. brucei AQP3 v T. suis AQP3 | 0.30 |
| T. brucei AQP2 v T. brucei AQP3 | 2.00 |

**Figure S1.**
A. Sequence alignment and individual sequences of the *T. congolense*, *T. b. brucei* and *T. suis*. The *T. brucei* and *T. congolense* sequences were obtained from tritrypDB, *T. suis* sequences (Kelly S, Gibson W and Carrington M. The genome of *Trypanosoma suis*. In preparation). The alignment was produced with Clustal Omega. The yellow highlighting indicates the N-terminus of the sequences used to determine non-synonymous v synonymous ratios.

B. Phylogenetic tree of these sequences. The tree is a Neighbour-joining tree produced in Clustal Omega with the lengths of the horizontals proportional to the differences.

C. The ratio of non-synonymous v synonymous (dN/dS) codon changes calculated for selected comparisons between *T. brucei* and *T. suis* AQPs. The ratios were calculated using a region of high confidence alignments from ~amino acid 60 (highlighted in Supplemental Figure 2A) to the C-terminus.

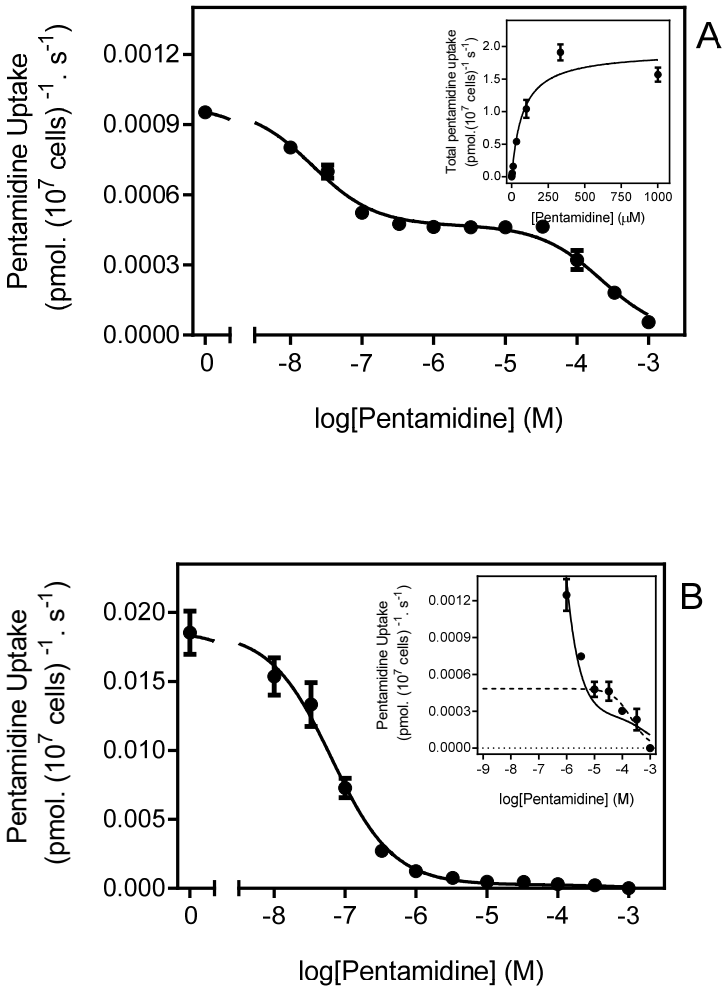


**Fig. S2. Pentamidine transport analysis for TbAQP2$^{I190T}$ and TbAQP2WT**. (A) Transport of 30 nM [$^3$H]-pentamidine by *tbaqp2/tbaqp3* null cells expressing TbAQP2$^{I190T}$, in the presence of unlabelled pentamidine at the indicated concentrations. Incubation time was 15 min, required to ensure sufficient radiolabel for accurate quantification, and uptake was linear and through zero over this period. The inhibition data were plotted to a double sigmoidal curve (Prism 7.0) with the bottom value fixed at 0. The high affinity component displayed an average an $IC_{50}$ of 30.9 ± 12.2 nM (n=3) and the lower affinity segment could be converted to a Michaelis-Menten plot for determination of $K_m$ and $V_{max}$ (inset), yielding an average $K_m$ of 59.9 ± 9.1 μM (n=3). The plot shown is one representative experiment in triplicate of three independent experiments. (B) Like (A) but with *tbaqp2/tbaqp3* null cells expressing TbAQP2WT. Incubation time was 20 s (linear phase). The high affinity phase had statistically identical $EC_{50}$ (41 ± 17 nM; P>0.05) as TbAQP2$^{I190T}$. The inset shows a zoom-in

on the low-affinity part of the curve, with the dotted line representing a theoretical sigmoid plot for 1 inhibitor, with the upper limit fixed at the value obtained for 10 μM pentamidine. The low affinity component was also statistically identical in the two strains (TbAQP2-WT $K_m$ = 82.7 ± 17.5 μM (n=3; P>0.05)). Note that the amount of [$^3$H]-pentamidine taken up by the low affinity component is highly similar for the mutant (A) and control (B) cell lines, at approximately 0.0005 pmol($10^7$ cells)$^{-1}$s$^{-1}$. Both frames show one representative experiment of three repeats, each performed in triplicate. Error bars are SEM, when not shown, fall within the symbol.

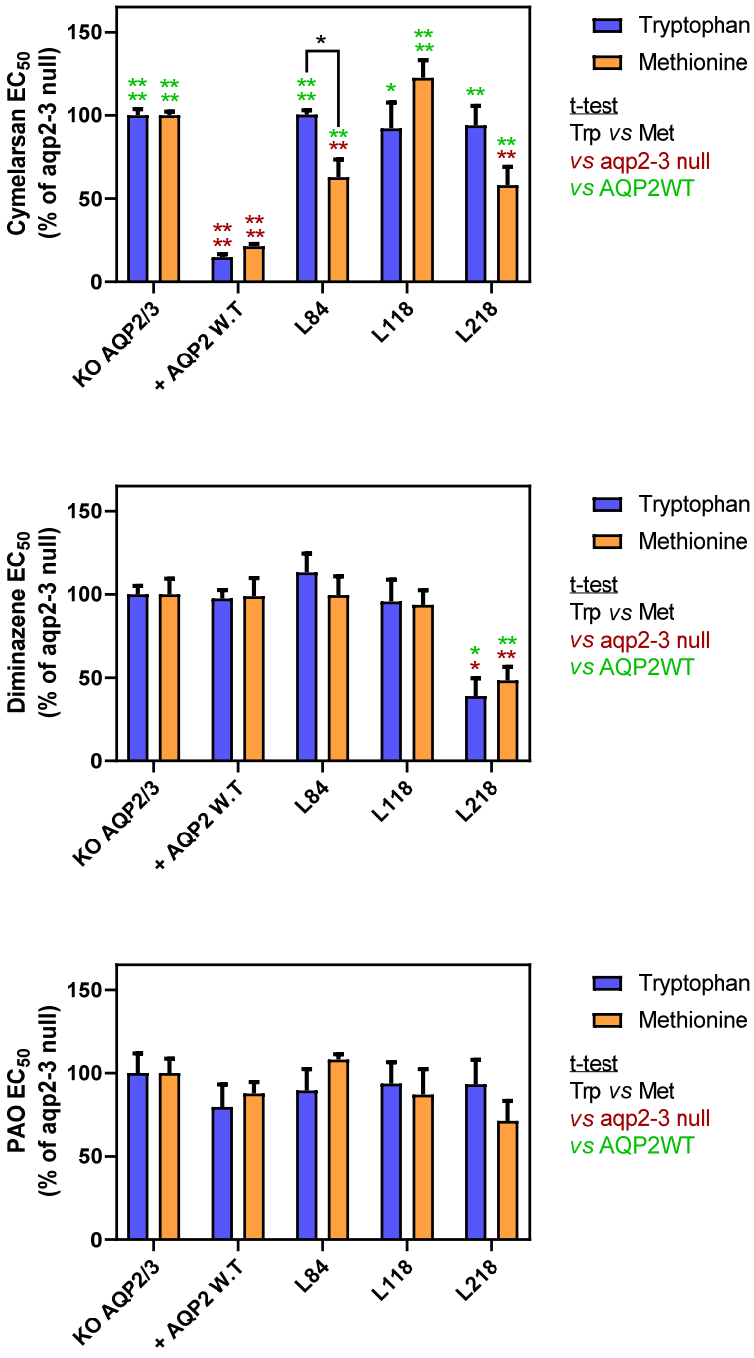


**Figure S3.** $EC_{50}$ values for Cymelarsan, diminazene aceturate and phenylarsine oxide (PAO) against the *tbaqp2-tbaqp3* null cell line. AQP2-WT and various mutant versions thereof (indicated) were expressed in this cell line. EC50 values were determined using the alamar blue (resazurin) assay. Bars represent the average and SEM for at least three determinations. nd, not done.

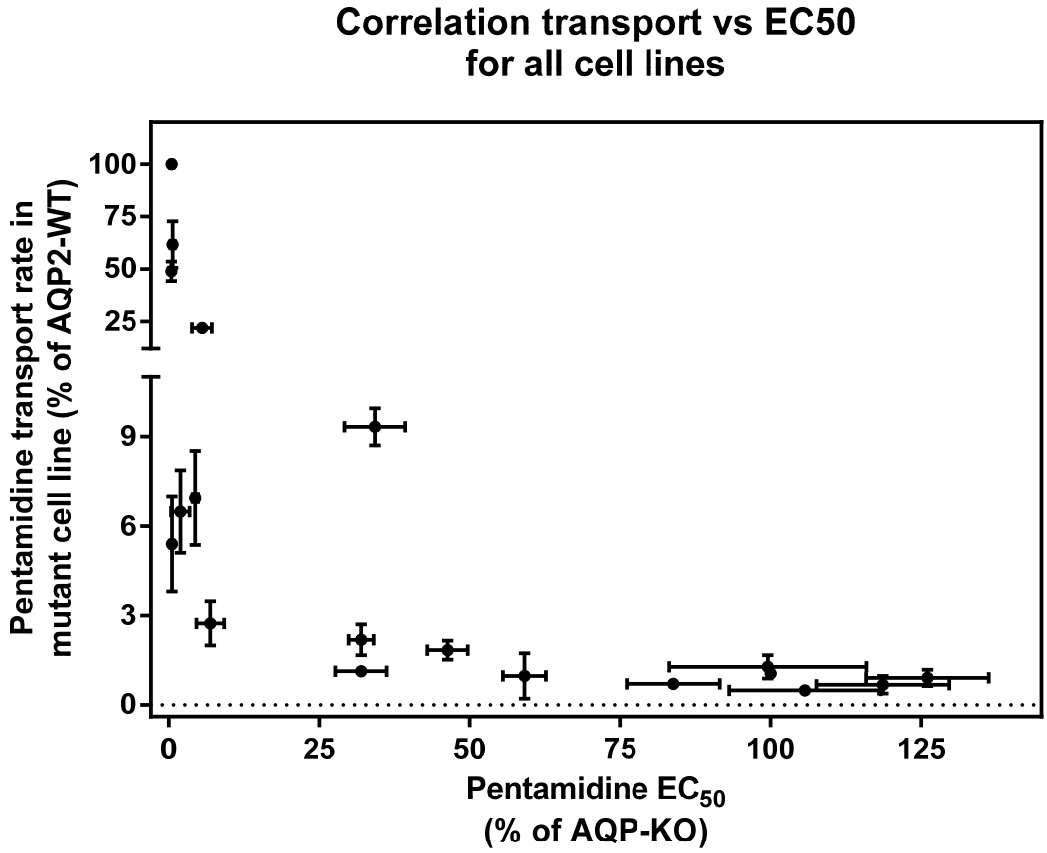


| Strain | EC50 | | Transport rate | |
|---|---|---|---|---|
| | AVG | SEM | AVG | SEM |
| 2T1 | 5.52 | 1.65 | 21.86 | 2.34 |
| AQKO | 100 | 0 | 1.05 | 0.16 |
| +AQP2-WT | 0.46 | 0.27 | 100 | 0 |
| +L264R | 126.1 | 10.2 | 0.91 | 0.28 |
| +L258Y | 0.5 | 0.24 | 5.4 | 1.6 |
| +S131P/S263A | 1.92 | 1.53 | 6.48 | 1.39 |
| +I190T/W192G | 99.52 | 16.4 | 1.27 | 0.4 |
| + I190T | 6.89 | 2.28 | 2.728 | 0.744 |
| +AQP2 I110W | 118.7 | 11.0 | 0.673 | 0.296 |
| +AQP3 WT | 105.7 | 12.6 | 0.48 | 0.1 |
| +AQP3 W102I/R256L | 83.83 | 7.7 | 0.7 | 0.18 |
| +AQP3 W102I/Y250L/R256L | 31.94 | 4.25 | 1.13 | 0.1 |
| +L218W | 4.4 | 0.45 | 6.94 | 1.58 |
| +L118W | 46.3 | 3.36 | 1.83 | 0.32 |
| +L84W | 31.98 | 2.08 | 2.18 | 0.52 |
| +L84W/L118W | 59.1 | 3.58 | 0.97 | 0.76 |
| +L84M | 0.43 | 0.09 | 48.84 | 4.68 |
| +L118M | 34.24 | 5.03 | 9.33 | 0.63 |

| | | | | |
|---|---|---|---|---|
| +L218M | 0.63 | 0.34 | 61.65 | 11.17 |

**Figure S4.** Correlation of the $EC_{50}$ value with the rate of pentamidine transport for all 19 cell lines expressing a wild-type or mutant TbAQP2 in the aqp2/3 null *T. b. brucei line*. All $EC_{50}$ values are expressed as percentage of the resistant control, aqp2/3 null transfected with an empty vector (no TbAQP2). 2T1 is the parental cell line of the aqp2/3 null. All values are the average of at least three independent determinations; the sensitive and resistant control cell lines were included in each independent experiment and the percentages taken are from the internal control rather than from the grand average over all experiments.

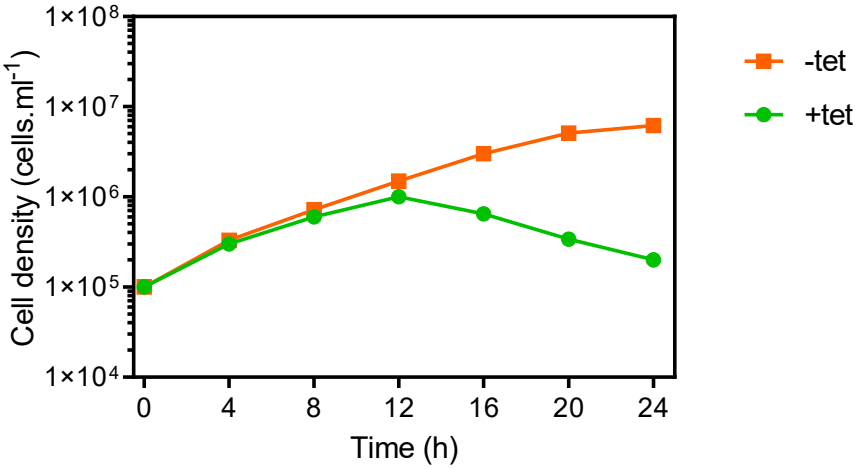


**Figure S5**. Growth Curve of CRK12 RNAi cells in full HMI-9 medium at 37 ºC/5% $CO_2$, in the presence or absence of 1 µg/ml tetracycline (tet). Cell counts were performed with a haemocytometer and the average of duplicate determinations is shown.

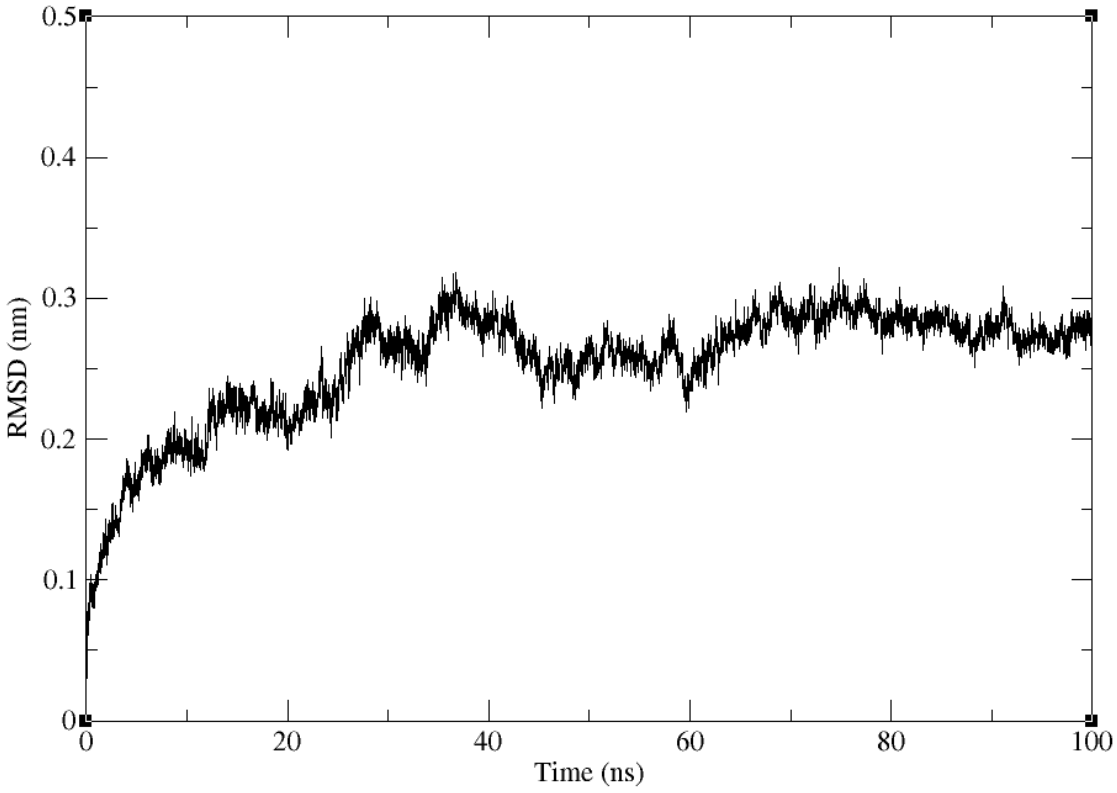


**Figure S6**. Backbone RMSD of the protein inserted into a lipid bilayer showing convergence to ~3 Å in a simulation of 100 ns length.

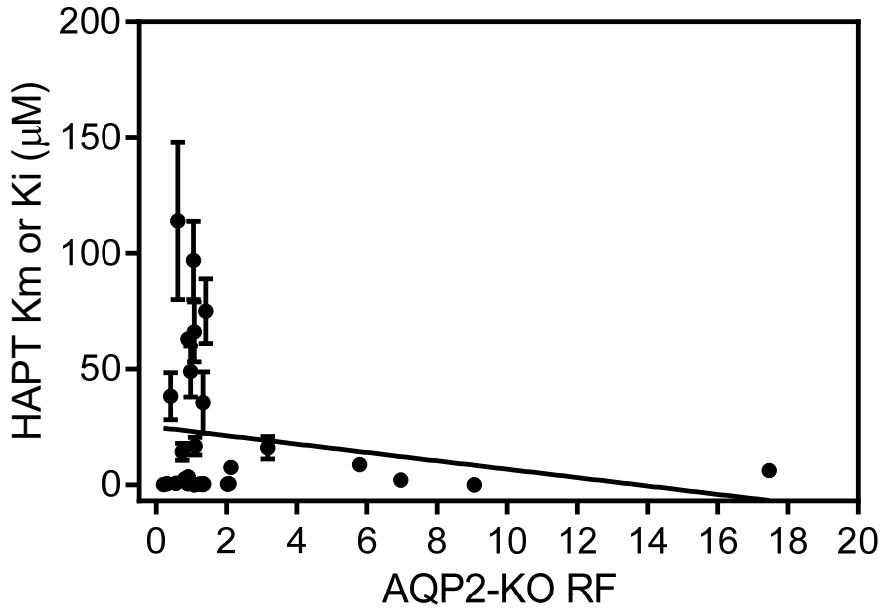


| | AQP2-KO RF | Ki value HAPT1 | |
|---|---|---|---|
| | AVG | AVG | SEM |
| pentamidine | 9.06 | **0.036** | **0.0006** |
| RT12 | 0.74 | 14.3 | 3.6 |
| RT14 | 1.08 | 0.061 | 0.015 |
| RT43 | 1.33 | 0.51 | 0.15 |
| RT52 | 5.79 | 8.84 | 0.88 |
| Diminazene | 0.9 | 63 | 3 |
| DB75 | 0.4 | 38.25 | 10.2 |
| DB902 | 0.61 | 114 | 34 |
| DB1111 | 0.2 | 0.14 | 0.03 |
| DB1213 | 0.55 | 0.72 | 0.17 |
| DB1225 | 0.3 | 0.54 | 0.25 |
| CHI/1/72/1 | 0.8 | 2.6 | 0.68 |
| RT05 | 2.07 | 0.57 | 0.18 |
| RT13 | 3.17 | 16.1 | 4.9 |
| RT18 | 2.02 | 0.26 | 0.09 |
| RT24 | 1.31 | 0.12 | 0.03 |
| RT26 | 1.28 | 0.34 | 0.07 |
| RT30 | 1.35 | 0.3 | 0.07 |
| RT36 | 0.9 | 0.43 | 0.07 |
| RT44 | 1.1 | 16.78 | 3.93 |
| RT45 | 2.13 | 7.52 | 0.14 |
| RT01 | 0.97 | 49 | 11 |
| RT02 | 1.08 | 66 | 13 |
| RT08 | 1.41 | 75 | 14 |
| RT10 | 1.33 | 35.6 | 13.4 |

| | | | |
|---|---|---|---|
| RT32 | 1.23 | 0.4 | 0.008 |
| RT48 | 6.97 | 2.01 | 0.86 |
| RT50 | 17.47 | 6.27 | 1.3 |
| Isometamidium | 0.91 | 3.5 | 0.5 |
| Ethidium | 1.05 | 97 | 17 |

**Figure S7.** Correlation between the Resistance Factor (RF; $EC_{50}$(aqp2/3 null)/$EC_{50}$(TbAQP2-WT)) and the $K_i$ value for inhibition of the High Affinity Pentamidine Transporter (HAPT1) encoded by TbAQP2. The pentamidine value (bold) is the $K_m$ determined with radiolabeled pentamidine. The table lists the data points shown in the plot. The line was made by linear regression (Prism 6.0); correlation coefficient $r^2$ is 0.039. F-test: slope is not significantly different from zero ($P = 0.29$).

**Supplemental Table S2: primers used for mutations in TbAQP2**

| Mutation | Primer | Sequence (altered base(s) underlined) | Generated Plasmid | Original Template |
|---|---|---|---|---|
| S131P/S263A | S131P: HDK1062 | CTCCGGTGGCCATCTCAACCCTGCCGTCACCGTTGGCAA | pHDK166 | pRPa$^{GFP-AQP2}$ |
| | S131P: HDK1063 | TTGCCAACGGTGACGGCAGGGTTGAGATGGCCACCGGAG | | |
| | S263A: HDK1064 | TCTCCCCTTGCGATGAATCCCGCACTTGATTTCGGTCCCAGGG | | |
| | S263A: HDK1065 | CCCTGGGACCGAAATCAAGTGCGGGATTCATCGCAAGGGGAGA | | |
| I110W | HDK607 | CTCGGTCTTACGATTGGTTGGGGTGTGGCTGTCACGATG | pHDK84 | pRPa$^{GFP-AQP2}$ |
| | HDK608 | CATCGTGACAGCCACACCCCAACCAATCGTAAGACCGAG | | |
| L264R | HDK609 | TCTCCCCTTGCGATGAATCCCTCACGTGATTTCGGTCCCAGGGTCTTC | pHDK167 | pRPa$^{GFP-AQP2}$ |
| | HDK610 | GAAGACCCTGGGACCGAAATCACGTGAGGGATTCATCGCAAGGGGAGA | | |
| I110W/L264R | L264R: HDK609 | TCTCCCCTTGCGATGAATCCCTCACGTGATTTCGGTCCCAGGGTCTTC | pHDK78 | pHDK84 |
| | L264R: HDK610 | GAAGACCCTGGGACCGAAATCACGTGAGGGATTCATCGCAAGGGGAGA | | |
| L258Y | HDK1109 | CAACTTCGGCTTAGCGTCTCCCTATGCGATGAATCCCTCACTTGAT | pHDK168 | pRPa$^{GFP-AQP2}$ |
| | HDK1110 | ATCAAGTGAGGGATTCATCGCATAGGGAGACGCTAAGCCGAAGTTG | | |
| I190T | HDK1056 | GCCTTCGGTGAAAAGGGGACTGCGTGGGTGTTTGCCATG | pHDK163 | pRPa$^{GFP-AQP2}$ |
| | HDK1057 | CATGGCAAACACCCACGCAGTCCCCTTTTCACCGAAGGC | | |
| W192G | HDK1058 | CGGTGAAAAGGGGATTGCGGGGGTGTTTGCCATGTACCC | pHDK164 | pRPa$^{GFP-AQP2}$ |
| | HDK1059 | GGGTACATGGCAAACACCCCCGCAATCCCCTTTTCACCG | | |
| I190T/W192G | HDK1060 | GCCTTCGGTGAAAAGGGGACTGCGGGGGTGTTTGCCATGTACCC | pHDK165 | pHDK163 |
| | HDK1061 | GGGTACATGGCAAACACCCCCGCAGTCCCCTTTTCACCGAAGGC | | |
| L84W | HDK1276 | AAACTTCGTCTGGATATATATCGCTAAGGG | pHDK210 | pRPa$^{GFP-AQP2}$ |
| | HDK1277 | CCCAGAAATTCAGCCACG | | |
| L118W | HDK1274 | CACCGCAGTGTGGCTGCTCTGTG | pHDK208 | pRPa$^{GFP-AQP2}$ |
| | HDK1275 | GAAATGAGTTCAGCAAAAATTG | | |
| L218W | HDK1272 | CACGATGGCTTGGTATGTTTCACTG | pHDK209 | pRPa$^{GFP-AQP2}$ |
| | HDK1273 | ACAGCCACACCAATACCA | | |
| L84W/L118W | HDK1276 | AAACTTCGTCTGGATATATATCGCTAAGGG | pHDK227 | pHDK208 |
| | HDK1277 | CCCAGAAATTCAGCCACG | | |
| L84M | HDK1364 | AAACTTCGTCATGATATATATCGCTAAGG | pHDK234 | pHDK210 |
| | HDK1367 | GAAATGAGTTCAGCAAAAATTGGATAAAATATAC | | |
| L118M | HDK1365 | CACGATGGCTATGTATGTTTCAC | pHDK235 | pHDK208 |
| | HDK1367 | GAAATGAGTTCAGCAAAAATTGGATAAAATATAC | | |
| L218M | HDK1366 | CACCGCAGTGATGCTGCTCTGTG | pHDK236 | pHDK209 |
| | HDK1367 | GAAATGAGTTCAGCAAAAATTGGATAAAATATAC | | |

**Supplemental Table S3: primers used for mutations in TbAQP3**

| Mutations | Primer | Sequence (altered base(s) underlined) | Plasmid | Template |
|---|---|---|---|---|
| W102I/R256L | W102I: HDK511 | CTCAGCATTACGCTTGGTATCGGCATTGCCGTCACGATG | pHDK71 | pRPa$^{GFP-AQP3}$ |
| | W102I: HDK512 | CATCGTGACGGCAATGCCGATACCAAGCGTAATGCTGAG | | |
| | R256L: HDK513 | TACGCAATAAATCCGGCTCTTGACTTCGGTCCCAGGGTC | | |
| | R256L: HDK514 | GACCCTGGGACCGAAGTCAAGAGCCGGATTTATTGCGTA | | |
| W102I/R256L/Y250L | Y250L HDK795 | CATCGGTTACTCAACGGGTCTCGCAATAAATCCGGCTCTT | pHDK121 | pHDK71 |
| | Y250L HDK796 | AAGAGCCGGATTTATTGCGAGACCCGTTGAGTAACCGATG | | |

# Chemistry of new compounds from Paul O'Neill laboratory.

**1,2-Bis (4-cyanophenoxy) ethane** (Ethamidine Precursor) **(1a)** [1]

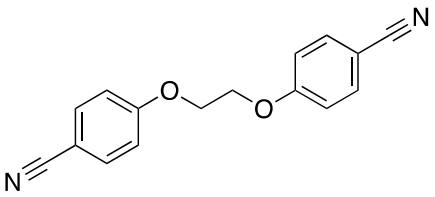

Sodium (0.16 g, 6.96 mmol) was added portionwise to anhydrous EtOH (4.0 mL) under an atmosphere of nitrogen. After dissolution of the sodium pieces, a solution of 4-cyanophenol (0.75 g, 6.38 mmol) dissolved in anhydrous EtOH (4.0 mL) was added followed by dropwise addition of 1,2-dibromoethane (0.28 mL, 3.19 mmol). The reaction mixture was allowed to stir at reflux under a nitrogen atmosphere for 3 days after which the mixture was cooled, filtered, the solid washed with water and dried under vacuum. Purification by column chromatography eluting with DCM: hexane (8:2) gave the desired dinitrile ethamidine precursor (**1a**) as a white solid (1.42 g, 84%). Mp 211-212°C; $^{1}$H NMR ($CDCl_3$, 400MHz) δ 7.61 (d, 4H, *J* = 9.0 Hz, ArH), 7.01 (d, 4H, *J* = 9.0 Hz, ArH), 4.39 (s, 4H, $CH_2$); $^{13}$C NMR ($CDCl_3$, 100MHz) δ 161.6, 134.1, 118.9, 115.3, 104.7, 66.4; $\nu_{max}$ (NujOI) /cm$^{-1}$ 3326 (C-O-C), 3033 (ArH), 2898 (OH), 2223 (CN), 1602 (Ar), 1509 (Ar), 1247 (C-O-C); *m/z* (CI) 282 ($[M+NH_4]^+$), found 282.12433, $C_{16}H_{16}O_2N_3$ requires 282.12424; anal. Found C 72.37, H 4.51, N 10.54, $C_{16}H_{12}O_2N_2$ requires C 72.71, H 4.57, N 10.60.

**4,4'-(ethane-1,2-diylbis(oxy))dibenzimidamide dihydrochloride dihydrate** (Ethamidine, Compound CHI/1/30/1) (**2**) [1]

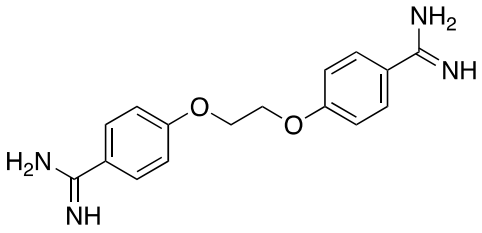

(0.51 g, 1.92 mmol) of **1a** was dissolved in a mixture of anhydrous benzene (54 mL) and EtOH (2.90 mL), cooled to 0 °C and saturated with HCl gas. The mixture was sealed and allowed to stir at room temperature for 3 days after which anhydrous $Et_2O$ (28 mL) was introduced and the mixture was allowed to stir for 10 minutes. The solids were filtered under nitrogen and dissolved in a mixture of anhydrous EtOH (36 mL) and EtOH.$NH_3$ (36 mL). The mixture was heated overnight (50 °C), cooled to room temperature and reduced by half *in vacuo*. Ether was added to precipitate the solid which was filtered, washed and dried under vacuum. Purification by recrystallisation (2N HCl) gave the desired compound **2** as fine white needles (0.54 g, 70%). Mp 333°C; $^{1}$H NMR (MeOD, 400MHz) δ 7.85 (d, 4H, *J* = 9.0 Hz, ArH), 7.23 (d, 4H, *J* = 9.0 Hz, ArH), 4.52 (s, 4H, $CH_2$); $^{13}$C NMR (MeOD, 100MHz) δ 167.9, 165.3, 131.5, 121.7, 116.7, 68.5; $\nu_{max}$ (Nujol) /cm$^{-1}$ 3362 (NH), 3037 (ArH), 2940 (C-H), 1658 (C=N-H), 1606 (Ar), 1505 (Ar), 1245 (C-0-C); *m/z* (ESP) 299 ($[M-H]^-$); anal. Found C 47.54 H 5.62 N 14.30, $C_{16}H_{24}N_4O_4Cl_2$ requires C 47.18, H 5.94, N 13.76.

**4, 4'-(propane-1,3-diylbis(oxy))dibenzonitrile** (Propamidine Precursor) (**1b**)[1]

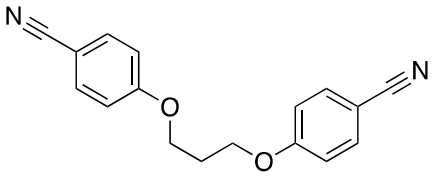

Sodium (0.16 g, 6.96 mmol) was added portionwise to anhydrous EtOH (4.0 mL) with stirring under an atmosphere of nitrogen. After dissolution of Na, a solution of 4-cyanophenol (0.75 g, 6.38 mmol) dissolved in dry ethanol (4.0 mL) was added followed by dropwise addition of 1,3-dibromopropane (0.32 mL, 3.19 mmol). The reaction mixture was allowed to stir at reflux under a nitrogen atmosphere for 3 days after which the mixture was cooled, filtered, the solid washed with water and dried under vacuum. Purification by column chromatography eluting with DCM: hexane (8:2) gave the desired compound **1b** as a white solid (1.40 g, 79%). Mp 190-191°C; $^{1}$H NMR ($CDCl_3$, 400MHz) δ 7.59 (d, 4H, *J* = 8.5 Hz, ArH), 6.96 (d, 4H, *J* = 8.5 Hz, ArH), 4.20 (t, 4H, *J* = 6.0 Hz, $CH_2$), 2.32 (m, 2H, $CH_2$); $^{13}$C NMR ($CDCl_3$, 100MHz) δ 161.9, 134.0, 119.1, 115.1, 104.2, 64.4, 28.8; $\nu_{max}$ (Nujol) /cm$^{-1}$ 3104 (Ar-H), 2823 (C-H), 2221 (C≡N), 1604 (Ar), 1509 (Ar), 1253 (C-O); *m/z* (CI) 296 ($[M+NH_4]^+$), found 296.14037, $C_{17}H_{18}N_3O_2$ requires 296.13992; anal. Found C 73.22, H 5.13, N 10.03, $C_{17}H_{14}N_2O_2$ requires C 73.37, H 5.07, N 10.07.

**4,4'-(propane-1,3-diyl*bis*(oxy))dibenzimidamide dihydrochloride dihydrate** (Propamidine, Compound CHI/1/25/5) (**3**)[1]

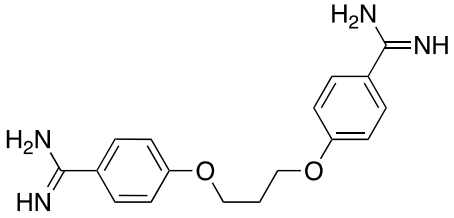

(0.50 g, 1.79 mmol) of **1b** was dissolved in a mixture of anhydrous benzene (55 mL) and anhydrous ethanol (3.0 mL), cooled to 0 °C and saturated with HCl gas. The mixture was sealed and allowed to stir at room temperature for 3 days after which ether (30 mL) was added and the mixture was allowed to stir for 10 minutes. The solids were filtered under nitrogen and dissolved in a mixture of anhydrous EtOH (36 ml) and $EtOH.NH_3$ (36 mL). The mixture was heated overnight (50 °C), cooled to room temperature and reduced by half *in vacuo*. $Et_2O$ (15 mL) was added to precipitate the solid which was filtered, washed and dried under vacuum. Purification by recrystallisation (2N HCl) gave the desired compound **3** as fine white needles (0.59 g, 78%). Mp 200°C; $^{1}$H NMR (MeOD, 400MHz) δ 7.82 (d, 4H, *J* = 9.0 Hz, ArH), 7.19 (d, 4H, *J* = 9.0 Hz, ArH), 4.34 (t, 4H, *J* = 6.0 Hz, $CH_2$), 2.46 (m, 2H, $CH_2$); $^{13}$C NMR (MeOD, 100MHz) δ 167.9, 165.5, 131.5, 121.5, 121.4, 116.6, 66.4, 30.3; $\nu_{max}$ (Nujol) /cm$^{-1}$ 3280 (N-H), 3038 (Ar-H), 2929 (C-H), 1504 (Ar), 1606 (Ar), 1240 (C-O-C); *m/z* (ESP) 313 ($[M-H]^-$); anal. Found C 48.60, H 6.10, N 13.25, $C_{17}H_{26}N_4O_4Cl_2$ requires C 48.46, H 6.22, N 13.30.

**4,4'-(Butane-1,4-diylbis(oxy))dibenzonitrile** (Butamidine precursor) (**1c**)[1]

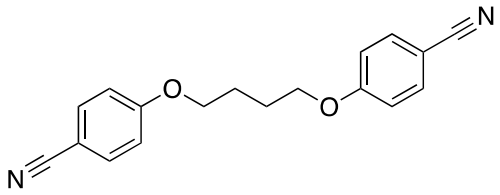

Sodium (0.10 g, 4.35 mmol) was added portionwise to dry EtOH (4.0 mL) stirring under an atmosphere of nitrogen. After dissolution of sodium, a solution of 4-cyanophenol (0.47 g, 3.95 mmol) dissolved in dry ethanol (4.0 mL) was added followed by dropwise addition of 1,4-dibromobutane (0.24 mL, 1.98 mmol). The reaction mixture was allowed to stir at reflux under a nitrogen atmosphere for 3 days after which the mixture was cooled, filtered, the solid washed with water and dried under vacuum. Purification by column chromatography eluting with DCM: hexane (8:2) gave the desired compound **1c** as a white solid (1.03 g, 89%). Mp 174°C; 'H NMR ($CDCl_3$, 400MHz) δ 7.59 (d, 4H, *J* = 8.9 Hz, ArH), 6.93 (d, 4H, *J* = 8.9 Hz, ArH), 4.08 (m, 4H, $CH_2$), 2.01 (m, 4H, $CH_2$); $^{13}C$ NMR ($CDCl_3$, 100MHz) δ 162,1, 134.0, 119.1, 115.1, 104.0, 67.7, 25.7; $\nu_{max}$ (Nujol) /$cm^{-1}$ 3332 (C-O-C), 3033 (Ar-H). 2956 (C-H), 2219 (C≡N), 1604 (Ar). 1506 (Ar), 1251 (C-O-C); *m/z* (CI) 310 ($[M+NH_4]^+$) found 310.15532, $C_{18}H_{20}N_3O_2$ requires 310.15555; anal. Found C 74.03, H 5.55, N 9.55, $C_{18}H_{16}N_2O_2$ requires 73.95, H 5.52, N 9.58.

**4,4'-(Butane-l ,4-diylbis(oxy))dibenzimiamide dihydrochloride dihydrate** (Butamidine, Compound CHI/1/41/1) (**4**)[1]

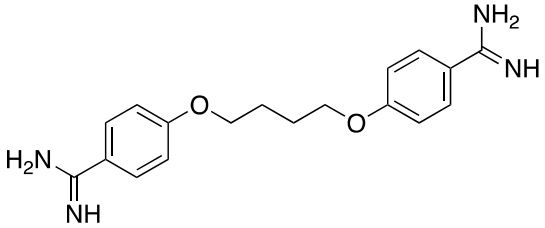

Compound **1c** (0.42 g, 1.44 mmol) was dissolved in a mixture of anhydrous benzene (46 mL) and anhydrous ethanol (2.50 mL), cooled to 0 °C and saturated with HCl gas. The mixture was sealed and allowed to stir at room temperature for 3 days after which anhydrous $Et_2O$ (40 mL) was introduced and the mixture was allowed to stir for 10 minutes. The solids were filtered under nitrogen and dissolved in a mixture of anhydrous EtOH (34 mL) and $EtOH.NH_3$ (34 mL). The mixture was heated overnight (50 °C), cooled to room temperature and reduced by half *in vacuo*. Ether (15 mL) was added to precipitate the solid which was filtered, washed and dried under vacuum. Purification by recrystallisation (2N HCl) gave the desired compound **4** as fine white needles (0.46 g, 73%). Mp 286-287°C', 'H NMR (MeOD, 400MHz) δ, 7.80 (d, 4H, *J* = 9.0 Hz, ArH), 7.14 (d, 4H, *J* = 9.0Hz, ArH), 4.19 (m, 4H, $CH_2$), 2.02 (m, 4H, $CH_2$); $^{13}$ CNMR (MeOD, 100MHz) δ 165.7, 131.4, 121.2, 116.7, 69.7, 27.2; $\nu_{max}$ (Nujol) /$cm^{-1}$ 3370 (N-H), 3129 (Ar-H), 2884 (C-H), 1650 (C≡N), 1606 (Ar), 1508 (Ar), 1257 (C-O); *m/z* (ESP) 327 ($[M+H]^+$); anal. Found C 49.87, H 6.46, N 12.67, $C_{18}H_{28}N_4O_4Cl_2$ requires C 49.66, H 6.48, N 12.87.

**4-(4-phenoxybutoxy) benzonitrile**

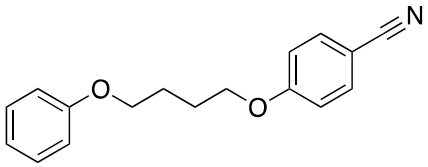

Sodium (0.16g, 6.96 mmol) was added dropwise to dry ethanol (5 mL) and dissolved under a nitrogen atmosphere. To this a solution of 4-cyanophenol (0.53g, 4.47 mmol) dissolved in anhydrous ethanol (5ml) was added followed by addition of 1,4-dibromobutane (0.53 mL, 4.47 mmol). The reaction mixture was allowed to stir at reflux and monitored by TLC. After consumption of 4-cyanophenol, the reaction mixture was allowed to cool to room temperature. In a separate flask sodium (0 16 g, 6.96 mmol) was added portionwise to ethanol (5 mL) stirring under nitrogen. A solution of phenol (0.42 g, 4.47 mmol) in ethanol (5ml) was added and stirred for 10 minutes. This mixture was added dropwise to the cooled mixture and allowed to stir under reflux for 3 days after which the mixture was cooled, filtered, the solid washed with water and dried under vacuum. Purification by column chromatography eluting with DCM: hexane (8:2) gave the desired compound 4-(4-phenoxybutoxy) benzonitrile as a white solid (0.98 g, 82%). Mp 130°C; $^{1}$H NMR ($CDCl_3$, 400MHZ) δ 7.57 (d, 2H, *J* = 8.9 Hz, ArH), 7.28 (d, 1H, *J* = 7.5 Hz, ArH), 7.26 (d, 1H, *J* = 8.1 Hz, ArH), 6.92 (m, 5H, ArH), 4.08 (t, 2H, *J* = 5.9 Hz, $CH_2$), 4.03 (t, 2H, *J* = 5.9 Hz, $CH_2$), 1.99 (m, 4H, $CH_2$); $^{13}$C NMR ($CDCl_3$, 100MHz) δ 162.6, 159.2, 134.3, 129.8, 121.1, 115.5, 114.8, 104.3, 68.3, 67.5, 26.2; $\nu_{max}$ (Nujol) /cm$^{-1}$ 3043 (Ar-H), 2884 (C-H), 2219 (C≡N), 1602 (Ar), 1504 (Ar), 1247 (C-O); *m/z* (CI) 285 ($[M+NH_4]^+$), found 285.16020, $C_{17}H_{21}N_2O_2$ requires 285.16031; anal. Found C 76.40, H 6.46, N 5.44, $C_{17}H_{17}NO_2$ requires C 76.38, H 6.40, N 5.24.

**4-(4-Phenoxybutoxy)benzimidamide hydrochloride hydrate** (Compound CHI/1/69/1)

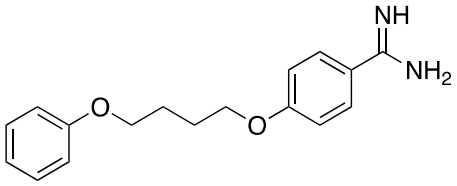

4-(4-phenoxybutoxy) benzonitrile (0.27 g, 1.01 mmol) was dissolved in a mixture of anhydrous benzene (100 mL) and ethanol (1.60 mL), cooled to 0 °C and saturated with HCl gas. The mixture was sealed and allowed to stir at room temperature for 3 days after which anhydrous $Et_2O$ (16 mL) was introduced and the mixture was allowed to stir for an additional 10 minutes. The solids were filtered under nitrogen and dissolved in a mixture of anhydrous EtOH (20 mL) and anhydrous $EtOH.NH_3$ (20 mL). The mixture was heated overnight (50 $^{o}$C), cooled to room temperature and reduced by half *in vacuo*. Ether (30 mL) was added to precipitate the solid which was filtered, washed and dried under vacuum. Purification by recrystallisation (2N HCl) gave the desired compound 4-(4-Phenoxybutoxy)benzimidamide hydrochloride hydrate as fine white needles (0.28 g, 82%). Mp 134-135°C; $^{1}$H NMR (DMSO, 400MHz) δ 9.28 (s, 2H, NH;), 9.08 (s, 2H, NHZ), 7.86 (d, 2H, *J* = 9.0 Hz, ArH), 7.29 (d, 1H, *J* = 7.0 HZ, ArH), 7.27 (d, 1H, *J* = 7.2 Hz, ArH), 7.16 (d, 2H, *J* = 9.0 Hz, ArH), 6.93 (d, 3H, *J* = 7.8 Hz, ArH), 4.16 (t, 2H, *J* = 5.9 Hz, $CH_2$), 4.03 (t, 2H, *J* = 5.9 Hz, $CH_2$), 1.89 (m, 4H, $CH_2$); $^{13}$C NMR (DMSO, 100MHZ) δ 165.0, 163.3, 158.9, 130.5, 129.8, 120.7, 119.6, 115.1, 114.7,

68.1, 67.2, 25.6, 25.5; $\nu_{max}$ (Nujol) /cm$^{-1}$ 3288 (N-H), 1656 (C=N-H), 1604 (Ar), 1506 (Ar), 1234 (C-O-C); *m/z* (ESP) 285 ([M+H]$^+$), found 285.1603, $C_{17}H_{24}N_2O_2$ requires 285.1599; anal. Found C 59.50, H 6.75, N 8.33, $C_{17}H_{23}N_2O_3Cl$ requires C 60.26, H 6.84, N 8.27.

**4-(5-(*p*-Tolyloxy)pentyloxy)benzonitrile**

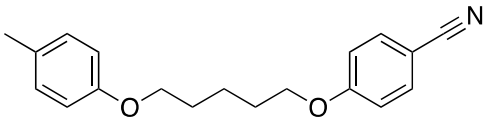


Sodium (0.12 g, 5.22 mmol) was added portionwise to anhydrous ethanol (4.0 mL) and dissolved under a nitrogen atmosphere. To this a solution of 4-cyanophenol (0.57 g, 4.79 mmol) dissolved in anhydrous ethanol (4.0 mL) was added followed by dropwise addition of 1,5-dibromopentane (0.65 mL, 4.79 mmol). The reaction mixture was allowed to stir at reflux and monitored by TLC. After consumption of 4-cyanophenol the reaction mixture was cooled to room temperature. In a separate flask, sodium (0.57 g, 4,79 mmol) was added portionwise to anhydrous EtOH (4.0 ml) with stirring under nitrogen. To this, a solution of *p*-cresol (0.5 ml, 4.79 mmol) in anhydrous EtOH (4.0 ml) was added and stirred for 10 minutes. This mixture was added dropwise to the cooled mixture and stirred under reflux for 3 days after which the mixture was cooled, filtered and the solid washed with water and dried under vacuum. Purification by column chromatography eluting with DCM: hexane (8:2) gave the desired compound as a white solid(1.02 g, 72%). Mp 133°C; $^1$H NMR ($CDCl_3$, 400MHz) δ 7.57 (d, 2H, *J* = 9 Hz, ArH), 7.07 (d, 2H, *J* = 8.6 Hz, ArH), 6.93 (d, 2H, *J* = 9.0 Hz, ArH), 6.79 (d, 2H, *J* = 8.6 Hz, ArH) 4.02 (t, 2H, *J* = 6.4 Hz, $CH_2$) 3.96 (t, 2H, *J* = 6.4 Hz, $CH_2$), 2.28 (s, 3H, CH3), 1.86 (m, 4H, $CH_2$), 1.64 (m, 2H, $CH_2$); $^{13}$C NMR ($CDCl_3$, 100MHz) δ 162.7, 157.2, 134.3, 130.3, 130.2, 115.5, 114.7, 104.1, 68.5, 68.0, 29.4, 29.1, 23.0, 20.8; $\nu_{max}$ (Nujol) /cm$^{-1}$ 3322 (C-O-C), 3031 (Ar-H), 2921 (C-H), 2223 (C≡N), 1602 (Ar), 1506 (Ar), 1234 (C-O-C); *m/z* (CI) 313 ([M+$NH_4$]$^+$), found 313.19092, $C_{19}H_{25}N_2O_2$ requires 313.19162; anal. Found C 77.19, H 7.13, N 5.02, $C_{19}H_{21}NO_2$ requires C 77.26, H 7.17, N 4.74.

**4-(5-(*p*-tolyloxy)pentyyloxy)benzimidamide hydrochloride hydrate** (Compound CHI/1/72/1)

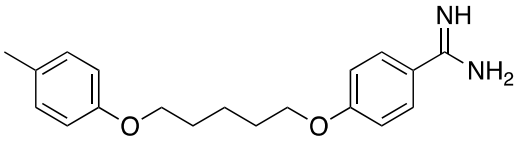


4-(5-(*p*-Tolyloxy)pentyloxy)benzonitrile (0.27 g, 0.91 mmol) was dissolved in a mixture of anhydrous benzene (100 mL) and anhydrous ethanol (1.60 mL), cooled to 0 °C and saturated with HCl gas. The mixture was sealed and allowed to stir at room temperature for 3 days after which anhydrous $Et_2O$ (20 mL) was introduced and the mixture was allowed to stir for 10 minutes. The solids were filtered under nitrogen and dissolved in a mixture of anhydrous EtOH (20 mL) and EtOH.$NH_3$ (20 mL). The mixture was heated overnight (50 °C), cooled to room temperature and reduced by half *in vacuo*. Ether (30 mL) was added to precipitate the solid which was filtered, washed and dried under vacuum. Purification by recrystallisation (2N HCl) gave the desired compound as fine white needles (0.25 g, 75%). Mp 132°C; $^1$H NMR (DMSO, 400MHZ) δ 7.84 (d, 2H, *J* = 9.1 Hz, ArH), 7.15 (d, 2H, *J* = 9.1

Hz, ArH), 7.06 (d, 2H, *J* = 8.4 Hz, ArH), 6.80 (d, 2H, *J* = 8.4 Hz, ArH), 4.11 (t, 2H, *J* = 6.4 Hz, $CH_2$), 3.93 (t, 2H, *J* = 6.4 Hz, $CH_2$), 2.22 (s, 3H, $CH_3$), 1.78 (m, 4H, $CH_2$), 1.56 (m, 2H, $CH_2$); $^{13}C$ NMR (DMSO, 100MHz) δ 165.0, 163.3, 158.9, 130.5, 130.1, 115.1, 114.5, 79.5, 79.3, 79.0, 20.4; $\nu_{max}$ (Nujol) /$cm^{-1}$ 3430 (NH), 3309 (C-O-C), 3093 (Ar-H), 1658 (C=N-H), 1606 (Ar), 1508 (Ar), 1245 (C-O-C); *m/z* (ESP) 313 ($[M+H]^+$), found 313.1916, $C_{19}H_{25}N_2O_2$ requires 313.1907; anal. Found C 62.19, H 7.42, N 7.66, $C_{19}H_{27}ClN_2O_3$ requires C 62.20, H 7.42, N 7.66.

**Synthesis of ER 1004**

**4-bromobenzothioamide**

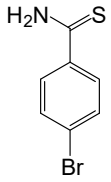


Triethylamine (3.8 mL) was added to a solution of 4-bromobenzonitrile (5 g, 27.5 mmol) in pyridine (17 mL). The solution was cooled to 10 °C and $H_2S$ (g) was bubbled through for 15 min. The resulting green solution was allowed to stir overnight (17 h). Nitrogen was bubbled through for 1 h to remove any excess $H_2S$. Water (27 mL) was added and the mixture was stirred for 10 min, a further portion of water (62 mL) was added and the pale yellow suspension left stirring overnight. The precipitate was filtered and rinsed with water to afford the title compound as bright yellow crystals (5.52 g, 93%). $^1H$ NMR ($d_6$-acetone, 400MHz) 9.07 (bs, 1H, NH), 8.92 (s, 1H, NH), 7.94 (dd, 2H, *J* = 2.0, 6.5 Hz, ArH), 7.62 (dd, 2H, *J* = 2.0, 6.5 Hz, ArH); $^{13}C$ NMR ($d_6$-acetone, 100MHz) 201.9, 140.2, 132.3, 130.4, 126.5; *m/z* (CI) 216 (100%, $[M^+]$)

**2,4-bis(4-bromophenyl)thiazole**

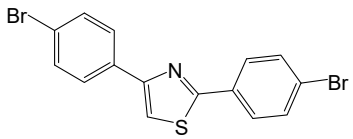


2,4'-dibromoacetophenone (1 g, 3.60 mmol) was added to a solution of 4-bromobenzothioamide (777 mg, 3.60 mmol) in EtOH (15 mL) and warmed to 45 °C for 1 h. The mixture was cooled to room temperature and left for 30 min before filtering. The precipitate was washed with EtOH: water (3:1, 10 mL) and dried to afford the thiazole as a pale solid (1.33 g, 94%). $^1H$ NMR ($CDCl_3$, 250MHz) 7.89 (d, 2H, *J* = 8.5 Hz, ArH), 7.85 (d, 2H, *J* = 8.5 Hz, ArH), 7.59 (d, 2H, *J* = 5.5 Hz, ArH), 7.56 (d, 2H, *J* = 5.5 Hz, ArH), 7.47 (s, 1H, CH); *m/z* (CI) 396 (10%, $[M+H]^+$).

**4,4'-(thiazole-2,4-diyl)dibenzonitrile**

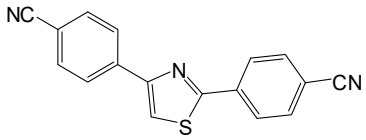


A suspension of 2,4-bis(4-bromophenyl)thiazole (1 g, 2.53 mmol) and CuCN (906 mg, 10.12 mmol) in anhydrous DMF (15 mL) were heated to reflux for 21 h. On cooling, the reaction mixture was poured into aqueous $NH_4OH$ (10%, 50 mL) and extracted with $CHCl_3$ (100 mL). Both layers were filtered to remove the dark precipitate. The organic layer was washed with water (2 x 50 mL), brine (50 mL) and dried $MgSO_4$. Removal of solvent gave a dark oily solid. Purification by column chromatography eluting with $CHCl_3$, afforded the title compound as a pale solid (361 mg, 50%). $^1$H NMR ($CDCl_3$, 400MHz) 8.15 (d, 2H, *J* = 8.5 Hz, ArH), 8.11 (m, 2H, ArH), 7.77 (d, 2H, *J* = 8.5 Hz, ArH), 7.73 (t, 2H, *J* = 3.0 Hz, ArH), 7.26 (s, 1H, CH); $^{13}$C NMR ($CDCl_3$, 100MHz) 166.5, 137.4, 133.2, 130.1, 127.3, 119.1, 117.1, 114.2, 112.4; *m/z* (CI) 288 (100 %, $[M+H]^+$).

**4,4'-(thiazole-2,4-diyl)dibenzimidamide (ER1004)**

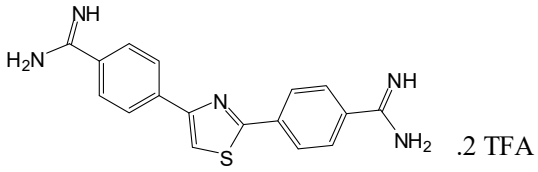


The Garigipati Reaction is a little known reaction which effects the conversion of hindered nitriles to unsubstituted amidines in a mild and effective manner [2, 3]. This is an efficient one step transformation involving direct nucleophilic addition of an amine to a nitrile, affording the corresponding amidine (Scheme 1).

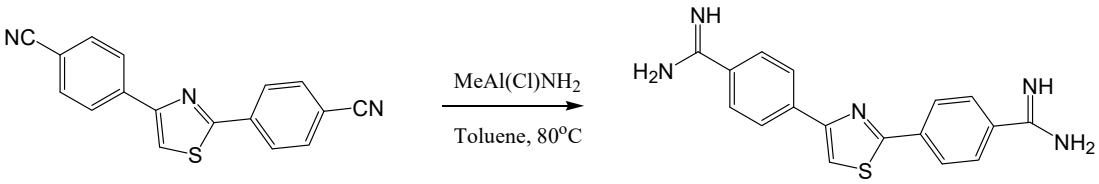


**Scheme 1.**

The alkylchloroaluminium amides are effectively generated from trimethyl aluminium and ammonium chloride and the intermediate aluminium complex is easily hydrolyzed by water adsorbed on silica gel (Scheme 2).

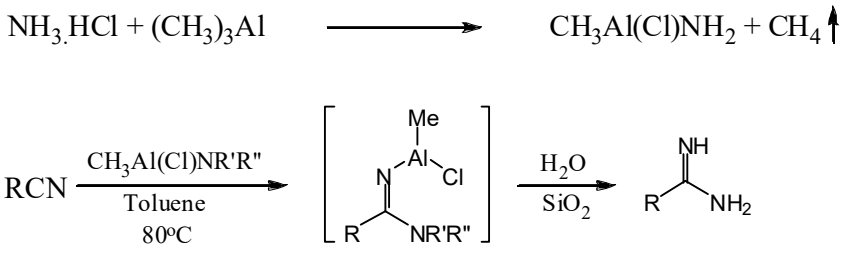


**Scheme 2.**

The freshly prepared alkylchloroaluminum reagents (4 mL, 0.67 M, 2.7 mmol) were added to 4,4'-(thiazole-2,4-diyl)dibenzonitrile (78 mg, 0.27 mmol) in anhydrous toluene (1 mL) and heated to 80 °C overnight under nitrogen. On cooling, the aluminium complex was decomposed by pouring into a slurry of silica gel (2 g) in $CHCl_3$. The mixture was stirred for 5 min before filtering, the filter cake was washed with MeOH (20 mL). Removal of solvent gave the crude amidine as a pale solid in quantitative yield. The crude product (100 mg) was purified by reverse phase HPLC using a YMC-pack ODS-A column (250 x 20 mm I.D, 5 µM) eluting with $CH_3CN$: Water 0.1% TFA (20-80 % gradient over 20 min). Removal of solvent afforded the desired compound as an off-white solid (38 mg, 22%). Mp 271-272 °C; $^1$H NMR (DMSO, 400MHz) 9.32 (bs, 6H, NH & $NH_2$), 8.54 (s, 1H, CH), 8.25 (d, 2H, *J* = 8.5 Hz, ArH), 8.22 (d, 2H, *J* = 8.5 Hz, ArH), 7.92 (d, 2H, *J* = 8.5 Hz, ArH), 7.90 (d, 2H, *J* = 8.5 Hz, ArH); $^{13}$C NMR (DMSO, 100MHz) 165.5, 165.4, 154.4, 138.7, 137.4, 129.6, 129.2, 127.9, 126.9, 126.8, 119.6; *m/z* (ES) 322 (88 % $[M+H]^+$); Found (ES) 322.1121 $C_{17}H_{16}N_5S$ requires 322.1126; anal. Found C 46.05, H 3.10, N 12.44, S 5.77, $C_{21}H_{18}N_5O_4F_6S$ requires C 45.91, H 3.12, N 12.74, S 5.83.

References

1. R. R. Tidwell, S. K. Jones, J. D. Geratz, K. A. Ohemeng, M. Cory and J. E. Hall, *Journal of Medicinal Chemistry*, 1990, **33**, 1252-1257.
2. Moss, R.A., et al., *Conversion of Obstinate Nitriles to Amidines by Garigipatis Reaction. Tetrahedron Letters*, 1995. **36**(48): p. 8761-8764.
3. Garigipati, R.S., *An Efficient Conversion of Nitriles to Amidines.* Tetrahedron Letters, 1990. **31**(14): p. 1969-1972.

# Chemistry of new compounds from David Boykin laboratory.

**General procedure for conversion of nitriles into amidine hydrochlorides (Method A).**
To a cold and stirred suspension of the nitrile or dinitrile (0.001 mol) in 15 ml dry THF was added 6.0 ml, (0.006 mol) $LiN(TMS)_2$ (1 M in THF), stirred for 24 h, cooled, acidified carefully with saturated ethanolic-HCl, the precipitated white solid stirred for 2 h, solvent removed under reduced pressure, diluted with ether, filtered. The collected solid was added to 10 ml ice water, basified with 2M NaOH, the precipitate was filtered, washed with water and air dried. The solid was suspended in anhydrous ethanol (15 ml) and 5 ml saturated ethanolic-HCl and stirred for 6 h, ethanol was distilled off, triturated with dry ether and filtered. The solid was dried under reduced pressure at $80^0$C for 12 h to yield (70-75%) amidine hydrochloride.

**General procedure for conversion of nitriles into amidine hydrochlorides (Method B).**
A suspension of the nitrile or dinitile (0.001 mole) in 20 ml saturated ethanol-HCl was stirred for 4 days in a closed stoppered flask, followed by precipitation with anhydrous ether. The precipitated light yellow solid imidate ester dihydrochloride was filtered and dried under reduced pressure for 3 h to yield (65% -70%) amidine hydrochloride. The imidate ester dihydrochloride (0.0005 mole) in 20 ml anhydrous ethanol was saturated with ammonia(g) or 0.03 equivalents of ethylene diamine stirred in ethanol (at reflux) for 12 h, solvent removed, 20 ml ice water added, basified to pH 10 with aqueous 2N NaOH, filtered, and washed with water. The precipitated solid was dried in air, suspended in 10 ml of saturated ethanolic-HCl, and stirred for 2 h. The solvent removed, dry ether 20 ml added, filtered, washed with ether and dried under reduced pressure for 12 h. The product amidine hydrochloride was obtained as yellow solid 60-66% yield.

**4-(5-(4-methoxyphenyl) furan-2-yl) benzimidamide hydrochloride (DB 607)**
A mixture of 5-(4-cyanophenyl)-2-bromo furan[1] (1.23 g, 0.005 mole) and 4-methoxyphenyl boronic acid (0.93 g, 0.006 mole) in 75 ml dioxane under nitrogen was added $K_2CO_3$ (1.38 g, 0.01 mole, in 5 ml $H_2O$), followed by $Pd(PPh_3)_4$ 0.12 g (0.0001 mole) and the solution was heated under reflux for 12-24 h (tlc monitored). The solvent was removed under reduced pressure, solid filtered, washed with hexane and dried in air. The solid was suspended in DCM (100 ml), filtered through celite, concentrated under reduced pressure, triturated with ether: hexane (2:1), and filtered to yield 4-(5-(4-methoxyphenyl)furan-2-yl)benzonitrile as a yellow brown solid 0.76 g (74%) mp 250-2 °C dec ; $^1$H NMR (DMSO-$d_6$): 7.94 (d, 2H, J= 10.4 Hz), 7.85 (d, 2H, J= 10.4 Hz), 7.78 (d, 2H, J= 10.8 Hz), 7.28 (d, 1H, J= 4.4 Hz), 7.02 (d, 2H, J= 10.8 Hz), 6.97 (d, 1H, J= 4.4 Hz), 3.81 (s, 3H); $^{13}$C NMR (DMSO-$d_6$): 159.3, 154.5, 150.0, 134.1, 132.9, 125.4, 123.5, 122.5, 119.0, 114.4, 111.8, 108.8, 106.9, 55.2; MS: HRMS-ESI-POS: Calcd. for $C_{18}H_{14}NO_2$ *m/z* 276.1024 ($M^+$+1), found *m/z* 276.1021.
The amidine hydrochloride was obtained as yellow solid (Method A) 0.24 g (74%) ; mp >318°C dec ; $^1$H NMR (DMSO-$d_6$): 9.41 (brs, 2H), 9.1 (brs, 2H), 8.01 (d, 2H, J= 8.4 Hz), 7.92 (d, 2H, J= 8.4 Hz), 7.82 (d, 2H, J= 8.4 Hz), 7.324 (d, 1H, J= 3.6 Hz), 7.04 (d, 2H), 7.02 (d, 1H, J= 3.6 Hz), 3.82(s, #H); $^{13}$C NMR (DMSO-$d_6$): 164.9, 159.2, 154.3, 150.2, 134.8, 128.8, 125.5, 125.4, 123.0, 122.5, 114.4, 111.4, 106.8, 55.2; ; MS: HRMS-ESI-POS.: Calcd. for $C_{18}H_{17}N_2O_2$ *m/z* 293.1289 ($M^+$+1), found *m/z* 293.1274; Anal. calcd. for $C_{18}H_{16}N_2O_2$-HCl: C, 65.75; H, 5.21; N, 8.52; Found: C, 65.78; H, 5.23; N, 8.44.

**4,4'-(thiophene-2,4-diyl) dibenzimidamide dihydrochloride (DB 1077)**

A mixture of 2, 4-dibromothiophene 1.21 g (0.005 mole), 4-cyanophenylboronic acid 1.75 g (0.012 mole) following procedure for DB 607, yielded 2,4-(4-cyanophenyl)thiophene as a yellow solid, 0.86 g (72%) mp >220°C dec ; $^{1}$H NMR ($CDCl_3$): 7.75-7.21 (m, 8H), 7.71 (d, 1H, J= 1.2 Hz), 7.64 (d, 1H, J= 1.2 Hz); $^{13}$C NMR ($CDCl_3$): 143.6, 141.6, 139.4, 138.0, 132.9, 132.8, 126.8, 126.1, 123.8, 123.7, 118.8, 118.6, 111.3, 111.1; MS: HRMS-ESI-POS: Calcd. for $C_{14}H_{11}N_2S$ *m/z* 239.0642 ($M^+$+1), found *m/z* 239.0639.
The diamidine hydrochloride was obtained as yellow solid (Method A) 0.32 g (74%) mp>300°C dec ; $^{1}$H NMR (DMSO-$d_6$): 9.55 (brs, 2H), 9.54 (brs, 2H), 9.31 (brs, 4H), 8.42 (s, 1H), 8.32 (s, 1H), 8.09 (d, 2H, J= 8.4 Hz), 8.03-7.97 (m, 6H); $^{13}$C NMR (DMSO-$d_6$): 164.9, 164.8, 142.5, 140.9, 139.5, 138.3, 129.1, 128.8, 126.6, 126.3, 126.2, 125.4, 125.0, 124.8; MS: HRMS-ESI-POS.: Calcd. for $C_{18}H_{18}N_4S$ *m/z* 161.0626 ($M^+$+2)/2, found *m/z* 161.0621; Anal. calcd. for $C_{18}H_{16}N_2S$-2HCl-2$H_2O$: C, 50.35; H, 5.16; N, 13.05; Found: C, 50.52; H, 5.23; N, 13.22.

**3,3'-(furan-2,5-diyl bis (4,1-phenylene)) dipropanimidamide dihydrochloride (DB 1061)**
To a mixture of 4-bromophenyl propionitrile 0.63 g (0.003 mole) and 2, 5-bis (tributylstannyl) furan in 30 ml anhydrous dioxane under nitrogen was added $Pd(PPh_3)_4$ 0.14 g (0.00012 mole) and the solution was heated under reflux for 12 h (tlc monitored). The solvent was removed under reduced pressure, the solid was filtered, washed with hexane and dried in air. The solid was suspended in DCM (50 ml), stirred 2 h with 20 ml 10% KF (aqueous), the organic layer separated, filtered through celite dried over anhydrous $MgSO_4$, filtered, concentrated, triturated with hexane and the solid filtered was filtered to yield 0.34 g (70%) of 3,3'-(furan-2,5-diylbis(4,1-phenylene))dipropanenitrile as a yellow solid mp 120-2°C dec; $^{1}$H NMR ($CDCl_3$): 7.73 (d, 4H, J= 8.4 Hz), 7.30 (d, 4H, J= 8.4 Hz),7.28 (s, 2H), 3.0 (t, 4H, J= 7.6 Hz), 2.66 (t, 4H, J= 7.6 Hz); $^{13}$C NMR ($CDCl_3$): 153.2, 137.2, 130.0, 128.9, 124.4, 119.2, 107.2, 31.5, 19.5; MS: HRMS-ESI-POS: Calcd. for $C_{22}H_{18}N_2ONa$ *m/z* 349.1317 ($M^+$+Na), found *m/z* 349.1332**.**
The diamidine dihydrochloride was obtained using Method B: 0.14 g (60%) mp>300°C dec ; $^{1}$H NMR (DMSO-$d_6$): 9.13 (brs, 4H), 8.74 (brs, 4H), 7.64 (d, 4H, J= 8.4 Hz), 7.49 (s, 2H), 7.33 (d, 4H, J=8.4 Hz), 3.0 (t, 4H, J= 7.2 Hz), 2.74 (d, 4H, J= 7.2 Hz); $^{13}$C NMR (DMSO-$d_6$): 170.6, 142.7, 139.4, 132.4, 129.6, 125.8, 125.2, 33.7, 32.03; MS: HRMS-ESI-POS: Calcd. for $C_{22}H_{26}N_4O$ *m/z* 181.1053 ($M^+$+2)/2, found *m/z* 181.1048; Anal. calc. for $C_{22}H_{24}N_4O$-2HCl-2$H_2O$: C, 56.29; H, 6.44; N, 11.93; Found: C, 56.35; H, 6.54; N, 11.86.

**2,5-bis(4-(2-(4,5-dihydro-1H-imidazol-2-yl) ethyl) phenyl) furan dihydrochloride (DB 1062)**
Similarly, 0.245 g (0.005 mole) of the above imidate ester in 20 ml of anhydrous ethanol was allowed to react under reflux (12 h) with 0.06 g (0.0015 mole) ethylene diamine. The solvent was removed under reduced pressure, diluted with water, solid was filtered, dried and converted to dihydrochloride using ethanolic-HCl to yield a yellow solid, 0.15 (62%), mp >325 $^{o}$C, H NMR (DMSO-$d_6$): 8.29 (br, 4H), 8.74 (brs, 4H), 7.77 (d, 4H, J= 8.4 Hz), 7.34 (s, 2H), 7.05 (d, 4H, J=8.4 Hz), 3.0 (t, 4H, J= 7.2 Hz), 2.74 (d, 4H, J= 7.2 Hz); $^{13}$C NMR (DMSO-$d_6$): 170.2, 152.4, 138.5, 128.8, 128.6, 123.6, 108.0, 44.0, 30.5, 27.4; MS: HRMS-ESI-POS: Calcd. for $C_{26}H_{30}N_4O$ *m/z* 207.1209 ($M^+$+2)/2, found *m/z* 207.1203; Anal. calc. for $C_{26}H_{28}N_4O$-2HCl-2.75$H_2O$: C, 58.37; H, 6.68; N, 10.47; Found: C, 58.45; H, 6.54; N, 10.63.

**3,3'-(thiophene-2,5-diylbis(4,1-phenylene)) dipropanimidamide dihydrochloride (DB 1063)**
The dinitrile, 3,3'-(thiophene-2,5-diylbis(4,1-phenylene))dipropanenitrile, was prepared as described for DB1061 yielding a yellow solid 0.77 g (75%); mp 124-6$^{0}$C dec.;$^{1}$H NMR

($CDCl_3$): 7.62 (d, 4H, J= 8.0 Hz), 7.29 (d, 4H, J= 8.0 Hz),7.28 (s, 2H), 3.0 (t, 4H, J= 7.2 Hz), 2.66 (t, 4H, J= 7.2 Hz); $^{13}$C NMR ($CDCl_3$): 143.3, 137.5, 133.5, 129.1, 126.2, 124.2, 119.2, 31.4, 19.4; MS: HRMS-ESI-POS: Calc. for $C_{22}H_{18}N_2SNa$ *m/z* 365.1088 ($M^+$+Na), found *m/z* 365.1089.

Similarly following the DB 1061 procedure the diamidine dihydrochloride was obtained as a yellow solid 0.16 g (66%), mp >280$^0$C dec; $^1$H NMR (DMSO-$d_6$): 9.19 (brs, 4H), 8.77 (brs, 4H), 7.64 (d, 4H, J= 8.0 Hz), 7.51 (s, 2H), 7.33 (d, 4H, J=804 Hz), 2.99 (t, 4H, J= 8.4 Hz), 2.73 (d, 4H, J= 8.4 Hz); $^{13}$C NMR (DMSO-$d_6$):170.0, 142.2, 138.9, 131.9, 129.1, 125.3, 124.7, 33.2, 31.6; MS: HRMS-ESI-POS: Calcd. for $C_{22}H_{26}N_4S$ *m/z* 189.0939 ($M^+$+2)/2, found *m/z* 189.0931; Anal. calcd. for $C_{22}H_{24}N_4S$-2HCl-1.5$H_2O$: C, 55.45; H, 6.13; N, 11.76; Found: C, 55.52; H, 6.34; N, 11.63.

**2, 5-bis(4-(2-(4,5-dihydro-1H-imidazol-2-yl) ethyl) phenyl) thiophene dihydrochloride (DB 1064)**

Similarly following the procedure for DB1062 the diamidine dihydrochloride was obtained as a yellow solid, 0.17 g (62%); mp >225°C dec.; $^1$H NMR (DMSO-$d_6$): 10.19 (s, 4H), 7.63 (d, 4H, J=7.6 Hz), 7.5 (s, 2H), 7.30 (d, 4H, J= 7.6 Hz), 3.78 (s, 8H),2.97 (t, 4H, J= 6.4 Hz), 2.81(t, 4H, J= 6.4 Hz); $^{13}$C NMR (DMSO-d6): 170.2, 140.2, 138.9, 131.9, 129.1, 125.4, 124.8, 44.1, 30.6, 27.4; MS: HRMS-ESI-POS: Calcd. for $C_{26}H_{29}N_4S$ *m/z* 429.2113 ($M^+$+1), found *m/z* 429.2109; Anal. calcd. for $C_{26}H_{28}N_4S$-2HCl-3.0$H_2O$: C, 56.21; H, 6.53; N, 10.08; Found: C, 56.34; H, 6.61; N, 10.24.

**4-(5-(1-methyl-1H-benzo[d]imidazol-2-yl) furan-2-yl) benzimidamide dihydrochloride (DB 960)**

To a stirred solution of 5-(4-cyanophenyl) furan-2-aldehyde[2] 1.23 g (0.005 mole), 1-amino-2-*N*-(methylamino) benzene 0.61 g (0.005 mol) in 20 ml dry DMF under $N_2$ was added sodium metabisulfite 0.95 (0.005 mol) and the mixture was heated at 130°C for 12 h (tlc monitored). The solvent was removed, the residue was triturated with cold water, separated solid was filtered, washed with water and air dried. The solid was stirred with 1:1 mixture of DCM-ether, filtered and dried in vac at 70°C for 4 h to give the nitrile, 4-(5-(1-methyl-1H-benzo[d]imidazol-2-yl)furan-2-yl)benzonitrile, as a yellow brown solid, 1.1 g (72%), mp >290°C dec ; $^1$H NMR (DMSO-$d_6$): 8.03 (d, 2H, J= 8.4 Hz), 7.92 (d, 2H, J= 8.4 Hz), 7.69-7.63 (m, 2H), 7.46 (d, 1H, J= 3.6 Hz), 7.40 (d, 1H, J= 3.6 Hz), 7.34-7.23 (m, 2H), 4.13 (s, 3H); $^{13}$C NMR (DMSO-$d_6$): 152.4, 145.9, 143.2, 142.4, 136.0, 133.2, 132.9, 124.2, 122.7, 122.2, 118.9, 118.5, 114.7, 111.1, 110.2, 109.9, 31.4; MS: HRMS-ESI-POS: Calcd. for $C_{19}H_{14}N_3O$ *m/z* 300.1136 ($M^+$+1), found *m/z* 300.1132.

The amidine hydrochloride was obtained as yellow solid (Method B) 0.3 g (78%); mp >300°C dec; $^1$H NMR (DMSO-$d_6$): 8.09 (d, 2H, J= 8.7 Hz), 7.90 (d, 2H, J= 8.7 Hz), 7.78-7.70 (m, 2H), 7.61 (d, 1H, J= 3.9 Hz), 7.48-7.42 (m, 2H), 7.45 (d, 1H, J= 3.9 Hz), 4.13 (s, 1H); $^{13}$C NMR (DMSO-$d_6$): 165.5, 155.6, 141.5, 141.3, 135.3, 134.8, 133.9, 129.5, 128.0, 126.0, 125.8, 125.5, 119.6, 116.4, 112.4, 112.0, 32.9; MS: HRMS-ESI-POS: Calcd. for $C_{19}H_{18}N_4O$ *m/z* 159.0740 ($M^+$+2)/2, found *m/z* 159.0733; Anal. calcd. for $C_{19}H_{16}N_4O$-2HCl-1$H_2O$: C, 56.02; H, 4.94; N, 13.76; Found: C, 56.18; H, 4.91; N, 13.51.

## References

1. Depauw, S.; Lambert, M.; Jambon, S.; Paul, A.; Peixoto, P.; Nhili, R.; Marongiu, L.; Figeac, M.; Dassi, C.; Paul-Constant, C.; Billoré, B.; Kumar, A.; Farahat, A.; Ismail, M.; Mineva, E.; Sweat , D. ; Stephens, C.; Boykin, D.; Wilson, W.; David-

Cordonnier, M-H. Heterocyclic Diamidines DNA ligands as HOXA9 Transcription Factor Inhibitors: Design, Molecular Evaluation and Cellular Consequences in HOXA9-Dependant Leukemia Cell Model. *J Med Chem* **62,** 1306-1329 (2019).

2. Mitsch, A., Wissner, P., Silber, K., Hacebel, P., Sattler, I., Klebe, G., Schlitzer, M. Non-thiol farnesyltransferase inhibitors: *N*-(4-tolylacetylamino-3-benzoylphenyl)-3-arylfurylacrylic acid amides. Bioorg. & Med. Chem. **12**, 4585-4600 (2004).